2012

NONINVASIVE ASSESSMENT AND MODELING OF DIABETIC CARDIOVASCULAR AUTONOMIC NEUROPATHY

Siqi Wang
University of Kentucky, siqi.lotus@gmail.com

STUDENT AGREEMENT:

I represent that my thesis or dissertation and abstract are my original work. Proper attribution has been given to all outside sources. I understand that I am solely responsible for obtaining any needed copyright permissions. I have obtained and attached hereto needed written permission statements(s) from the owner(s) of each third-party copyrighted matter to be included in my work, allowing electronic distribution (if such use is not permitted by the fair use doctrine).

I hereby grant to The University of Kentucky and its agents the non-exclusive license to archive and make accessible my work in whole or in part in all forms of media, now or hereafter known. I agree that the document mentioned above may be made available immediately for worldwide access unless a preapproved embargo applies.

I retain all other ownership rights to the copyright of my work. I also retain the right to use in future works (such as articles or books) all or part of my work. I understand that I am free to register the copyright to my work.

REVIEW, APPROVAL AND ACCEPTANCE

The document mentioned above has been reviewed and accepted by the student's advisor, on behalf of the advisory committee, and by the Director of Graduate Studies (DGS), on behalf of the program; we verify that this is the final, approved version of the student's dissertation including all changes required by the advisory committee. The undersigned agree to abide by the statements above.

Siqi Wang, Student

Dr. Abhijit R. Patwardhan, Major Professor

Dr. Abhijit R. Patwardhan, Director of Graduate Studies

NONINVASIVE ASSESSMENT AND MODELING OF DIABETIC CARDIOVASCULAR AUTONOMIC NEUROPATHY

DISSERTATION

A dissertation submitted in partial fulfillment of the
requirements for the degree of Doctor of Philosophy in the
College of Engineering
at the University of Kentucky

By
Siqi Wang

Lexington, Kentucky

Director: Dr. Abhijit R. Patwardhan, Professor of Biomedical Engineering

Lexington, Kentucky

2012

ABSTRACT OF DISSERTATION

NONINVASIVE ASSESSMENT AND MODELING OF DIABETIC CARDIOVASCULAR AUTONOMIC NEUROPATHY

Noninvasive assessment of diabetic cardiovascular autonomic neuropathy (AN): Cardiac and vascular dysfunctions resulting from AN are complications of diabetes, often undiagnosed. Our objectives were to: 1) determine sympathetic and parasympathetic components of compromised blood pressure regulation in patients with polyneuropathy, and 2) rank noninvasive indexes for their sensitivity in diagnosing AN. Continuous 12-lead electrocardiography (ECG), blood pressure (BP), respiration, regional blood flow and bio-impedance were recorded from 12 able-bodied subjects (AB), 7 diabetics without (D0), 7 with possible (D1) and 8 with definite polyneuropathy (D2), during 10 minutes supine control, 30 minutes 70-degree head-up tilt and 5 minutes supine recovery. During the first 3 minutes of tilt, systolic BP decreased in D2 while increased in AB. Parasympathetic control of heart rate, baroreflex sensitivity, and baroreflex effectiveness and sympathetic control of heart rate and vasomotion were reduced in D2, compared with AB. Baroreflex effectiveness index was identified as the most sensitive index to discriminate diabetic AN.

Four-dimensional multiscale modeling of ECG indexes of diabetic autonomic neuropathy: QT interval prolongation which predicts long-term mortality in diabetics with AN, is well known. The mechanism of QT interval prolongation is still unknown, but correlation of regional sympathetic denervation of the heart (revealed by cardiac imaging) with QT interval in 12-lead ECG has been proposed. The goal of this study is to 1) reproduce QT interval prolongation seen in diabetics, and 2) develop a computer model to link QT interval prolongation to regional cardiac sympathetic denervation at the cellular level. From the 12-lead ECG acquired in the study above, heart rate-corrected QT interval (QTc) was computed and a reduced ionic whole heart mathematical model was constructed. Twelve-lead ECG was produced as a forward solution from an equivalent cardiac source. Different patterns of regional denervation in cardiac images of diabetic patients guided the simulation of pathological changes. Minimum QTc interval of lateral leads tended to be longer in D2 than in AB.

Prolonging action potential duration in the basal septal region in the model produced ECG and QT interval similar to that of D2 subjects, suggesting sympathetic denervation in this region in patients with definite neuropathy.

KEYWORDS: blood pressure regulation, spectral power, baroreflex, twelve-lead ECG, forward solution

Multimedia Elements Used: TIFF (.tif), JPEG (.jpg), PNG (.png), WMV (.wmv)

NONINVASIVE ASSESSMENT AND MODELING OF DIABETIC CARDIOVASCULAR AUTONOMIC NEUROPATHY

By

Siqi Wang

Dr. Abhijit R. Patwardhan
Director of Dissertation

Dr. Abhijit R. Patwardhan
Director of Graduate Studies

December 12th, 2012

I would like to dedicate this work to my respective parents who have been my constant source of inspiration. They have given me the drive and discipline to tackle any task with enthusiasm and determination. Without their love and support this project would not have been made possible.

ACKNOWLEDGEMENTS

The completion of this work would not be possible without the help of many, many people. My first and foremost acknowledgement is to my advisors, Joyce Evans and Abhijit Patwardhan. In the four and half years that I've worked with you, you've taught me about important disciplines in science, and also about life and work.

I would like to thank the members of my committee, David Randall, Charles Knapp and Guoqiang Yu for their knowledge, guidance and encouragement.

Thank you to everyone in the research team: Kevin Nelson, Dennis Karounos, Samy Elayi, Todd Schlegel, Andrea Hartman, Daniel Silcox and Rebecca Schneider, Mead Ferris, Mark Howarth, Lindsey Krompak, Lindsay Mohney, Conner Ferguson, Janet Kaenzig and other staff of the UK GCRC. Adam Lindstrom, of the UK SSTARS Center guided the statistical analysis. Dr. David Brown, Biomedical Engineering, University of Kentucky wrote the program for R wave detection. Natalia Arzeno, NASA Johnson Space Center Cardiovascular Laboratory developed the software used for beat-to-beat analysis. I would also like to thank our subjects who willingly gave their time and information to this study.

I would also like to thank the students, staff and faculty of the University of Kentucky Center for Biomedical Engineering. Wenner-Gren has been my home during this journey, and it was a pleasure working with all of you.

Finally, I would like to thank my parents for, not only raising and providing for me, but for their support and encouragement in pursuing academic achievements. Their passions in work and the spirit of continuous learning have influenced me and give me the passion on my study and work.

TABLE OF CONTENTS

LIST OF FIGURES

LIST OF TABLES

LIST OF FILES

WANG_dissertation.pdf

Heart Model and ECG.wmv

Part 1. Noninvasive assessment of diabetic cardiovascular autonomic neuropathy

1.1 Chapter One: Introduction

Neuropathy is one of the complications of diabetes. Diabetic neuropathy affects sensory, motor and autonomic nerves. Cardiovascular autonomic neuropathy (CAN) is a common and serious type of neuropathy, that involves the damage of both sympathetic and parasympathetic branches of autonomic nerves innervating the heart and blood vessels, causing abnormal regulation of heart rate and vascular dynamics (128).

The pathogenesis of neuropathy in diabetic patients is still not clear. Current hypotheses concerning the multiple etiologies of diabetic neuropathy include metabolic insult to nerve fibers, neurovascular insufficiency, autoimmune damage and neurohormonal growth factor deficiency, resulting in nerve degeneration or gene-related neural damage (128, 130). The prevalence of CAN has been determined to be 25.3% for individuals with Type 1 diabetes and 34.3% for individuals with Type 2 diabetes, as diagnosed by clinical cardiovascular reflex tests currently in use (see below) (143).

Cardiovascular autonomic neuropathy is associated with increased risk of occurrence of cardiac events including myocardial infarction, heart failure, ventricular tachycardia or fibrillation (128). The 5-year mortality of diabetics with CAN is three times higher than in diabetics without CAN (128). The quality of life was decreased in diabetic patients with severe CAN due to orthostatic hypotension, amputation, or other symptoms. Treatment of cardiovascular manifestations of diabetic autonomic neuropathy includes intensive glycemic control to prevent the onset of diabetic autonomic neuropathy and slow the progression (129) . In addition, a variety of treatments are available to alleviate the symptoms of autonomic neuropathy (130). The onset of CAN occurs early in diabetes, and patients are usually asymptomatic for years and are not able to

sense when they are becoming hypoglycemic or having a heart attack (130). Early diagnosis and treatment is the key to effectively treating CAN.

Current clinical tests of CAN rely on a battery of cardiovascular reflex tests called Ewing tests (39). Although useful, these tests require voluntary participation and the sensitivity of these tests is limited. For example, the direct measure of cardiac sympathetic innervation determined from metaiodobenzylguanidine (MIBG) scintigraphy revealed that abnormal cardiac sympathetic innervation occurred earlier than previously known from Ewing, and other, tests and, in fact, was evident in diabetic patients whose Ewing tests were still normal (49). However, MIBG scintigraphy is expensive, invasive and time consuming, and is thus not suitable for routine screening of CAN. In the last two decades, alterations in power spectral analysis of heart rate variability have been related to abnormal Ewing tests in diabetic patients, reflecting mostly parasympathetic dysfunction (32, 45, 60, 144).

1.1.1 Objective

The present study aimed to assess the function of both sympathetic and parasympathetic braches of the autonomic nervous system in diabetic patients, in order to develop indexes suitable for screening of diabetic autonomic neuropathy. Passive head-up tilt was used to stimulate autonomic regulation of cardiovascular responses to orthostatic stress. Cardiovascular variables were acquired from able-bodied subjects, diabetic patients without neuropathy, diabetic patients with mild neuropathy and diabetic patients with severe neuropathy. The specific goals of this study were to 1) assess dysfunction of autonomic regulation of cardiovascular system in diabetic patients, 2) develop indexes of diabetic cardiovascular autonomic neuropathy that are noninvasive, sensitive, cost-effective and easy to acquired and 3) further explore mechanisms of autonomic regulation of the cardiovascular system of normal humans by comparing with autonomic failure in diabetics.

In this study, 12-lead ECG was also acquired to assess cardiac function in supine diabetic patients. Because of the lack of cardiac imaging data of sympathetic innervation, a heart-torso computer model was developed to assess dysfunction of sympathetic innervation of the heart in diabetic patients. Because of the extended length of the content, 12-lead ECG and modeling are included in Part 2 of this document. Part 1 focuses on blood pressure regulation in diabetic and nondiabetic subjects in response to head-up tilt.

1.2 Chapter Two: Background

1.2.1 Physiological Response to Orthostatic Stress

Demands for autonomic regulation of blood pressure at supine position are minimum, therefore passive head-up tilt (47) was used to activate autonomic regulation by challenging the cardiovascular system during exposure to gravity while minimizing activation of postural muscles, primarily the legs. The hydrostatic pressure gradient along the length of the body, due to the drag of gravity, increases transmural pressure of the vessels below the heart, thus increasing venous volume by approximately 500 mL (79). In healthy subjects, reflexes elicited by the unloading of arterial baroreceptors and cardiopulmonary mechanoreceptors restore blood pressure rapidly. The reflexes act by increasing heart rate, contractility and vascular resistance. After the initial response, hormonal regulation predominates in blood pressure regulation by further vasoconstriction and maintaining plasma volume. These responses are described in detail below.

Arterial baroreceptors and cardiopulmonary receptor are sensory stretch receptors, which sense arterial and cardiac filling pressures. This information is transmitted to the brainstem where it is integrated with information from other sensors. Sympathetic and parasympathetic outflows from the brainstem are adjusted to initiate the desired cardiovascular response. These reflexes function via negative feedback (79).

The cardiac pre-ganglionic parasympathetic fibers synapse the post-ganglionic parasympathetic fibers near the heart. Parasympathetic fibers innervate the sinoatrial (SA) and atrioventricular (AV) nodes. Post-ganglionic parasympathetic fibers release the neurotransmitter acetylcholine (ACh) from the nerve terminal, which acts by binding to muscarinic M_2-receptors on the myocyte membrane (79). ACh slows the pacemaker potential decay and hyperpolarizes the membrane, resulting in slowing of heart rate. ACh reduces the pacemaker slope via an inhibitory G protein-adenylate cyclase-cAMP-PKA pathway. On the

other hand, the hyperpolarizing effect of ACh is mediated through a G-protein-K_{ACh} channel pathway, which is a rapid pathway. ACh is quickly removed from the junctional region by the enzyme cholinesterase. These mechanisms account for the rapidity of the response, with which vagal stimulation slows the heart and the reduction of vagal activity speeds the heart, within one heart beat (79).

The efferent cardiac pre-ganglionic sympathetic fibers arise from the thoracic spinal cord, segments T1 – T5, and synapse in the sympathetic chain. The post-ganglionic fibers innerve the SA node, the AV node, and the myocardium of atria and ventricles. Post-ganglionic sympathetic fibers release the neurotransmitter norepinephrine (NE), which binds to adrenergic receptors in the heart. There are α-, β_1 and β_2 –receptors in the heart, while β_1 receptors predominate. Activation of the β_1 receptors induces the following effects over several beats: increased heart rate, increased AV node conduction velocity, shortened myocyte action potential, increased contractile force and increased rate of relaxation. These responses are induced by β_1 receptors activating the cAMP-PKA pathway, which leads to changes in ion channel and pump activity. The termination of the action of NE is partly by diffusion into the bloodstream, which washes it away; and partly by reuptake into the sympathetic nerves. The slow activation and termination processes explain the slow response to, and recovery from, sympathetic stimulation. Epinephrine, which is secreted into the bloodstream by the medulla of the adrenal gland in response to preganglionic sympathetic fiber activity, acts in a similar way as NE at the heart (79).

In addition to the control of the heart, sympathetic neural activity controls vascular resistance by controlling the contraction and relaxation of vascular smooth muscle (VSM) cells. The post-ganglionic sympathetic neurotransmitter, NE, binds to α-adrenoreceptors on the membrane of VSM cells. Activation of α-adrenoreceptors induces VSM contraction by increasing cytosolic free [Ca^{2+}], due to 1) sustained membrane depolarization through PLC-IP_3-DAG pathway in many arteries, 2) firing of action potentials in response to strong sympathetic

stimulation in arterioles, small arteries and veins, and 3) mechanisms independent of membrane depolarization in large arteries. Activation of sympathetic fiber is tonic, and reduced sympathetic activity results in vasodilation (79).

Within the first few minutes of head-up tilt, healthy persons usually have an initial drop in blood pressure, sensed by arterial baroreceptors and cardiopulmonary receptors, which rapidly bring back blood pressure by withdrawal of parasympathetic outflow and an increase in sympathetic outflow. Withdrawal of parasympathetic outflow to the heart causes an increase of heart rate. Increased sympathetic outflow to the heart results in increases of heart rate and heart contractility. In addition, increased sympathetic outflow to peripheral vasculature causes constriction of resistance vessels and thus an increase in total peripheral resistance. At the capillary level, constriction of arterioles causes decreased hydrostatic pressure thereby increasing osmotic absorption of interstitial fluid in to the plasma compartment which helps to increase blood return. Finally, increased sympathetic outflow results in venoconstriction, which can displace blood from the big reservoirs in the intestinal tract, liver and skin (79, 109).

During longer head-up tilt, regulation by hormones predominates. The effective hormones at different times are epinephrine, norepinephrine, renin, angiotensin II, aldosterone, vasopressin, etc, to vasoconstrict and maintain plasma volume (109).

It should be noted that skin is an important organ in both regulation of blood pressure and thermoregulation. In human, approximately 95% of the skin is hairy skin and the other 5% is non-hairy skin which is primarily at palmar surface of the hands, soles of the feet and part of the face (59). Circulations in both types of skin are controlled by the sympathetic nervous system: hairy skin is controlled by both cholinergic (active vasodilation) and adrenergic (vasoconstriction) branches of the sympathetic nerves and non-hairy skin is controlled by

adrenergic (vasoconstriction) sympathetic nerves (21). Arteriovenous anastomoses (AVA) are present in the non-hairy skin and are innervated by adrenergic sympathetic nerves which are tonically active, while in hairy skin, AVA rarely exist (21). It was reported that there is a reflex vasoconstriction in hairy skin in response to head-up tilt, while the non-hairy skin is not involved in this response (109).

1.2.2 Detection of Diabetic CAN

The damage of nerve fibers in autonomic neuropathy is believed to be length dependent. It occurs earliest in parasympathetic fibers which are longer fibers, followed by damage in shorter sympathetic fibers (128, 130). Ewing tests were developed several decades ago and serve as a noninvasive measure of cardiovascular autonomic neuropathy in both branches (39). Ewing tests consist of 5 reflex tests, including heart rate response to Valsalva maneuver, heart rate variation during deep breathing, immediate heart rate response to standing, (controlled predominantly by parasympathetic nerves), blood pressure response to standing and blood pressure response to sustained handgrip, (controlled predominantly by sympathetic nerves) (39). If the results of two or more of these tests are abnormal, the patient is diagnosed to have CAN. Although it is useful in detection of cardiovascular autonomic neuropathy, this battery of tests requires voluntary participation of patients and involves specialized operations from heath care providers. In addition, its manifestations lag behind abnormalities in spontaneous baroreflex function (44) and cardiac imaging of sympathetic innervation to the myocardium (49).

A direct measure of cardiac sympathetic innervation to the myocardium can be performed by using a radio-labeled norepinephrine analog and tomography of uptake of this analog into nerve terminals. The most commonly used neuronal tracers are MIBG, used with single photon emission computed tomography (SPECT), and ^{11}C-meta-hydroxyephedrine (HED), used with positron emission tomography (PET) (63). In normal human subjects, cross sections of MIBG-SPECT or HED-PET images demonstrated homogeneous

uptake of tracer and a complete ventricular structure, while in diabetic patients, reduced tracer uptake in the whole left ventricle or regions of the left ventricle have been observed, even in those without signs of neuropathy (22, 49, 56, 75, 91, 93, 112-115, 123). These techniques provide insight to sympathetic innervation of the heart, although they are not suitable for routine screening.

Other techniques are being examined for their potential to provide in-depth, easy to administer, diagnostic tools. Comparisons of heart rate variability, low (LF) and high (HF) frequency components of heart rate oscillations, have been correlated with abnormal results of Ewing tests (32, 45, 60, 144). Diabetic patients with abnormal Ewing results also demonstrated reduced LF spectral power of systolic blood pressure compared to able bodied controls or compared to diabetics with normal results in Ewing tests, during one hour supine or a short period of standing (32, 144). In diabetics with no signs of autonomic neuropathy, the numbers of spontaneous baroreflex sequences were reduced and slopes of baroreflex sequences were smaller compared to controls (32, 44). Heart rate variability and baroreflex sequences, acquired during a short period of time, demonstrate parasympathetic dysfunction in modulating heart rate in diabetic patients. Longer recordings of blood pressure revealed sympathetic dysfunction in modulating peripheral vasculature. The ultimate goal of this study is to develop indexes of both sympathetic and parasympathetic function from noninvasive recordings taken over a short period of time.

1.2.3 Models of Autonomic Failure

Studies of sino-aortic denervated (SAD) animals (cats and dogs), a form of ‘dysautonomia’, showed that not only were harmonic components (LF or HF peaks) of heart rate and blood pressure oscillations affected by SAD, but nonharmonic components were also altered over a wide frequency range (very low, low and high frequencies) (29, 133). In addition to the alteration in heart and blood pressure variability over a wide frequency range, the baroreflex effectiveness index, which represents the percentage of systolic blood pressure (SBP) ramps followed by reflex RR interval responses to all SBP ramps, was

reduced by 89% in SAD cats (31). In humans with pure autonomic failure, heart rate and blood pressure variability have been shown to be altered at all frequencies (97). Finally, we reported previously that spinal cord injury resulted in reduced baroreflex effectiveness index in tetraplegic patients compared to able bodied controls (5). Results of these previous human and animal studies indicated similarities between diabetic autonomic neuropathy, sinoaortic denervation and primary autonomic failure that appeared to be proportional to the level of neuropathy and observable in noninvasive indexes of autonomic function.

1.3 Chapter Three: Methods

1.3.1 Subjects

Twelve healthy able-bodied volunteers (AB) were recruited from the local community using word of mouth, newspaper advertisements and flyers mounted on boards across the university campus and hospital. Twenty-two diabetic subjects were recruited. The diabetic subjects were evaluated at the day of study by Dr. Kevin Nelson, Department of Neurology, UK College of Medicine, for distal symmetrical polyneuropathy using neuropathic symptoms, depressed ankle reflexes, distal sensory loss, distal muscle weakness or atrophy, and nerve conduction studies (18). Subjects were then distinguished by consensus criteria that determined the likelihood of neuropathy using an ordinal scale from highest 4 to lowest 1 (35). 'Possible neuropathy' was defined by a likelihood ranking of two or three, and 'definite neuropathy' by the likelihood of 4. Diabetic subjects without neuropathy had no signs or symptoms of neuropathy, in addition to normal nerve conduction studies. Based upon the results of these evaluations the neuropathy of diabetic subjects was categorized as absent (D0), possible (D1) or definite (D2). In addition to the tests for peripheral neuropathy, and for fasting blood glucose levels on the day of study, all subjects underwent a familiarization tilt and 12 lead ECG. Medications affecting autonomic function were discontinued for the day of study. Demographic characteristics of the participants are shown in Table 1.

Table 1 *Demographic characteristics of participants*

		Diabetic		
	Able-bodied (AB)	No Peripheral Neuropathy (D0)	Possible Peripheral Neuropathy (D1)	Definite Peripheral Neuropathy (D2)
Age, yr	48.2 ± 3.9	39.7 ± 5.6	53 ± 4.1	55.1 ± 2.7
Weight, kg	93.0 ± 9.0	84.2 ± 8.1	110.7 ± 15.9	97.9 ± 11.4
Height, cm	171.5 ± 3.0	164.6 ± 3.0	176.8 ± 4.6	174.2 ± 3.3
n (Male/Female)	12 (5/7)	7 (1/6)	7 (5/2)	8 (5/3)
n of Type 1/ Type 2		3/4	2/5	3/5

Values are means ± SEM

1.3.2 Tilt Protocol

We utilized passive head-up tilt to challenge the autonomic regulation of arterial blood pressure. Before entering the study all subjects gave written informed consent and the protocol was approved by the University of Kentucky Institutional Review Board. Prior to head-up tilt testing, subject's height, age, weight and diabetic status were recorded. Later, after blood glucose level had been determined, an IV cannula was placed in an antecubital vein. Subjects then rested in the supine position for 30 min when instrumentation was applied followed by 10 minutes of supine control and 30 minutes of 70-degree head-up tilt. If presyncopal symptoms developed during tilt, subjects were brought back to supine immediately. All subjects were followed for a supine recovery period of five minutes.

1.3.3 Measured Variables

Mixed venous blood samples were drawn from the antecubital vein catheter at the end of control, at three and seven min of tilt, and during the second minute of recovery. Results of blood assays, body fluid shifts and impedance measures of cardiac output are not reported here, but are components of the next manuscript, see Future Work.

Lead II ECG (Pilot Colin) was acquired from three electrodes. Noninvasive continuous arterial blood pressure (BP, Portapres model-2) was acquired from a cuff placed at finger. Respiratory activity (Respitrace) was acquired by measuring respiratory inductance plethysmography with two bands enclosed chest and abdomen. Two laser Doppler probes (Perimed) were placed at two skin sites: one on the palm of hand (non-hairy skin) and the other on the forearm (hairy skin). The measuring depth of the probe was 0.5 – 1 mm with the fiber separation 0.25 mm and the wavelength of the laser 780 nm (77, 121). Fluid shifts between body segments were assessed by measuring bio-impedance (UFI THRIM) of thorax, abdomen, upper leg and lower leg. Tilt angle (Crossbow CXL 04LP3) was acquired from an accelerometer mounted on the tilt table. Recordings were commenced during supine control, and continued uninterrupted during the 70 degree head-up tilt and supine recovery. The blood pressure sensor was maintained at heart level. Manual blood pressure using an arm cuff was acquired at the end of supine control, the beginning of tilt and at the end of recovery. The hand with blood pressure finger cuff and laser Doppler probe was covered by a mitten, in order to keep the hand warm and allow for a measurable blood pressure signal during the whole study. A 12-lead ECG was acquired from supine subjects breathing at 15 breaths/min. Data acquisition of 12-lead ECG lasted for approximately 5 min or until at least 256 heart beats were recorded for signal averaging. Room temperature was maintained at 22 ± 0.25^{o}C (mean ± SEM), ranging from 20.6-23.9 ^{o}C.

1.3.4 Data Acquisition and Analysis

Blood pressure, ECG, respiratory activity, skin perfusion, bio-impedance and tilt angle recordings were digitized at 1000 Hz by using a commercial data acquisition system (DATAQ). 12-lead ECGs were digitized at 1000 Hz and recorded by using a commercial device and software (Cardiax).

Mean values. Heart rate (HR) and RR interval were computed by identifying R waves in the last 5 min of control, 0-3 min, 3-7 min, and 7-12 min of tilt and the first 3 min of recovery. Data were analyzed using custom written

programs in C++ and MATLAB (the MathWorks, Natick, MA). Artifacts in HR and BP signals, including premature beats and Portapres servo adjustments (approximately 5% of the beats per time series), were manually removed. The cleaned signals were then aligned in time. Systolic (SBP) and diastolic (DBP) blood pressures were determined by computing the maximum and minimum values of clean arterial BP for each heart beat. Beat-to-beat skin perfusion sequences were determined by integrating the pulsatile skin perfusion between two R waves. Mean values of RR interval, SBP, DBP and skin perfusions of palm and forearm were computed in each time segment. All subsequent data analyses were performed in MATLAB.

Spectral analysis. RR interval, SBP, DBP and skin perfusions in control, tilt and recovery periods were resampled at 4 Hz using a cubic spline. Power spectral densities of RR interval, SBP and DBP were analyzed in the last 5 min of control, 0-3 min, 3-7 min, and 7-12 min of tilt and the first 3 min of recovery. Power spectral densities of skin perfusions were analyzed in 10 min of control and the first 10 min of tilt to acquire a better accuracy at lower frequencies. Each segment was then linearly detrended. Power spectral densities were estimated using Welch's method of averaged periodograms (480-point Hamming windows with 440-point overlap). Spectral powers of RR interval, SBP and DBP in the LF (0.04-0.15 Hz) and HF (0.15-0.4 Hz) regions were obtained using trapezoidal integration over the specified frequency range. Spectral power of DBP was used as an index of sympathetic control of vasomotion because DBP correlated better than did SBP with vascular resistance (13). Power spectral density of SBP, however, was used as an index of baroreflex-mediated buffering of blood pressure. Power spectral densities were plotted in a log-power vs. log-frequency scale, and the slope of the linear regression of this plot within the LF range was calculated. This power law scaling relationship was quantified for RR interval, SBP and DBP to determine their harmonic and nonharmonic characteristics (34, 50). The magnitudes of the power spectral density of skin perfusions were determined from the mean value of the logarithm of the power spectral density in

specific frequency regions: very low frequency (VLF, 0.004-0.04 Hz), low frequency (LF, 0.04 -0.15 Hz) and high frequency (HF, 0.15-0.4 Hz).

Coherences. The coherences between skin perfusions and blood pressure were analyzed across 10 min of control and the first 10 min of tilt. The 95% confidence level of non-zero coherence was estimated by the following method. If the theoretical coherence between the input and output signals of a linear time-invariant system is zero, then the random variable

$$\frac{(v-2)r_{xy}^2(f)}{2(1-r_{xy}^2(f))}$$

is approximately distributed with an F distribution $f_{2,v-2}$, where r^2_{xy} is the squared coherence between skin perfusion and blood pressure, and v is the degree of freedom associated with Hamming window, which was estimated by

$$v = 2.51\frac{N}{M}.$$

2M is the window length and N is the data length. Therefore, we have

$$\frac{(v-2)r_{xy}^2(f)}{2(1-r_{xy}^2(f))} = f_{2,v-2} \qquad <1>$$

Rearranging <1> and replacing the f function in <1> with its 95% critical value give the 95% confidence level of non-zero coherence as

$$r^2 = \frac{2f_{2,v-2}(0.95)}{(v-2)+2f_{2,v-2}(0.95)}$$

Because able-bodied subjects and diabetics without neuropathy had similar skin perfusion responses to head-up tilt, and diabetics with possible and those with definite neuropathy had similar responses, able-bodied subjects and diabetics without neuropathy were combined into one, non-neuropathy, group,

and diabetics with possible and those with definite neuropathy were combined into one neuropathy group.

Baroreflex sequences. The sequence method (12) was adopted to quantify the number of blood pressure ramps and baroreflex sequences, as well as baroreflex sensitivity. Sequences of three or more consecutive heartbeats were identified, in which progressively increasing (or decreasing) SBP with at least 1 mmHg beat-to-beat change were followed within 1 heart beat by progressively lengthening (or shortening) of RR interval with at least 4 msec beat-to-beat change. A sequence was accepted as a baroreflex sequence if the correlation coefficient of the regression line between SBP and RR interval within the sequence was 0.85 or greater (12). The slope of the regression line for each sequence was taken as spontaneous baroreflex sensitivity (BRS). The ratio between the number of baroreflex sequences and the total number of increasing or decreasing SBP ramps determined the baroreflex effectiveness index (BEI) (31). Because the numbers of SBP ramps and baroreflex sequences depend on the number of analyzed heartbeats, which varied among and within subjects, the numbers of SBP ramps and baroreflex sequences were normalized by the number of analyzed heartbeats of each subject in each time segment.

Arterial pulse transit time. An index of arterial compliance, arterial pulse transit time (PTT), was measured by adapting the technique of Foo et al. (42). Arterial PTT was recorded as the time interval between the R peak in ECG and the SBP peak in the arterial pressure measured at the finger. Average values from ten beats selected from clean data were taken in the last minute of supine control and the second minute of 70-degree head-up tilt.

Statistical analysis. SAS (The SAS Institute, Cary, NC) software was used to test a linear mixed model for differences within and among four groups (able-bodied, diabetic without neuropathy, diabetic with possible neuropathy, diabetic with definite neuropathy) during supine control, at three time segments during tilt, and in recovery. The group factor was used to test differences among the four

groups. The time factor was used to test the tilt effect. The group × time factor was used to test for differences in tilt effects across groups. The changes from control to the first three minutes of tilt were tested with one-way ANOVA and two-tail t tests. For *a priori* hypothesized differences between variables, for which we predicted a specific difference (greater or less) before we analyzed the data, changes from control were analyzed using one-tail t tests. Data were transformed by using logarithm or square root if the residual plots showed heteroscedasticity. Nonparametric test, the Mann-Whitney U test, was used to test the changes from supine control to tilt when the distribution of data did not meet the requirement of t test. Outliers were identified if residuals were larger than two standard deviations and thus were not included in the statistical testing. Differences were considered significant if $p \leq 0.05$. Results are presented as mean ± SEM.

1.4 Chapter Four: Results

Upon testing, one able-bodied subject was diagnosed with nondiabetic sensory and motor neuropathy; his data were not included in any group. Five able-bodied subjects, and three diabetics with possible neuropathy demonstrated symptoms of presyncope before finishing 30 min of head-up tilt and were returned to supine immediately.

Typical RR interval, arterial BP, skin perfusion of palm and forearm, and tilt angle of an asymptomatic able-bodied subject and a diabetic patient with definite neuropathy during supine and during 30 min head-up tilt are shown in Figure 1.1. In the nonsyncopal, able bodied subject, RR interval decreased and BP increased modestly during head-up tilt. In the same subject, skin perfusion of palm increased and skin perfusion of forearm decreased during head-up tilt. In the diabetic patient with definite neuropathy, RRI decreased to a smaller extent and BP decreased during head-up tilt. In the same subject, skin perfusion of palm was higher than that in the able-bodied subject at control and did not increase during head-up tilt. Skin perfusion of forearm of this subject also decreased during head-up tilt.

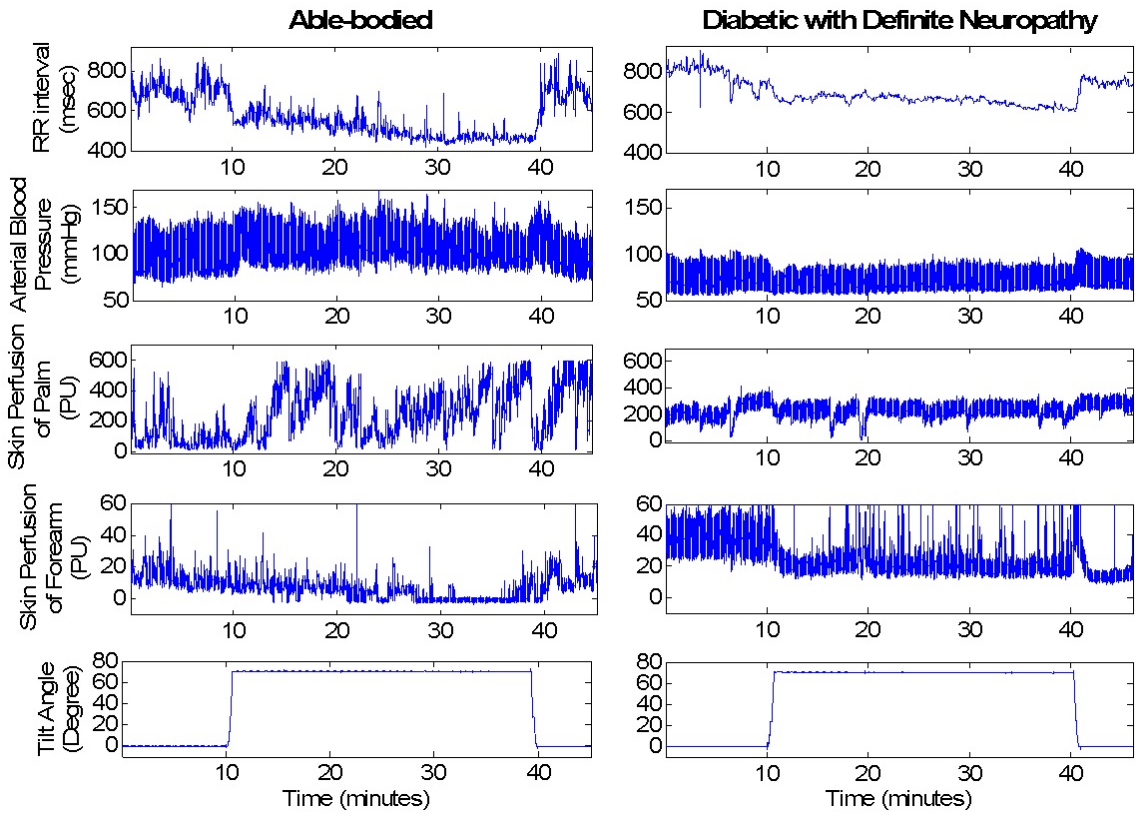

Figure 1.1 Typical RR interval, arterial blood pressure and skin perfusions of palm and forearm during 10 min supine control, 30 min 70-degree head-up tilt and 5 min recovery, in an able-bodied subject (left), and a diabetic subject with definite neuropathy (right).

1.4.1 Mean Values

Figure 1.2 shows group averaged (± SEM) RR interval and SBP for able-bodied (AB; blue line) subjects, diabetics without neuropathy (D0; pink line), diabetics with possible neuropathy (D1; red line) and diabetics with definite neuropathy (D2; dark red line). Data are given for supine control, three stages of tilt and supine recovery. All groups decreased RR interval (Figure 1.2A) in response to head-up tilt. The magnitudes of SBP responses to the first three minutes of head-up tilt (Figure 1.2B2) were significantly different between able-bodied subjects and diabetics with definite neuropathy (one-tailed t-test); for able-bodied, SBP increased from 124 ± 5.8 mmHg in supine control to 132 ± 7.9 mmHg; for diabetics with definite neuropathy, SBP decreased from 128.7 ± 7.8

mmHg in supine control to 119.2 ± 10.7 mmHg. Supine control values of RR interval and SBP were not different between the groups.

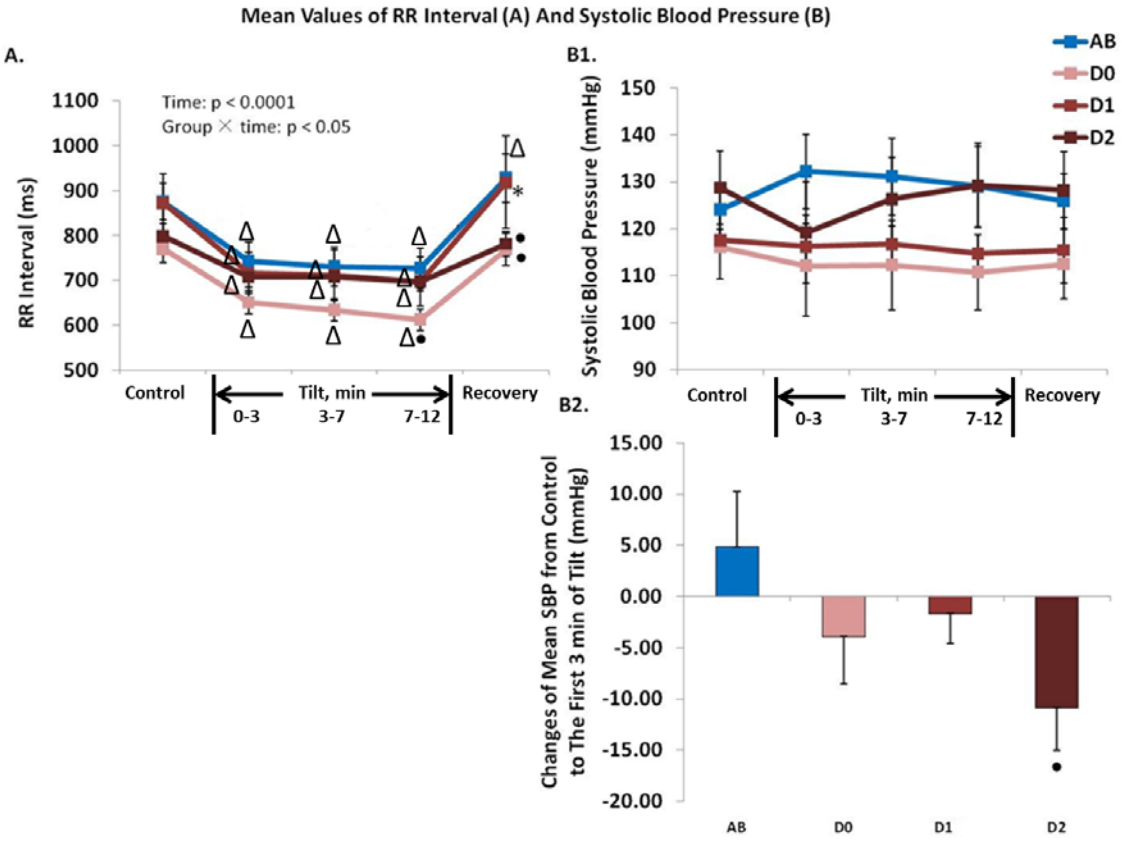

Figure 1.2 Average ± SEM RR interval (Figure A) and systolic blood pressure (Figure B1) for able-bodied subjects (AB; n=11), diabetics without neuropathy (D0; n=6), diabetics with possible neuropathy (D1; n=5) and diabetics with definite neuropathy (D2; n=8) in response to head up tilt. Figure B2 shows changes of SBP from supine control to the first 3 min of tilt. Δ, significantly different from control (same group); •, significantly different from AB (same time segment); *, significantly different from D0 (same time segment).

Figure 1.3 shows group averaged (± SEM) skin perfusion of the forearm for combined groups of subjects without neuropathy (able-bodied and diabetics without neuropathy) and those with neuropathy (diabetics with possible and definite neuropathy). Skin perfusion of forearm decreased in both groups (tilt main effect, p = 0.0078) during all time segments of head-up tilt compared to

control and recovery. The neuropathy group tended to have higher skin perfusion of forearm than the non-neuropathy group (group main effect, p = 0.189, Figure 1.3). We interpret this tendency to be due to the larger number of male subjects in the neuropathy group compared to the non-neuropathy group (Figure 1.4). Male subjects had higher skin perfusion than did females in both groups at control (gender main effect P<0.05 in two-way ANOVA with the factors of gender and presence of neuropathy).

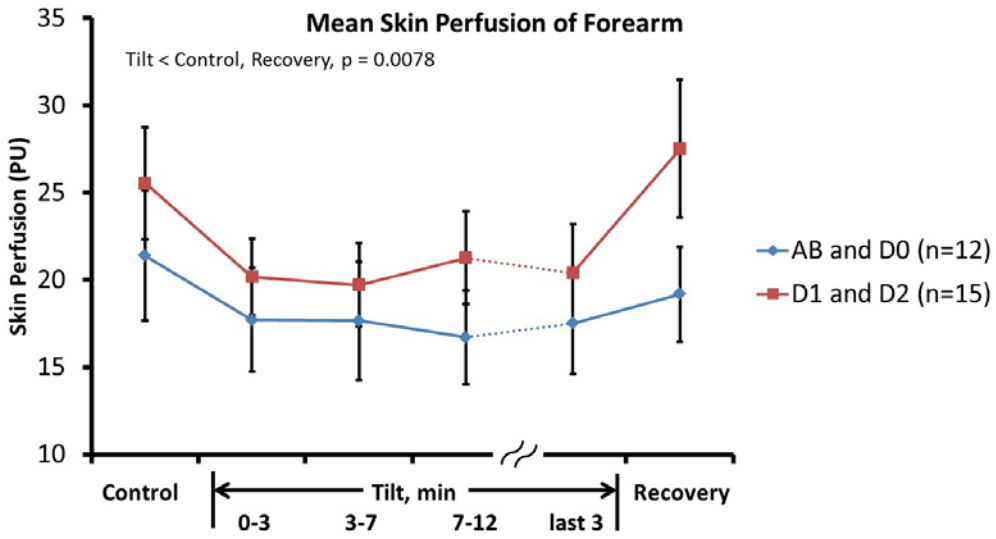

Figure 1.3 Average ± SEM skin perfusion of the forearm in the non-neuropathy group [able bodied (AB), diabetics without neuropathy (D0)], and the neuropathy group [diabetics with possible neuropathy (D1) and diabetics with definite neuropathy (D2)] during 5 min of supine control, 0-3 min, 3-7 min, 7-12 min and the last 3 min of head-up tilt and during 3 min of supine recovery.

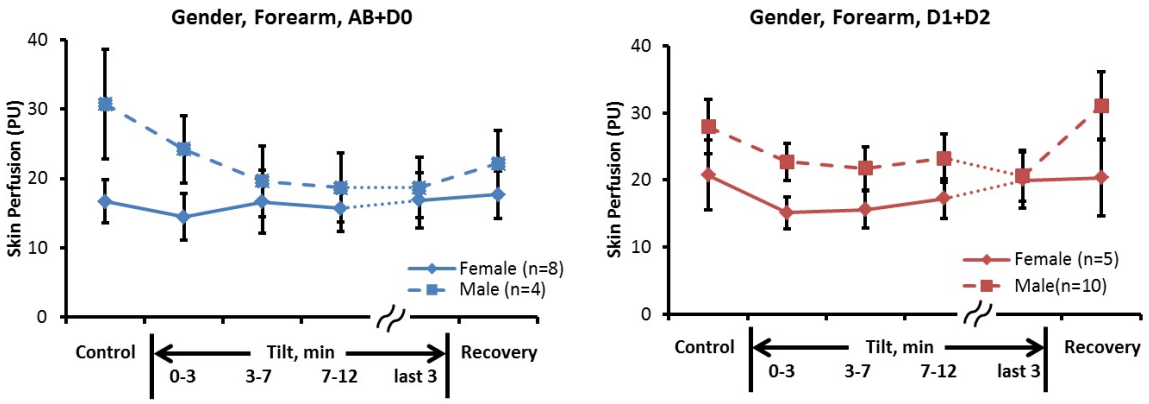

Figure 1.4 Gender differences in average ±SEM skin perfusion of the forearm in non-neuropathy (AB+D0, left) and neuropathy (D1+D2, right) groups during 5 min of supine control, 0-3 min, 3-7 min, 7-12 min and the last 3 min of head-up tilt and during 3 min of supine recovery.

Figure 1.5 shows group averaged (± SEM) skin perfusion of the palm for combined non-neuropathy and neuropathy groups. Skin perfusion of palm was significantly higher in the neuropathy group than in the non-neuropathy group during supine control. Skin perfusion of the palm of the non-neuropathy group increased significantly after the third minute of head-up tilt, while skin perfusion of the palm of the neuropathy group decreased during the first 3 min of head-up tilt. During recovery, palmar skin perfusion of the non-neuropathy group was higher than control, while that of neuropathy group was not different from control. Group differences in response to head-up tilt are easier to see, when palmar skin perfusion is plotted as tilt-induced changes from control (Figure 1.6). The changes of palmar skin perfusion in the neuropathy group were significantly different from those in the non-neuropathy group after the third minute of head-up tilt and during recovery. When each group was further divided into male and female subjects, gender differences were not significant either in the control values or in the responses to head-up tilt (Figure 1.7).

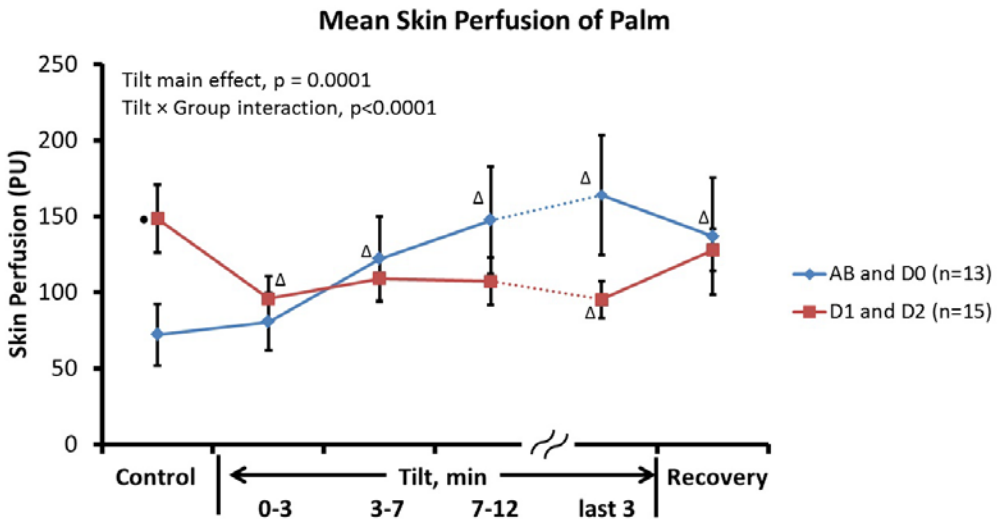

Figure 1.5 Average ± SEM skin perfusion of the palm of the hand in the non-neuropathy (AB and D0) and neuropathy (D1 and D2) groups during 5 min of supine control, 0-3 min, 3-7 min, 7-12 min and the last 3 min of head-up tilt and during 3 min of supine recovery. ●, significantly different between groups in the same time segment. Δ, significantly different from control in the same group.

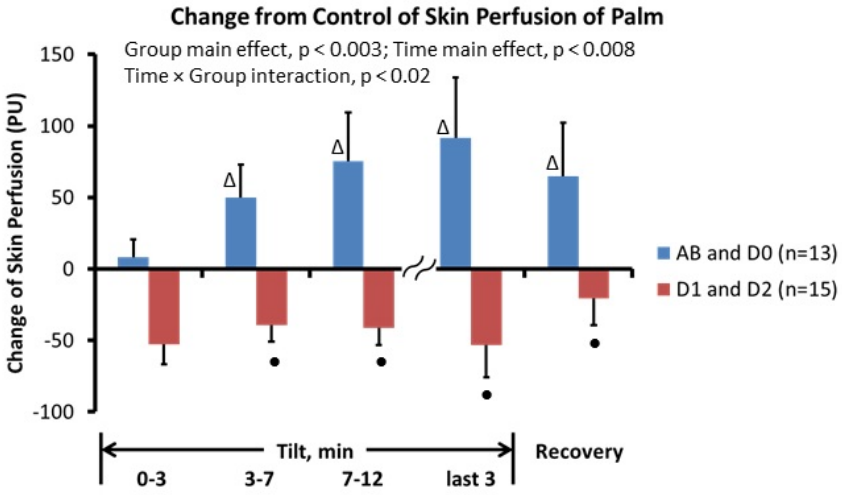

Figure 1.6 Average ± SEM changes from control of palmar skin perfusion for non-neuropathy (AB and D0) and neuropathy (D1 and D2) groups during 0-3 min, 3-7 min, 7-12 min and the last 3 min of head-up tilt and during 3 min of supine recovery. ●, significantly different between groups in the same time segment. Δ, significantly different from the first 3 min of tilt in the same group.

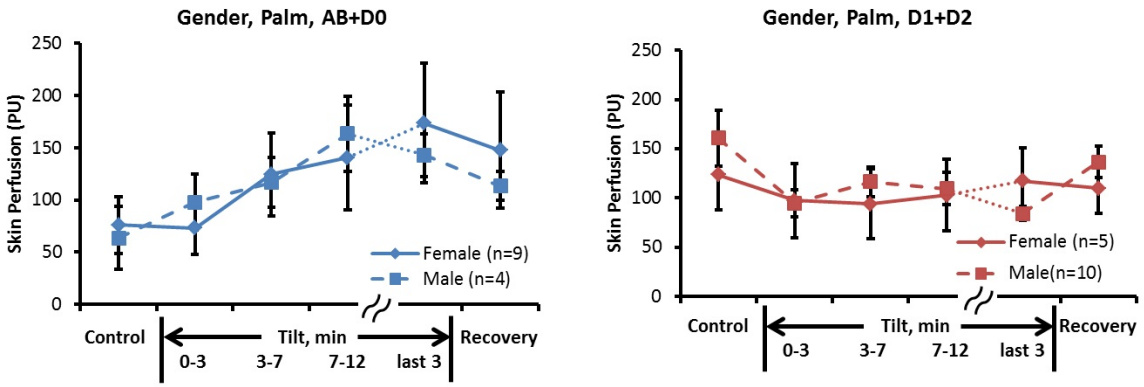

Figure 1.7 Gender differences in average ±SEM skin perfusion of the palm in non-neuropathy (AB+D0, left) and neuropathy (D1+D2, right) groups during 5 min of supine control, 0-3 min, 3-7 min, 7-12 min and the last 3 min of head-up tilt and during 3 min of supine recovery.

1.4.2 Spectral Power

Figure 1.8 gives average high frequency spectral power of RR interval (HFRRI, Panel A, left) and low frequency spectral power of diastolic blood pressure (LFDBP, Panel B1, upper right) for each of the four groups. In Figure 1.8A, HFRRI decreased during head-up tilt for all groups. In addition, able-bodied subjects and diabetics without neuropathy had higher HFRRI than did diabetics with definite neuropathy (group main effect). Figure 1.8B1 shows that diabetics with possible neuropathy and those with definite neuropathy tended to have lower LFDBP than did able-bodied subjects and diabetics without neuropathy during head-up tilt (group × time, $p=0.06$). The change in LFDBP during the first 3 min of tilt, Figure 1.8B2, differed significantly ($p<0.05$) between able-bodied (2.1 ± 0.4 mmHg^2 supine, to 4.9 ± 1.6 mmHg^2) and diabetics with definite neuropathy (2.1 ± 0.5 mmHg^2 supine, to 1.6 ± 0.7 mmHg^2).

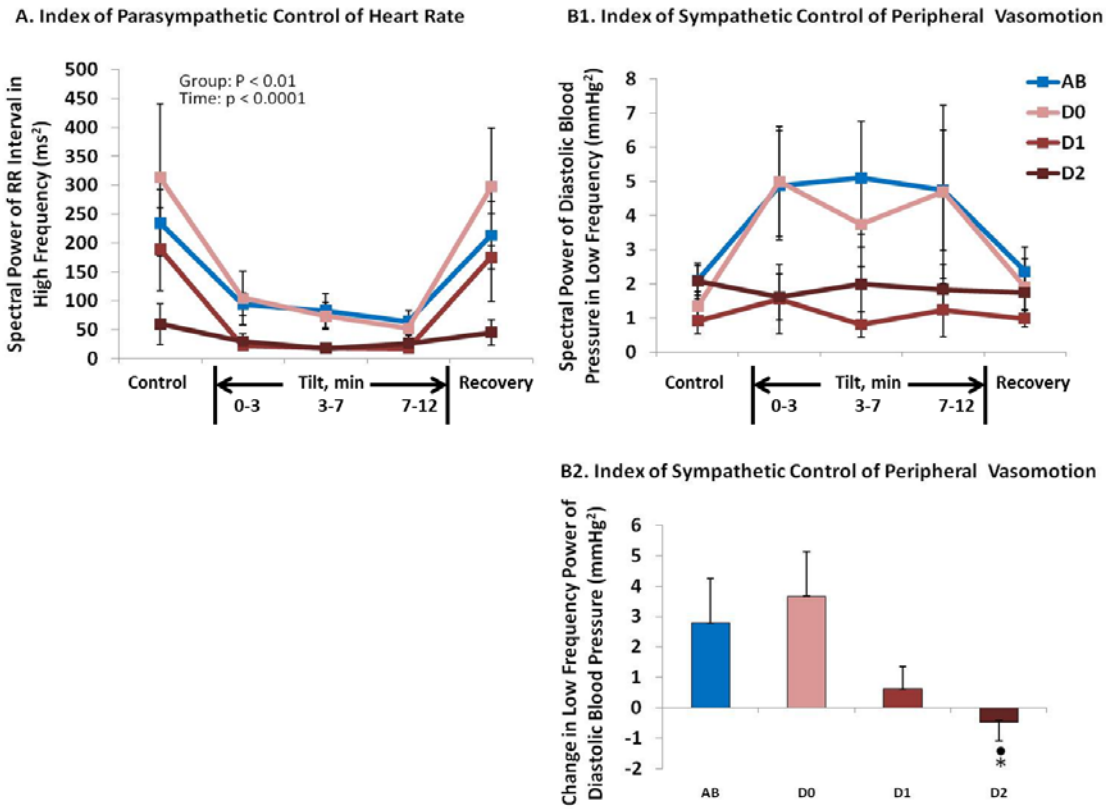

Figure 1.8 Panel A: Average ± SEM spectral power of RR interval in the high-frequency region for able-bodied subjects (AB; n = 11), diabetics without neuropathy (D0; n = 6), diabetics with possible neuropathy (D1; n=5) and diabetics with definite neuropathy (D2; n =8) at rest and in response to head-up tilt. Panel B1: The spectral power of DBP in the low-frequency region for the four groups in response to head-up tilt. These group differences in response to the first 3 min of tilt are shown in Figure B2. •, significantly different from AB; *, significantly different from D0.

Figure 1.9 shows group averaged log of power spectral density of SBP (PSD SBP; Figure 1.9A and Figure 1.9B, top) and log of RR interval (PSD RRI; Figure 1.9D and Figure 1.9E bottom) versus log of frequency for able-bodied subjects (left panels) and diabetics with definite peripheral neuropathy (middle panels). The analyses are from recordings taken during five minutes of supine control. Data shown are means (solid lines) ± SEM (shaded area above and below the mean). Spectral power of SBP was significantly greater (four fold,

which is not immediately evident on logarithmic scales) in diabetics with definite neuropathy than in able-bodied subjects (Figure 1.9B vs. Figure 1.9A) across the very low frequency (0.003 - 0.04 Hz) and high frequency (0.15 - 0.4 Hz) regions. However, in contrast to able-bodied subjects, the SBP spectral power of diabetics with definite neuropathy dipped at frequencies around 0.1 Hz (Figure 1.9B). In addition, the slope of the linear portion of this SBP curve in the low frequency region tended to be steeper in diabetics with definite neuropathy (-2.64 ± 0.44) than in able-bodied subjects (-1.54 ± 0.37) (Figure 4C). SBP powers for diabetics without, and those with, possible neuropathy, were similar to that of able-bodied subjects (not shown). In contrast to SBP, the variability of RR interval for diabetics with definite neuropathy was significantly (four fold) lower than that of able-bodied subjects over the range of frequencies (0.003 - 0.4 Hz) (Figure 1.9D vs. Figure 1.9E). Log-log plots of RRI for diabetics without neuropathy and diabetics with possible neuropathy were intermediate between able-bodied subjects and diabetics with definite neuropathy (not shown). Slopes of the log-log RR interval/frequency curve were significantly steeper in the low frequency region (0.04 - 0.15Hz) in diabetics with possible (-2.19 ± 0.35) and definite neuropathy (-2.77 ± 0.24) than slopes of able-bodied (-1.05 ± 0.35) and diabetics without neuropathy (-1.15 ± 0.4), Figure 1.9F.

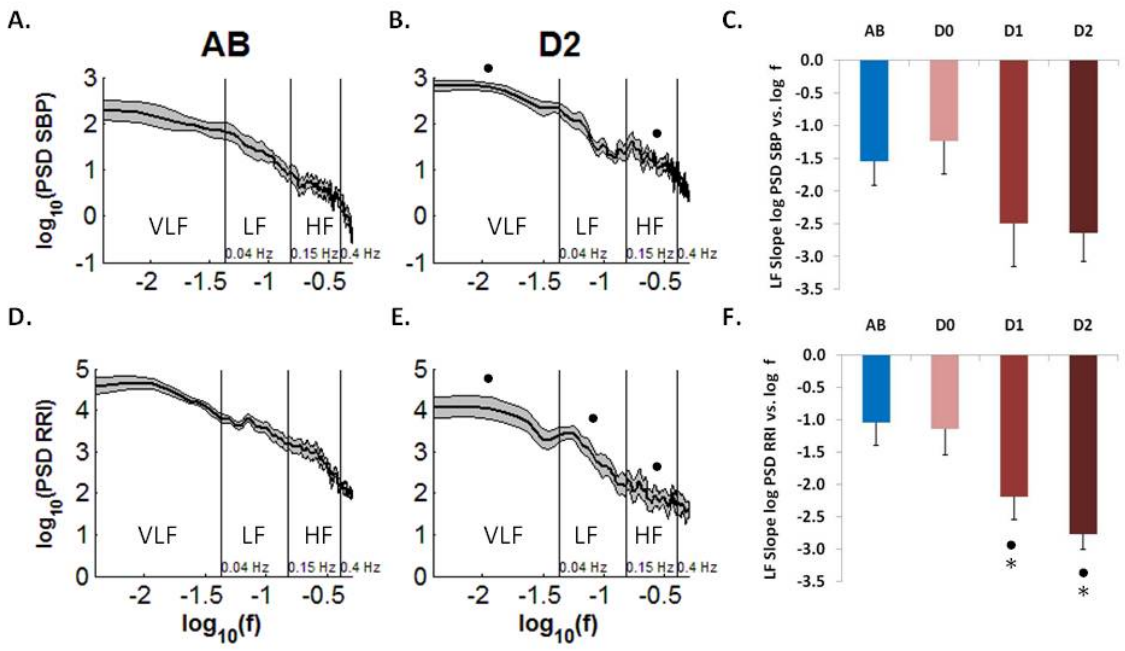

Figure 1.9 Average ± SEM logarithm of power spectral density of systolic blood pressure (PSD SBP) and RR interval (PSD RRI) taken from 5 min supine control (means shown in solid lines and SEM shown in shaded area above and below the mean in A, B, D and E). Plots A and B show log (PSD SBP) vs log (f) for AB (n = 11) and D2 (n=8) respectively. Plot C shows the average value of the slopes of the linear portion of log (PSD SBP) vs log (f) curves in the low frequency (0.04 - 0.15 Hz, LF) region for all four groups. Plots D and E show log (PSD RRI) vs log (f) for AB and D2 respectively. Plot F shows the average value of the slopes of log (PSD RRI) vs log (f) curves in the low frequency. •, significantly different from AB; *, significantly different from D0.

Figure 1.10 shows power spectral density (PSD) of diastolic blood pressure (DBP) on a logarithmic scale, during 10 min supine control (left panel) and the first 10 min of tilt (right panel) in non-neuropathy (blue) and neuropathy (red) groups. The PSD of DBP demonstrated similar response to that shown in Figure 1.8B, but with a more obvious difference between the two groups. During head-up tilt the mean magnitude of PSD in the low frequency region increased in the non-neuropathy group but did not change in the neuropathy group. In addition, mean LF PSD was lower in the neuropathy group than in the non-

neuropathy group. High frequency PSD of DBP decreased from control to tilt in the neuropathy group.

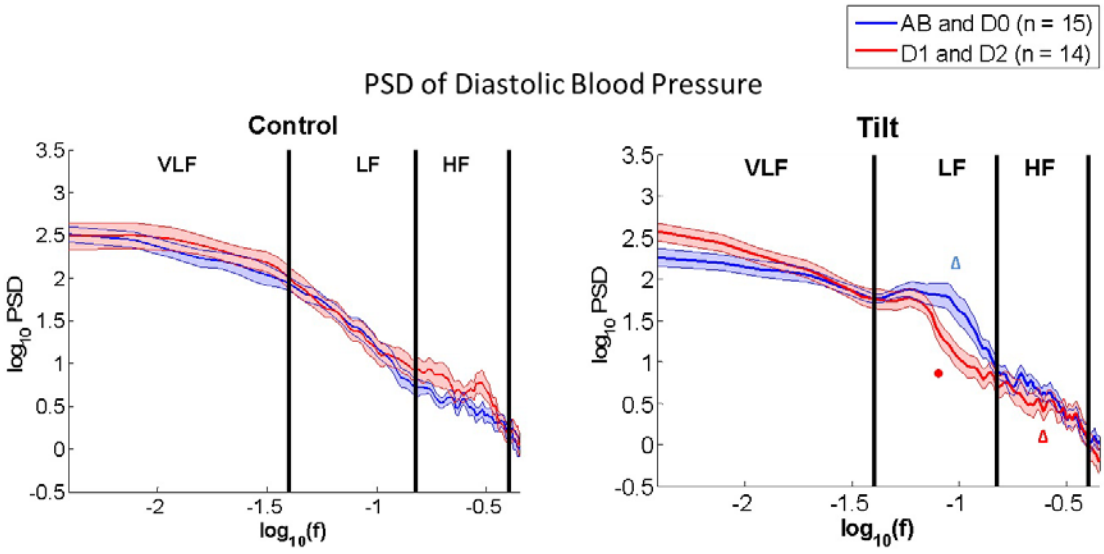

Figure 1.10 Average ± SEM logarithm of power spectral density of diastolic blood pressure taken from10 min supine control and the first 10 min of head-up tilt. ●, significantly different between groups in the same time segment. Δ, significantly different from control in the same group.

Figure 1.11 shows PSD of skin perfusion of the forearm on a logarithmic scale, during 10 min supine control (left panel) and the first 10 min of tilt (right panel) in non-neuropathy and neuropathy groups. Low frequency PSD decreased during tilt in the neuropathy group but did not change in the non-neuropathy group (group × time interaction p=0.03). The changes of mean LF PSD of skin perfusion of the forearm from control to tilt are shown in Figure 1.12. The change of LF PSD was significantly different between the non-neuropathy and neuropathy groups (Mann-Whitney Test, p = 0.05). The group difference was more obvious in the frequency range between 0.075 and 0.1 Hz (time × group interaction, p= 0.02; the non-neuropathy group tended to be greater than the neuropathy group during tilt, p = 0.1). In the high frequency region, mean PSD in the neuropathy group was higher than that in the non-neuropathy group in control and decreased during tilt (Figure 1.11, group × time interaction, p=0.012).

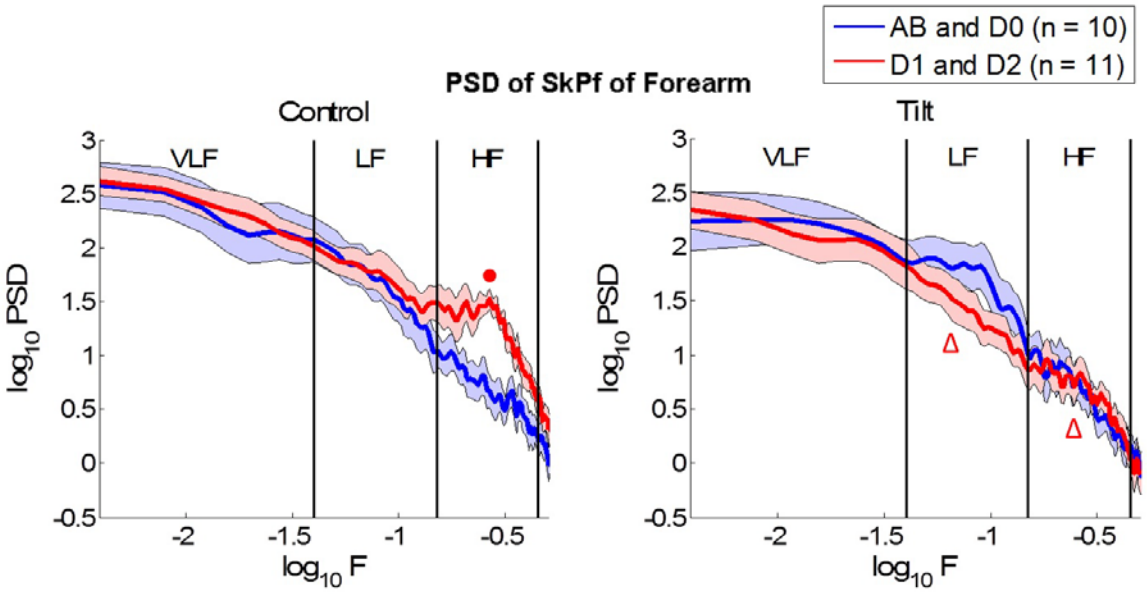

Figure 1.11 Average ± SEM logarithm of power spectral density of skin perfusion of forearm taken from10 min supine control and the first 10 min of head-up tilt. ●, significantly different between groups in the same time segment. Δ, significantly different from control in the same group.

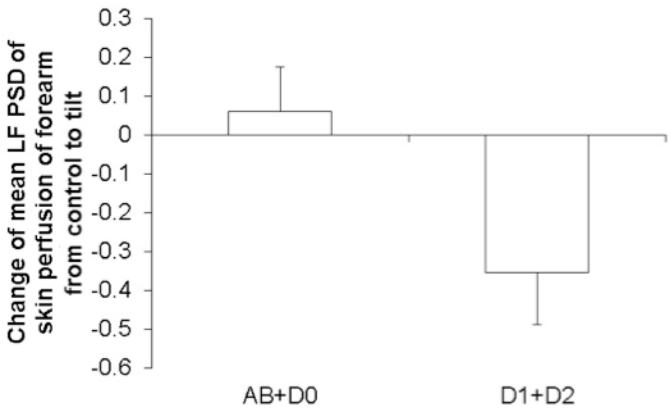

Figure 1.12 Change of mean low frequency PSD of skin perfusion of the forearm from control to the first 10 min of head-up tilt. P = 0.05, Mann-Whitney Test.

Figure 1.13 shows the power spectral density of skin perfusion of palm on a logarithmic scale, during 10 min supine control and the first 10 min of tilt in non-neuropathy and neuropathy groups. Mean magnitude of PSD in the very low frequency region decreased in both groups from control to tilt (main tilt effect). High frequency PSD tended to decrease in the neuropathy group but did not change in the non-neuropathy group (group × time interaction p=0.06).

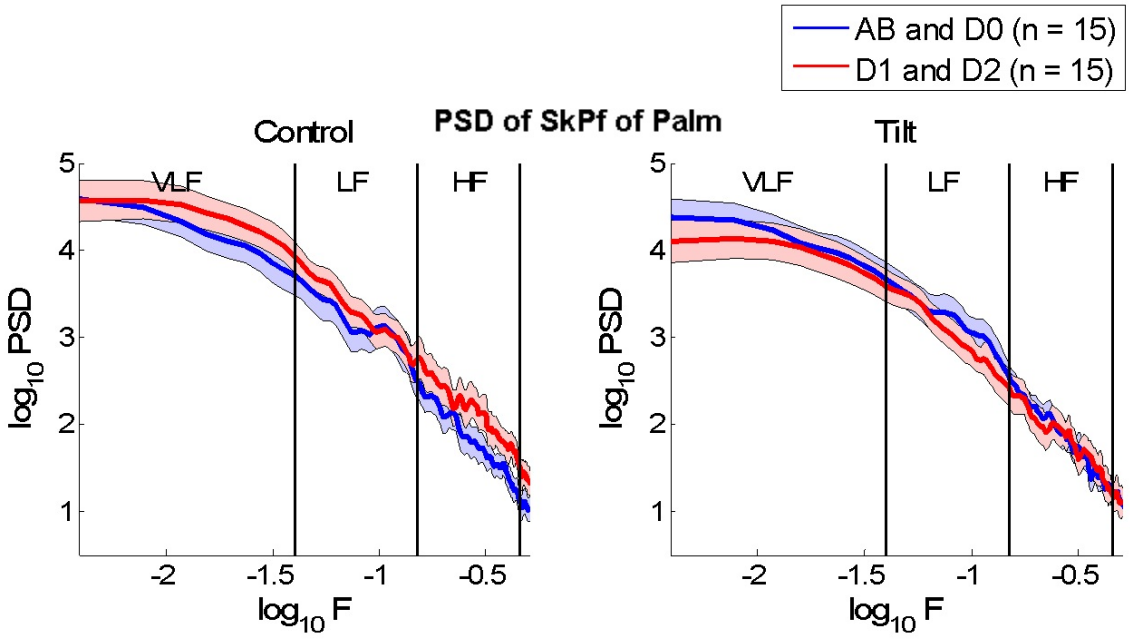

Figure 1.13 Average ± SEM logarithm of power spectral density of skin perfusion of palm taken from10 min supine control and the first 10 min of head-up tilt.

1.4.3 Coherences

Coherences between skin perfusion of the forearm and SBP during 10 min supine control and 10 min tilt for non-neuropathy and neuropathy groups are shown in Figure 1.14. At control, coherences between skin perfusion and SBP in the low frequency region were significant in the non-neuropathy group and were at the borderline of significance in the neuropathy group. In response to tilt, coherences in the low frequency region increased in the non-neuropathy group but decreased in the neuropathy group. At respiratory frequencies, coherences were significant in the neuropathy group in control and tilt. In the non-neuropathy group, coherences at respiratory frequencies were not significant during control, but approached significance during tilt. The responses were similar in the coherence between skin perfusion of forearm and DBP (Figure 1.15).

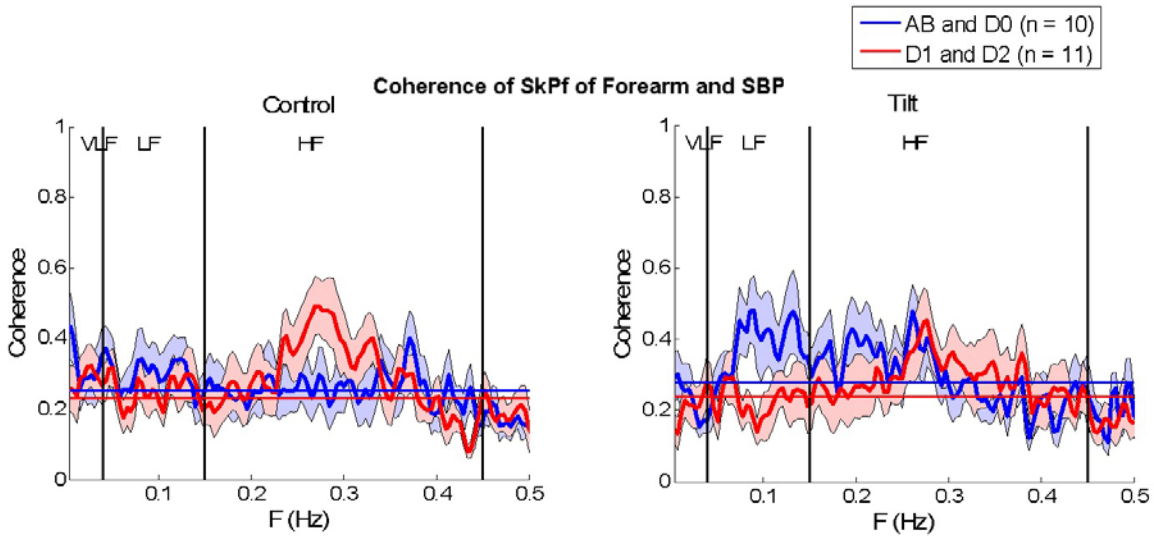

Figure 1.14 Average ± SEM coherence of skin perfusion of forearm and systolic blood pressure during 10 min supine control and the first 10 min of head-up tilt. Horizontal lines: 95% confidence level of non-zero coherence.

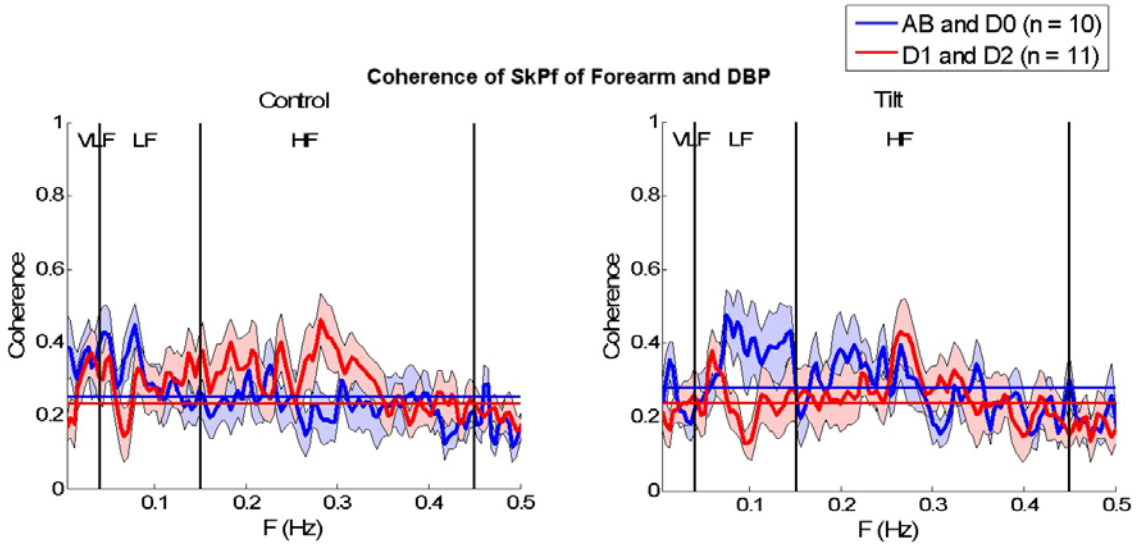

Figure 1.15 Average ± SEM coherence of skin perfusion of forearm and diastolic blood pressure during 10 min supine control and the first 10 min of head-up tilt. Horizontal lines: 95% confidence level of non-zero coherence.

The LF coherence between skin perfusion of the palm and SBP was not significant during supine control in both groups, but increased during tilt in the

non-neuropathy group. The LF coherence did not change in the neuropathy group (Figure 1.16). At respiratory frequencies, coherences were significant in the neuropathy group in control and tilt. In the non-neuropathy group, coherences at respiratory frequencies were not significant during control, but approached significance during tilt. The responses were similar in the coherence between skin perfusion of palm and DBP (Figure 1.17).

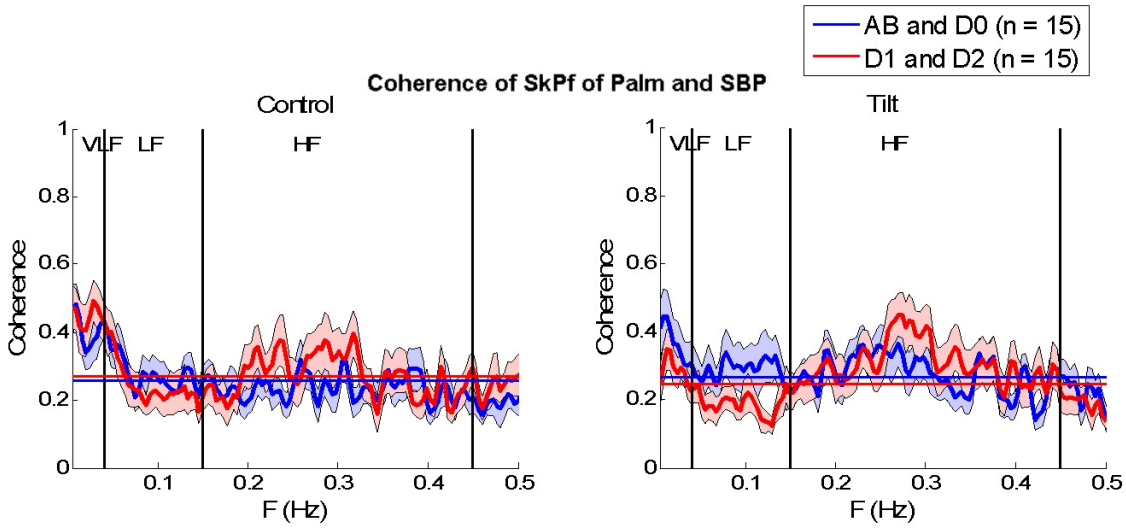

Figure 1.16 Average ± SEM coherence of skin perfusion of palm and systolic blood pressure during 10 min supine control and the first 10 min of head-up tilt. Horizontal lines: 95% confidence level of non-zero coherence.

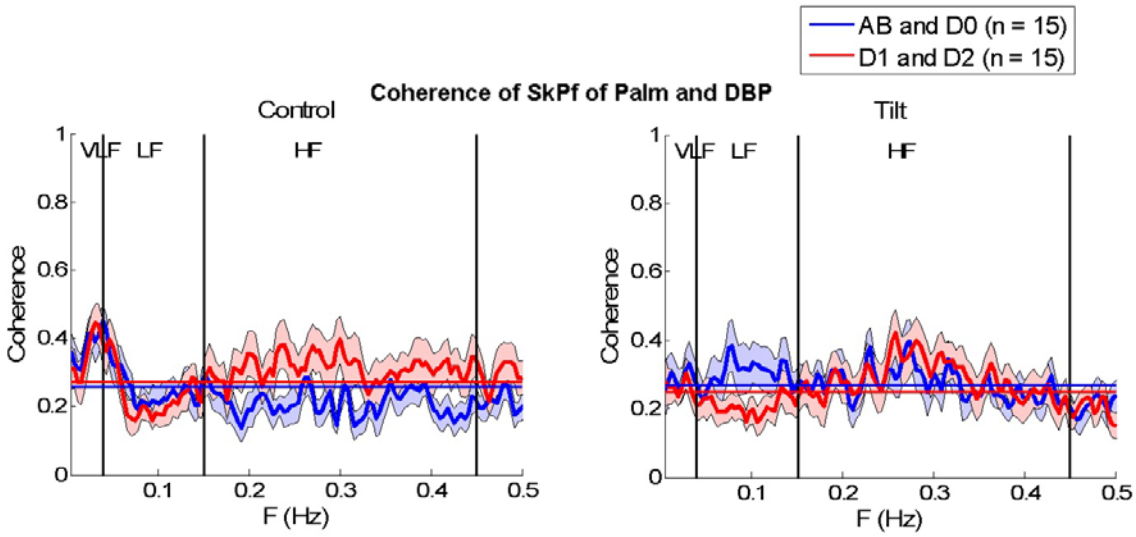

Figure 1.17 Average ± SEM coherence of skin perfusion of palm and diastolic blood pressure during 10 min supine control and the first 10 min of head-up tilt. Horizontal lines: 95% confidence level of non-zero coherence.

1.4.4 Baroreflex Sequences

Figure 1.18 provides the normalized number of SBP ramps (A), normalized number of baroreflex sequences (B), baroreflex effectiveness index (BEI; C), baroreflex slope (D) and high frequency spectral power of systolic blood pressure (HFSBP; E) for each of the four groups. In supine control, both diabetics with possible, and those with definite, neuropathy had greater numbers of SBP ramps than did able-bodied subjects (Figure 1.18A). During head-up tilt, diabetics with definite neuropathy also had more SBP ramps than did diabetics without neuropathy during all three time segments, most clearly illustrated at 7-12 min of tilt. However, diabetics with definite neuropathy had a significantly smaller number of baroreflex sequences than did able-bodied subjects and diabetics without neuropathy (group main effect; Figure 1.18B). As a result, BEI values for diabetics with possible, and for those with definite, neuropathy were significantly lower than those for able-bodied subjects and diabetics without neuropathy during head-up tilt (Figure 1.18C). One able-bodied subject had BEI residuals larger than 2 standard deviations at all time segments. When this subject's data were excluded from the analysis, the group x time interaction became significant.

Other factors remained significant with or without exclusion of this subject, with no effect on the direction of the results. In addition, baroreflex slope significantly decreased in all groups in response to head-up tilt (Figure 1.18D). Diabetics with possible neuropathy had significantly lower baroreflex slopes than able-bodied subjects, and diabetics with definite neuropathy had significantly lower slopes than both able-bodied subjects and diabetics without neuropathy (group main effect). Finally, the diminution of baroreflex activity to buffer breathing frequency blood pressure oscillations in diabetics with definite neuropathy is illustrated in Figure 1.18E indicating a four fold greater magnitude of HFSBP oscillations in those subjects compared to the other groups (similar to the results illustrated in Figure 1.9 A and B).

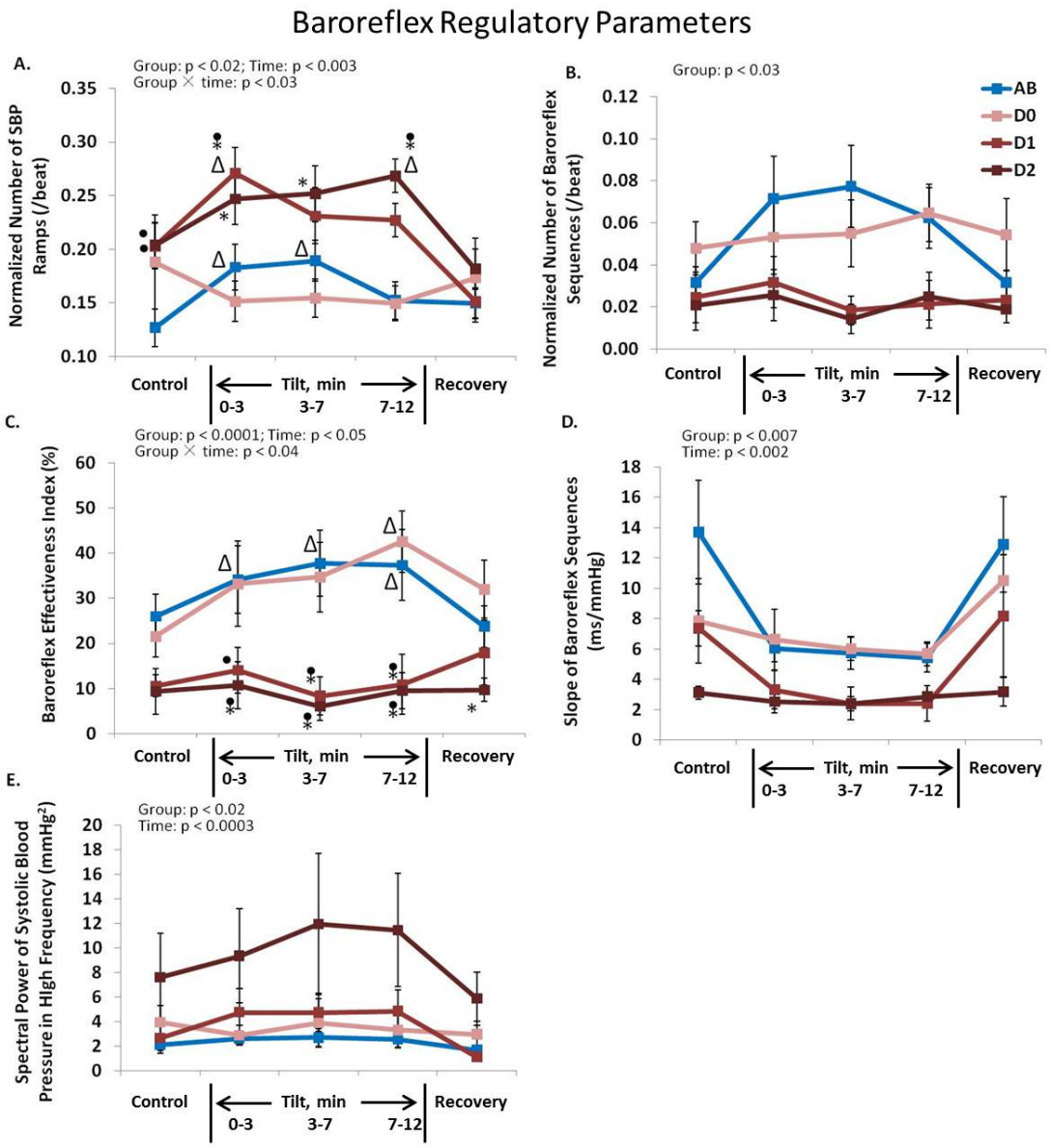

Figure 1.18 Baroreflex regulation: Average ± SEM normalized number of SBP ramps (A), normalized number of baroreflex sequences (B), baroreflex effectiveness index (C), baroreflex slope (D), and high frequency spectral power of SBP (E) for AB (n = 11), D0 (n=6), D1 (n=5) and D2 (n=8) at rest and in response to head-up tilt. Δ, significantly different from control (same group); •, significantly different from AB (same time segment); *, significantly different from D0 (same time segment).

1.4.5 Gender

Because of known gender differences in autonomic regulation of heart rate (parasympathetic dominance in high frequency power of heart rate in women compared to men) and peripheral vasculature (sympathetic dominance in control of vascular regulation in men) (7, 37, 52, 80), we examined heart rate, blood pressure and baroreflex variables for gender differences. The results of these analyses indicated that, for these groups, gender effects were obscured by effects of diabetes (data not shown).

1.4.6 Arterial Pulse Transit Time (PTT)

Arterial PTT was not significantly different among the four groups in supine or during the second minute of tilt, nor the tilt-induced increases of PTT were significantly different among the four groups.

1.5 Chapter Five: Discussion

1.5.1 Mean Values of Blood Pressure and RR Interval

The inability of diabetics to increase, or even maintain, blood pressure during tilt (Figure 1.2), indicated that sympathetic pathways to cardiovascular effectors were impaired in diabetics with peripheral neuropathy compared to able-bodied subjects. In healthy humans, orthostatic stress induces vasoconstriction at the arteriolar level, which increases absorption of fluid into the plasma. The drop of blood pressure in diabetic patients with definite neuropathy, and the lack of increase of blood pressure in diabetic patients without or with mild neuropathy during the first three minutes of tilt, may reflect impairment of normal orthostatic vasoconstriction (109). Moreover, the importance of the baroreflex in regulating blood pressure over longer time periods is illustrated in the very low frequency region of Figure 1.9. These results also support the comment made by many of the patients that they had learned to move slowly into the upright position and if they move slowly they are okay. The slow speed (approximately 38 seconds to move from supine to 70 degrees head up) of our tilt was probably responsible for the fact that presyncopal symptoms were relatively rare in our diabetic subjects.

1.5.2 Mean Values of Skin Perfusion

In all subjects, the skin perfusion of the palm was higher than that of the forearm as expected (62), an effect related to the presence of arteriovenous anastomoses in the microcirculation of the non-hairy skin (79). A higher evaporation rate from the skin of the palm of hand than that from the forearm at a thermoneutral environment has also been reported (57).

In the current study, in response to head-up tilt, the skin perfusion of the forearm decreased in the subjects without neuropathy, as expected (4, 62, 84, 109, 111, 117). The neuropathy group had similar responses to head-up tilt compared to the non-neuropathy group, indicating a normal reflex adrenergic control of cutaneous vasoconstriction, or the withdrawal of cholinergic control of

vasodilation in the forearm, in the neuropathy group (58). However, the neuropathy group tended to have a greater skin perfusion of the forearm at all time segments. This was probably due to a larger number of male subjects in this group compared to the non-neuropathy group, since men tended to have higher skin perfusion than did women in both groups as shown in Figure 1.4.

In the palm, the mean skin perfusion in the non-neuropathy group did not change during the first 3 min of head-up tilt (Figure 1.1), supporting the absence of vasoconstriction in the hand during orthostasis (109). It was also reported that direct baroreflex stimulations on carotid sinus nerve did not have discernible effect on the outflow of the skin sympathetic nerve (134). In the present study, the unchanged skin perfusion of the palm during the first 3 min of head-up tilt may be due to a lack of increase in sympathetic outflow during orthostasis. After the first 3 min of head-up tilt, skin perfusion of the palm increased in the non-neuropathy group (**Error! Reference source not found.**, Figure 1.6). We interpret this increase to be due to an increase of core temperature, previously observed in both men and women during graded head-up tilt to 60 degrees (84). Therefore, vasoconstriction of hairy skin during head-up tilt (Figure 1.3) appears to be acting to prevent heat loss (109). If core temperature increases, as a result of hairy skin vasoconstriction to preserve blood pressure, the vasomotor drive to AVAs from the hypothalamus could be reduced and thereby provide a mechanism to shunt blood to the skin for cooling through AVA dilation, increasing blood flow and allowing heat dissipation (109). This hypothesis is consistent with our observations from the non-neuropathy group. Alternatively, or in addition to prevention of heat loss, metabolic rate has been shown to rise during head up tilt (20).

Johnson et al. (65) have shown that adrenergic blockade by bretylium increased baseline palmar skin blood flow. In patients with familial dysautonomia, baseline skin blood flow at finger pulp tended to be higher than that in healthy subjects (121). This study also reported that sinusoidal neck suction at 0.1 Hz caused reduction in skin blood flow at finger pulp in healthy control subjects,

while the reduction of pulpar finger blood flow was much smaller in patients with familial dysautonomia (121). In our study, elevated control values of palmar skin perfusion in the neuropathy group, compared to the non-neuropathy group, may reflect impaired tonic sympathetic control of vasoconstriction of palmar skin in patients with neuropathy. During head-up tilt, the different palmar skin perfusion responses between the two groups appears to indicate an abnormal function of heat dissipation via opening AVAs in the neuropathy group. It is known that palmar skin lacks active vasodilation (65). In our study, the absence of tilt-induced increase of skin perfusion of the palm in the neuropathy group suggested a loss of tonic vasoconstriction at rest and an impaired ability to increase blood flow by withdrawal of vasoconstriction of the palmar skin.

1.5.3 RR Interval Spectral Power Indexes of Sympathetic and Parasympathetic Control of Heart Rate

The magnitude of the RR interval harmonic component at respiratory frequencies (HFRRI) is a marker of vagal control of the SA-node (101). The rapid decline of HFRRI in response to head-up tilt and rapid recovery of HFRRI when AB subjects were returned to supine (within a minute of the change in posture, Figure 1.8A) supports neural, reflex- mediated modulation of HR at respiratory frequencies in these people. During supine rest and head-up tilt, diabetics with definite neuropathy had lower HFRRI than did able-bodied subjects or diabetics without neuropathy, indicating impaired parasympathetic control of HR in diabetics with signs of peripheral neuropathy (124). The reduced reserve of parasympathetic control of HR in response to head-up tilt in diabetics with possible or definite neuropathy also confirmed a diminished orthostatic response and progressive loss of parasympathetic control of heart rate with increasing neuropathy (97).

A previous study of sino-aortic denervated (SAD) cats determined that the wide band spectra of pulse interval was significantly lower in SAD cats than that in controls (29). In our study, the decreases of wide band RR interval spectra in diabetics with definite neuropathy may be due to diminished baroreflex function,

or perhaps more specifically, to cardiac parasympathetic neuropathy. Moreover, the LF RRI component was different in diabetics with definite neuropathy: a steeper slope of the 1/f relationship was evident at the LF range of diabetics with definite neuropathy. This 1/f relationship of power spectrum exists in dynamic systems that have multiple control mechanisms with different time constants and the steeper slope of the 1/f relationship suggests a less complex control system (15, 16, 50, 133) in diabetics with definite neuropathy. If so, the complexity of the sympathetic regulation of heart rate in diabetics with definite neuropathy was diminished, possibly reflecting a diminution of sympathetic regulation of the SA node, perhaps secondary to diabetic sympathetic neuropathy. In patients with Chagas disease, which damages autonomic neurons, the slope of the linear part of the log-log plot of PSD RRI was significantly steeper than that of controls, indicating dysautonomia in these patients (27, 107). Therefore, the slope of log-log plot of heart rate power spectral density of resting diabetic subjects calculated from a five-minute measurement appears to be a sensitive discriminator of autonomic neuropathy in the LF region.

1.5.4 Blood Pressure Spectral Power Index of Sympathetic Control of Peripheral Vasculature

Significant coherence between low frequency spectral power of diastolic blood pressure (LFDBP) and muscle sympathetic nerve activity has been reported in able-bodied humans (25). In particular, muscle sympathetic nerve activity increased with head-up tilt and remained elevated during tilt in able-bodied subjects (46). In our study, LFDBP increased in response to tilt and remained high in able-bodied and in diabetic subjects without neuropathy (Figure 1.8B). Conversely, in diabetics with possible, and those with definite, neuropathy, LFDBP did not change indicating that reflex-mediated sympathetic pathways to peripheral vasculature were impaired in diabetics, including those with milder symptoms of neuropathy.

The log-log plot (Figure 1.9A, B) of the power spectral density of systolic blood pressure (PSD SBP) taken during five minutes of supine rest, showed a

significant elevation of harmonic and nonharmonic components of blood pressure variability in the VLF and the HF regions but not in the LF range (presumably because of a loss of the harmonic component) in diabetics with definite neuropathy compared to able bodied subjects. These findings confirm the previously reported reduction of sympathetically mediated harmonic vasomotion in diabetic autonomic neuropathy (32, 144).

1.5.5 Dynamics of Skin Perfusion

The measured skin perfusion using laser Doppler technique is mainly from capillaries and post-capillary venules of the upper horizontal plexus. These vessels exhibit little variation in their diameter and thus have little contribution to the rhythmic change in skin perfusion. Oscillations in skin perfusion are probably related to constriction/dilation of upstream arterioles (23). The origin of the vasomotion of skin blood flow was believed to be a combination of central/neural and local/myogenic mediated mechanisms (119). The known impairment of vasomotion of skin perfusion in diabetics was considered to be due to nerve dysfunction, vascular abnormalities, or both (119). In the current study, the comparison of the dynamics of skin perfusion between diabetics without and those with neuropathy during supine control and head-up tilt in a thermoneutral environment, allowed us to explore neural origins of skin perfusion oscillations and effect of diabetic neuropathy on reflex control of skin perfusion under orthostatic stress.

It was reported that passive change in posture increased the cross-correlation between skin blood flow (volar surface of the forearm) and heart rate, in which the maximum correlation during upright posture was always due to oscillations in the range of 0.1 Hz (10). In the same study, sympathetic blockade reduced the cross-correlation between skin blood flow and heart rate (10). Our study support the influences of central autonomic control on skin blood circulation via demonstrating significant coherence between skin perfusion of the forearm and blood pressure in the LF region in subjects without neuropathy. The LF coherence increased in response to tilt in the subjects without neuropathy, but

decreased in those with neuropathy. This group difference indicated an impaired central autonomic control of skin perfusion in diabetics with neuropathy.

In our study, the group difference in LF power spectral density of skin perfusion of the forearm was not significant during supine control, but became significant during head-up tilt, supporting the reduction of vasomotion in diabetic patients with neuropathy (85). Bernardi et al reported that, when supine, there was a significant difference in the LF skin blood flow oscillations in the forearm between diabetic patients and able-bodied subjects, with the magnitude of oscillations smaller in diabetics (11). However, in our study, the group difference was significant during tilt but not during supine control, which may due to an age difference between our able-bodied subjects and those in the study by Bernardi et al (48 vs. 38 yrs), which had a known effect on the dynamics of skin perfusion (11).

At the respiratory frequencies, the mean PSD of skin perfusion of the forearm was greater in the neuropathy group than in the non-neuropathy group, at supine control. It has been reported that respiratory oscillations is passively transmitted from blood pressure to skin blood flow (9). In our study, the elevated PSD of skin perfusion of forearm at respiratory frequencies in subjects with neuropathy may be due to elevated blood pressure oscillations in these subjects. Bernardi et al have reported that HF PSD of the skin perfusion of the forearm was not different between diabetics and able-bodied subjects (11). This discrepancy of HF PSD of skin perfusion between our and their studies may, again, be due to a difference in age (~10 yrs older in our study) or breathing patterns (spontaneous in our study vs. controlled breathing in that of Bernardi et al). Controlled breathing may have effects on HF PSD of skin perfusion, since controlled breathing reduced cardiac parasympathetic influences (102).

Similar to the skin blood flow of the forearm, in the palmar skin, sympathetic nerve stimulation caused high-power peaks in the palmar skin blood flow oscillations in healthy human, between 0.025 to 0.1 Hz, with the maximum response within 0.075 - 0.1 Hz (120). In our study, the LF coherence between

palmar skin perfusion and blood pressure became significant during head-up tilt confirming a central sympathetic control of skin blood circulation (8, 9). In our diabetics with neuropathy, the tilt-induced increase in LF coherence was not observed, indicating an impaired central sympathetic control of peripheral vasomotion. Significant LF coherences between skin blood flow (volar surface of the finger) and blood pressure during supine was reported (8, 9). However, in our study, the coherence between palmar skin perfusion and blood pressure at LF was not significant during supine control in the non-neuropathy group. This may due to the difference in the age of subjects (26 and 31 yrs in the previous studies vs. 45 yrs in our able-bodied subjects and diabetics without neuropathy), or the difference in the location of skin (finger vs. palm).

In our study, the mean LF power spectral density of palmar skin perfusion in the non-neuropathy group did not increased in response to head-up tilt, in contrast to the standing-induced increase in LF power of skin at fingertip in a previous study (9). This discrepancy may due to the difference in the location of the skin (fingertip vs. palm). The location of the measured skin may also explain the absence of group difference in LF PSD of palmar skin perfusion during supine control in our study, contrary to the reduction of oscillation below 0.1 Hz in skin blood flow at pulpar surface of the index finger, in diabetics with neuropathy (119).

Altered skin blood flow in diabetic patients could interfere with nutrient supply, causing ulcers and gangrene (131). Our diabetic subjects did not demonstrate these symptoms. However, autonomic regulation of skin perfusion was impaired in these subjects. Manifestation of dysfunction in skin perfusion regulation could occur earlier than symptoms of skin diseases in diabetic patients.

1.5.6 Baroreflex

The greater numbers of blood pressure ramps at rest and during tilt in diabetics with definite and suspected autonomic neuropathy (Figure 1.18A), was an unexpected finding of the present study. The combination of increased

numbers of BP ramps with reduced numbers of baroreflex sequences (44, 144), suggests that diabetics with neuropathy experience diminished effectiveness of the baroreflex in driving the sinus node. As is clearly illustrated in Figure 1.18C: BEI was significantly increased compared to supine control in able-bodied subjects during all phases of head-up tilt and in diabetics without neuropathy during 7-12 min of tilt, but remained unchanged in diabetics with possible, or definite, neuropathy. Further, Figure 1.18 clearly illustrates the ability of this measure to differentiate diabetics with neuropathy (definite or possible) from diabetics without neuropathy. Therefore, in our study, BEI was the most sensitive discriminator of neuropathy. Other studies have proposed LF power of SBP (32) as a sensitive discriminator of AN, but for our study, BEI was significantly better at discriminating differences, perhaps because this measure combines loss of sympathetic modulation of vasomotion with loss of parasympathetic control of heart rate into one parameter. Previous studies showed a severe impairment of baroreflex effectiveness in diabetic chronic renal failure patients compared with non-diabetic patients at supine rest (64). However, as far as we can determine, the present study is the first to demonstrate a reduction in baroreflex effectiveness in diabetics with neuropathy, without the simultaneous complication of chronic renal failure.

Baroreflex sequences may reflect physiological activities in a portion of these sequences. Baroreflex effectiveness index was 33% in intact cats and 4% in sinoaortic denervated cats (31). Therefore, in cats, the number of sequences due to physiological mechanisms was 29% of that of SBP ramps. Similarly, in our study, BEI was 26% in healthy subjects, and 9.4% in diabetics with severe neuropathy, during supine control. Therefore, in human, the number of sequences due to physiological mechanisms was 16.6% of that of SBP ramps. In addition, BEI increased in healthy subjects in response to head-up tilt, but did not change in diabetics with neuropathy in our study. Therefore, baroreflex may be engaged in a part of blood pressure regulation if it is measured by using the baroreflex sequences technique. Baroreflex may be important in maintaining homeostasis because the VLF and HF PSD of SBP were four fold higher, while

the VLF, LF and HF PSD of RRI was four fold lower in diabetics with severe neuropathy, compared to able-bodied subjects during supine control. Therefore, BEI may reflect a fast response, while baroreflex is engaged at all frequencies.

Baroreflex sensitivity has been proposed to reflect the strength of the baroreflex when it is effective (31). In our study, all groups demonstrated decreased baroreflex slope in response to head-up tilt (Figure 5D) as expected (67, 95, 96). However during both supine control and head-up tilt, diabetics with definite neuropathy had significantly smaller BRS than did able-bodied subjects and diabetics without neuropathy. During supine rest, diabetics without neuropathy tended to have smaller BRS than able-bodied subjects and larger BRS than diabetics with definite neuropathy. These findings support the widely held notion that diabetes reduces BRS and that reduced BRS is an early sign of AN (44, 104, 144). When we compared our significant reduction of BRS and BEI to the trend towards greater arterial pulse transit time in diabetics with definite neuropathy, we conclude that, for our study, baroreflex impairment was a more sensitive indicator of neuropathy than alterations in arterial stiffness (110).

Increased BP variability has been shown to predict nephropathy and retinopathy (71), and to correlate with endothelial and cardiovascular damage (28, 141) and higher mortality (70). Blood pressure variability, measured by standard deviation over 24 h, has been reported to be significantly higher in diabetic patients (43, 61, 87, 135) and was highest in those with cardiovascular autonomic neuropathy (24). In our study, we further explored the specific frequency ranges of increased BP variability and determined that diabetics with definite neuropathy had significantly higher VLF and HF power spectral density of SBP compared with able-bodied subjects. In addition, in all frequency ranges, our able bodied subjects demonstrated an ability to engage heart rate to buffer SBP fluctuations while diabetics with neuropathy demonstrated a reduced ability.

Arterial baroreflex buffering at respiratory frequencies may be more dominant in older persons. The fact that HF power of SBP was greater in our diabetics with neuropathy than in able-bodied subjects, but has been shown to

be smaller in diabetic children and adolescents than in healthy controls (72), may be a matter of age, but may, more accurately, reflect the presence of neuropathy in our subjects. In addition, in middle-aged to older diabetics, HF power of SBP was reported to be smaller than in able-bodied during conditions of controlled breathing (32). The act of controlling breathing itself, however, may be responsible for this effect since it was previously determined that controlled breathing reduced cardiovascular parasympathetic influence (102).

An important indicator of impaired baroreflex-buffering of BP lies in the four-fold increase in the harmonic and nonharmonic components of VLF power spectral density of SBP in diabetics with definite neuropathy compared with able-bodied subjects (Figure 1.9A, B). Although enhanced VLF SBP has been reported to result from SAD in animals (19, 30), VLF SBP power in humans is believed to reflect renin-angiotensin system activity, endothelial factors and thermoregulation (101). However, in patients with primary autonomic failure, enhanced VLF oscillations of SBP have been documented (97). Our study's enhanced VLF SBP power and decreased VLF RR interval power in diabetics with definite neuropathy, indicated that intact baroreflex function is important for normal BP regulation in the VLF range for both harmonic and nonharmonic components in able-bodied humans. Finally, in our study, VLF SBP was similar between able bodied and diabetics without neuropathy. This phenomenon has been reported previously in children and adolescents with Type 1 diabetes mellitus who have not developed other signs of neuropathy (72). These results suggest that in addition to BEI, increased VLF SBP spectral power may be a strong, early, indicator of diabetic neuropathy.

Our study did not show significantly increased standard deviation of SBP in diabetics with neuropathy. Similar to the finding of Frattola et al.(44), this may be due to the relatively short period of time over which the standard deviation was calculated (3 - 5 min in our study and 15 min in the study by Frattola et al.) compared to the greater standard deviation measured from 24h recordings (24, 43, 61, 87, 135).

At frequencies centered around 0.1 Hz (Figure 4B), the log-log power spectral density curve of SBP of diabetics with definite neuropathy demonstrated a dip, indicating that the loss of the harmonic component at LF (Fig 3B) is apparent in the log-log plot of SBP. This loss of power in the LF region is similar to that previously reported following sino-aortic denervation in animals (29, 132) and total autonomic failure in humans (97). Sympathetic nerve activity (SNA) with a frequency around 0.1 Hz in man is similar to the 0.4 Hz rhythm in rat and, at this frequency, there is a tight coherence in unanesthetized rat between changes in SNA and changes in arterial BP (14). We conclude that the dip in oscillations of SBP in the LF region of diabetics with definite neuropathy is consistent with effects of neuropathy on sympathetically mediated vasomotion. This change is exposed by the corresponding loss of parasympathetically (baroreflex) -driven changes in heart rate in subjects with definite neuropathy. In addition, altered BP and RR interval power spectral densities over the range of frequencies between 0.003 and 0.45 Hz in diabetics with neuropathy indicate that an intact baroreflex is an important component of healthy human BP regulation at all frequencies. Each of these measures is relatively easy to determine from a short (five minute) recording of continuous blood pressure and heart rate from resting subjects.

1.5.7 Limitations

The time of onset, the prevalence and the development of diabetic neuropathy, and treatment effects have been reported to be different between Type 1 and Type 2 diabetes (130, 142). Because of our limited number of subjects, diabetic patients were not separated based on the type of diabetes. Therefore the relative ability of our indices of autonomic dysfunction to identify autonomic neuropathy in Type 1 vs. Type 2 diabetes is unknown. Direct measures of sympathetic autonomic function (like MIBG SPECT imaging) were not performed, thus comparisons between direct measures and our indices are not available. Again, because of the limited numbers of subjects in each group, we were not able to establish age effects on the autonomic indices we report. The D0 group was younger than the D2 group; however, major differences in this

study lay between AB and D2 groups where there was no meaningful difference in age. Greater numbers of subjects would be required to establish significant interactions of study variables with gender and age.

The rate of presyncope (5 of 11) in the able-bodied subjects of the present study was similar to the able-bodied subjects that have reported by our lab in the past (78). In that study, 8 of 16 controls had symptoms within 30 minutes of head-up tilt. In another recent study of subjects who underwent 70-degree head-up tilt, 56% (9 of 16) had presyncopal symptoms during the 30 min tilt (36). Results from a third study of head-up tilt-mediated presyncope in healthy humans suggested that unexplained syncope was a result of altered cardiorespiratory interaction involving cerebral hemodynamics but with a normal neural control system (73). Similar to our results, other investigators have determined that the initial response to head-up tilt was similar between patients with vasovagal syncope and nonsyncopal subjects, and sympathetic nerve activity withdrawal did not occur until symptoms began (88). We do not believe that the incidence of presyncopal events in the AB subjects is remarkable, nor does it call into question any aspect of the interpretation of our findings.

Finally, abnormal findings in the battery of Ewing tests have been reported in 13% of the normal population (99). In our study, two able-bodied subjects with tingling of hands and/or feet were found to be free of peripheral neuropathy by standard clinical tests. Both subjects, however, decreased their BEI to near 0% in response to tilt while other able-bodied subjects increased or maintained their BEI at greater than 10%. In the group of diabetics with definite neuropathy, 6 of 8 subjects had BEI smaller than 10%. The similar behavior of the two able-bodied subjects to the behavior of the six diabetics with definite peripheral neuropathy suggests that BEI during tilt may be an index of autonomic neuropathy that is more sensitive, and/or more selective for autonomic involvement than are standard sensory/motor neuropathy findings. Also for other variables, when we removed these two subjects from the able-bodied group, the statistical significance of the group differences reported here were dramatically

increased, but without a physiological reason to remove them, the results reported here include these subjects with the able-bodied group.

1.6 Chapter Six: Conclusions

The much reduced ability to regulate blood pressure, characterized by decreased RRI buffering of an increased number of SBP ramps, the four-fold increases in VLF and HF SBP power spectral densities and the four-fold decrease in VLF, LF and HF RR interval power spectral densities indicated serious deficits in maintenance of cardiovascular homeostasis in diabetics with neuropathy. The major contributor to this loss of blood pressure regulation appeared to be the combination of a loss of sympathetically mediated control of vasomotion, with a reduced contribution from parasympathetically mediated responses of heart rate to buffer these changes in blood pressure. Our results indicate that preservation of baroreflex function needs to become a focus of diabetic neuropathy treatment. The present study also indicates that, in healthy subjects, baroreflex function is an important component of blood pressure regulation in all (very low, low and high) frequency regions and pertains to both self-similar as well as harmonic components. In addition, sympathetic control of skin perfusion was impaired in diabetic patients with neuropathy, which manifested earlier than signs of skin diseases. Finally, the results of our study indicate that noninvasive indexes of autonomic regulation were able to discriminate diabetics with autonomic neuropathy from subjects with reduced, or no, neuropathic damage.

1.7 Chapter Seven: Future Work

The measurement of plasma volume and hormone levels from blood samples, as well as stroke volume from bio-impedance will give further indication of blood pressure regulation by fluid shift, hormones and cardiac function. In addition, phase analysis of the time relationship between oscillations of skin perfusion and blood pressure will provide further information on mechanisms of reflex control of skin blood flow. These data are available for analysis and therefore will be included in the next manuscript which will be focused on group differences in distribution of blood flow and hormonal responses during the orthostatic stress.

In order to compare our noninvasive indexes with standard tests, comparisons to Ewing tests and MIBG-SPECT image need to be made to correlate these indexes with current clinical diagnoses of autonomic neuropathy and the gold standard method of detection of autonomic neuropathy to the myocardium. These comparisons have been, and will be, the topic of proposals submitted to extramural funding agencies.

Part 2. Four-dimensional multiscale model of ECG indexes of diabetics with autonomic neuropathy

2.1 Chapter One: Introduction

Prolongation of heart-rate corrected QT (QTc) interval of the ECG is well known in diabetic patients with autonomic neuropathy, and is correlated with the extent of autonomic neuropathy (51, 69, 83, 100, 125). Prolongation of QTc is associated with the risk of dying unexpectedly in diabetic patients with autonomic neuropathy (38) , and predicts long-term cardiac death in patients with non-insulin dependent diabetes mellitus (17, 81, 90, 106), and insulin dependent diabetes mellitus (108, 127). However, the mechanism of QTc prolongation in diabetic patients with autonomic neuropathy is still unknown. QTc interval prolongation does reflect an alteration of myocardial repolarization (137). Direct comparison of maximal QTc interval and global or visual defects in patterns of myocardial MIBG uptake in diabetic patients demonstrated a relationship between QTc interval and regional cardiac sympathetic denervation (74). The aims of this part of the study are to 1) verify that the QT interval prolongation in our diabetic patients were similar to the prolongation reported in previous studies and 2) link QT interval prolongation to regional cardiac sympathetic denervation, at the cellular level using a computer heart-torso model.

2.2 Chapter Two: Background

2.2.1 Cellular Basis of Autonomic Control of Ventricular Repolarization

Sympathetic stimulation increases the contractility and rate of relaxation of the heart (79). In normal heart ventricles, postganglionic sympathetic fibers release the neurotransmitter norepinephrine which binds to β-adrenergic receptor on the cell membrane of myocytes. One subtype of β-adrenergic receptor, the β_1-receptor dominates in ventricular myocytes (79). β_1-receptor stimulation activates the cAMP-dependent PKA pathway, resulting in an increase in L-type calcium current through $C_{av}1.2$ channels and a faster rate of closure of the channels through negative feedback (145). In addition, β_1-receptor stimulation augments potassium current through the slowly activating, delayed-rectifier, potassium channel. This activation results in the shortening of cardiac action potential in order to maintain adequate diastolic filling between beats, in the face of an increase in heart rate that occurs upon sympathetic nerve stimulation (145). Finally, sympathetic signaling modulates the rapidly activating, delayed-rectifier, potassium channel in a highly complex manner, resulting in opposite effects on current amplitude (145).

Sympathetic denervation by β-blockers exerts opposite effects on repolarization of cardiac myocytes. For example, administration of β-blockers such as atenolol and sotalol caused action potential duration (APD) prolongation (66, 103), while esmolol caused APD shortening by inhibiting L-type calcium current (40). Similarly, sympathetic denervation by stellate ganglionectomy (dogs) or phenol (rabbits) resulted in prolongation of repolarization (139, 140) , while bilateral sympathetic ganglionegtomy resulted in shortening of APD in a study of rats (136).

2.2.2 Autonomic Innervation of Ventricles

Sympathetic stimulation improves synchrony of excitation and contraction (3). Stimulation of individual cardiac nerve induces highly localized and differential changes in automatic, conductile and contractile function (3). For

example, right stellate ganglionectomy in dogs resulted in larger prolongation of functional refractory period at the anterior surface of the heart than at the posterior surface, while additional left stellate ganglionectomy resulted in larger prolongation of functional refractory period at the posterior surface than at the anterior surface (139). In addition, a single sympathetic nerve modulates finer myocardial segment. For example, electrical excitation of distal ventrolateral cardiac nerve induces increased contraction of posterior papillary muscle without noticeable alteration in the anterior papillary muscle of the same ventricle (3); comparable stimulation of ventromedial cardiac nerve increases anterior papillary muscle contraction without affecting the posterior muscle (3).

Distribution of sympathetic nerves in epicardium, endocardium and midmyocardium of animal heart has been reported (26). Percentage stained area of tyrosine hydroxylase- and neuropeptide Y-immunoreactive nerves (sympathetic nerves) are largest in epicardium, smaller in endocardium and smallest in midmyocardium (26).

2.2.3 Cardiac Autonomic Dysfunction in Diabetes

Direct measure of cardiac sympathetic innervation can be performed by MIBG-SPECT and HED-PET imaging (54, 63). The measures of cardiac autonomic neuropathy by MIBG-SPECT and HED-PET (122) have revealed inhomogeneous sympathetic innvervation of the left ventricle in diabetic patients (22, 56, 91, 92, 113-116). Low uptake of tracer has been observed in the posterior, inferior, or dorso-septal areas of the left ventricle in diabetic patients. The region with low uptake of MIBG extended to other areas in patients with autonomic neuropathy. A recent study, using MIBG-SPECT imaging, showed that in patients with innervation defects, 46% of the innervation defects were located at the inferior region, 18% were located at more than one region, 16% showed diffuse diminished uptake, 14% were located at the apex and 6% were located at the anterior region (115). Proximal hyperinnervation complicating distal denervation in diabetic patients with normal myocardial perfusion has also been reported (123).

2.2.4 Previous Simulation Studies

The forward problem and inverse problem of electrocardiography have been the focus of simulation studies attempting to locate the site of abnormal electrical activity of the heart in patients with myocardial infarction (41), Wolff-Parkinson-White syndrome (48), long-QT syndrome (68) and bundle branch block (2). The forward problem estimates the body surface potential from an equivalent source of cardiac electrical activity while the inverse problem approximates the electrical properties of the heart from measured body surface potential (53). The relationship between increases in QTc interval and the extent of diabetic autonomic neuropathy, diagnosed by clinical methods, implies that the change in ventricular repolarization of myocardium may be a result of alterations in cardiac innervation. To our knowledge, this study is the first to describe possible mechanisms of QTc interval prolongation in diabetics with autonomic neuropathy by using *a priori* changes in membrane potentials at the cellular level directly to predict changes in body surface potentials. This study aims to link the QT interval prolongation observed in diabetic patients with autonomic neuropathy to the patterns of regional cardiac sympathetic denervation.

2.3 Chapter Three: Methods

2.3.1 Experimental Study

2.3.1.1 Subjects

The subjects of this part of study were the same as in Part 1, which consisted of 12 able-bodied subjects, 7 diabetics without neuropathy, 7 with mild neuropathy and 8 with severe neuropathy.

2.3.1.2 Data acquisition

Twelve-lead ECG was acquired from supine subjects breathing at15 breaths/min. Data acquisition of 12-lead ECG lasted for approximately 5 min or until at least 256 heart beats were recorded for signal averaging.

2.3.1.3 Signal Preprocessing

Before performing QT interval measurement, ECG signals were processed to remove baseline wander (< 1Hz), power line noise (~60 Hz) and muscle noise for accurate characteristic wave detection (1). Baseline wander and power line noise were removed by two digital filters, a highpass and a lowpass filter, designed to meet American Heart Association (AHA) recommendations for minimizing distortion: amplitude response should be flat to within 6% (0.5 dB) over a range of 1.0-30 Hz; the 3 dB points should be less than or equal to 0.67 Hz (6). A butterworth filter is known to have a flat response at pass band and was therefore applied in this study. The MATLAB command ‘buttord’ was used to determine the order and cutoff frequency with these specifications. A highpass filter with 3 dB point at 0.67 Hz, and 60 dB point at 0.025 Hz, required a minimum order of 3, rendering the response at 1 Hz to be -0.38 dB. A lowpass filter with 3 dB point of 40 Hz, and 60 dB point of 250 Hz, required a minimum order of 4, rendering the response at 30 Hz to be -0.41dB. Then, filter coefficients were generated by using the MATLAB command ‘butter’, and signals were filtered forward and then backward to give a response with zero phase shift, by using the MATLAB command ‘filtfilt’.

After filtering, ECG waveforms of multiple beats were coherently averaged to remove muscle noise in the signal and improve signal-to-noise ratio (1, 76). Before averaging, the R peak of each beat was determined by setting a magnitude threshold manually, from which RR intervals (RRI) were calculated. Only beats having an RRI with the difference from the mean RRI less than 10%, were accepted for averaging (76). Segments which started 400 msec before the R peak and ended at the end of the P wave of the next beat (accepted beats) were aligned at the R peak, summed point by point, and then divided by the number of beats. QT interval was measured from the averaged waveform in each lead.

2.3.1.4 QT Interval Measurement

QT interval was measured by observing the signal and clicking in the graph of the signal at the Q wave onset and T wave end (Figure 2.1). The measurement was done without knowing the classification of subjects. The Q wave beginning was determined at the first deflection from baseline after the P wave. The T wave end was determined at the time when the signal went back to the TP baseline. If the T wave went asymptotically to the baseline, then the T wave end was determined as the intercept of the slope of the fastest decreasing segment of the T wave and the TP baseline. If a T wave was followed by a U wave, the T wave end was taken as the nadir between the T wave and the U wave. Merging of T wave with U/P wave, low T wave amplitude and various T wave morphologies have been reported to cause measurement error (82). If any of these features was present, the measurement was abandoned for that lead. Seventeen subjects had 1~3 leads abandoned. QT interval was not measured for one subject because of the presence of these features in most leads. QT interval was averaged from three measurements at different times. The heart rate corrected QT interval (QTc) was computed with Bazett's equation

$$corrected\ QT\ interval\ (QTc) = \frac{QT\ interval}{\sqrt{RR\ interval}}$$

Maximum and minimum QTc of all leads were determined from the 12 leads. Minimum QTc of inferior leads (leads II, III and aVF), septal leads (leads V1 and V2), anterior leads (leads V3 and V4) and lateral leads (leads I, aVL, V5 and V6) were also determined (94).

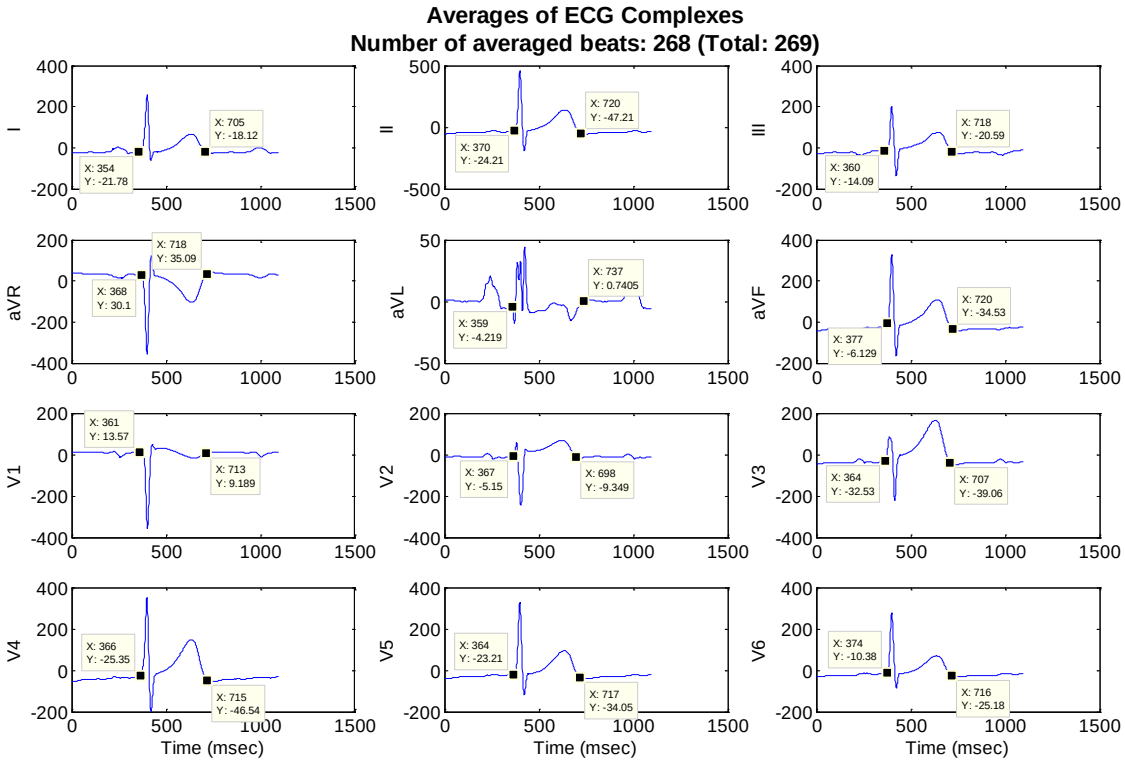

Figure 2.1 Typical averaged ECG complexes and manual QT interval measurement.

2.3.2 Simulation Study

2.3.2.1 Structure of Ventricles

The geometry of the ventricles was constructed by forming 90 cross-sections along planes perpendicular to the base to apex axis. Each cross-section contained a ring with 9 concentric circles with different radiuses, constructing the transmural layers of left ventricle, and 3 concentric partial circles with different radiuses, constructing the transmural layers of right ventricle. This was done by the following steps:

1) Construct a 90mm*60mm*90mm cubic consisting of a rectangular grid of discrete points with 1mm distance between points.

2) Determine the centers of the circles of left ventricle at all cross-sections, which was a vertically straight line consisting of points with the same x and y coordinates at all cross-sections.

3) Determine the radiuses of the circles of the left ventricle of all cross-sections, which was determined by an ellipse equation representing the curved shape of the ventricular walls.

4) Recruit elements in the cubic, one cross-section by one cross-section, and one transmural layer by one transmural layer, with every transmural layer determined by their distances to the center of the circles. An ID of the transmural layer was assigned to every element ranging from 1 to 9 (Figure 2.2).

5) Determine the centers of partial circles of right ventricles as points along the right side of the septum. Because the centers of right ventricle formed a curve, the lateral wall of right ventricle was more curved than that of the left ventricle.

6) Determine the radiuses of the partial circles of the right ventricle, one cross-section by one cross-section, which decreased from base to apex, according to an ellipse equation.

7) Recruit the elements in the cubic to form the right ventricle, one cross-section by one cross-section, and one transmural layer by one transmural layer, with every transmural layer determined by their distances to the center of the partial circles, which are equal to the radiuses. An ID of each transmural layer was assigned to every elements ranging from 1 to 3 (Figure 2.2).

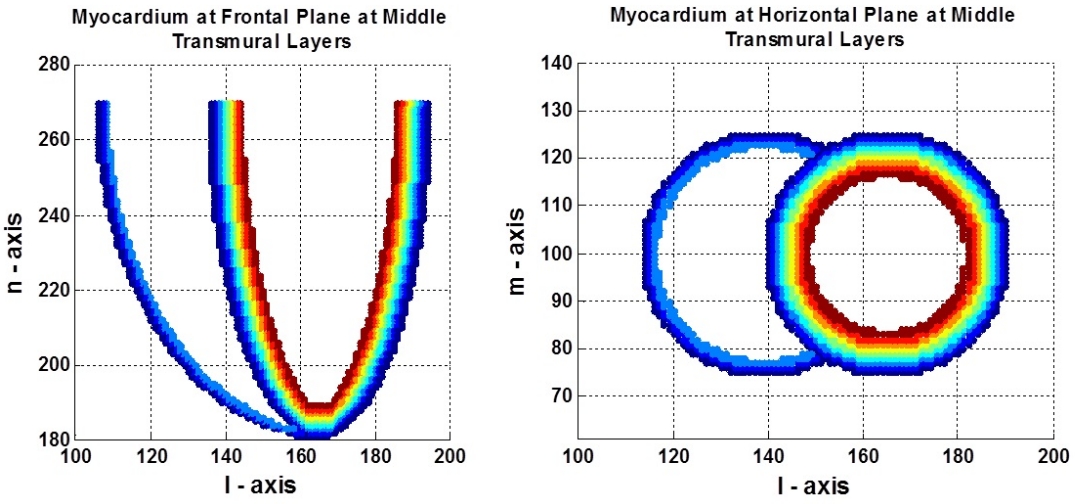

Figure 2.2 Transmural layers of left and right ventricles, from endocardium to epicardium.

8) In addition to the ID of transmural layers, the ID of endo-, mid- or epi-myocardium was also assigned (Figure 2.3).

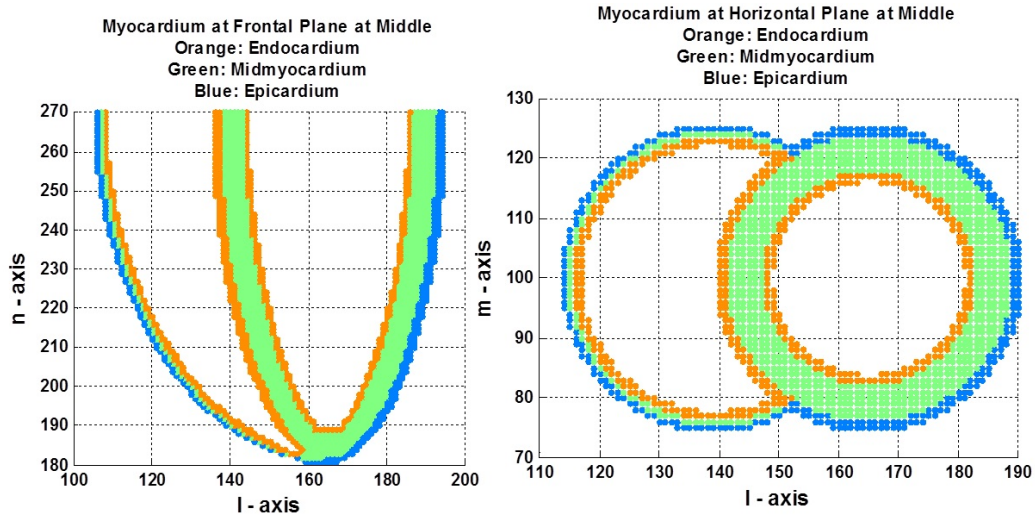

Figure 2.3 Determination of endocardium (orange), midmyocardium (green) and epicardium (blue).

9) A region ID was also assigned to every element (Figure 2.4). The regions were divided according to the polar map of the left ventricle in MIBG-SPECT imaging (55): apical, distal/basal anterior, distal/basal inferior, distal/basal septal and distal/basal lateral regions.

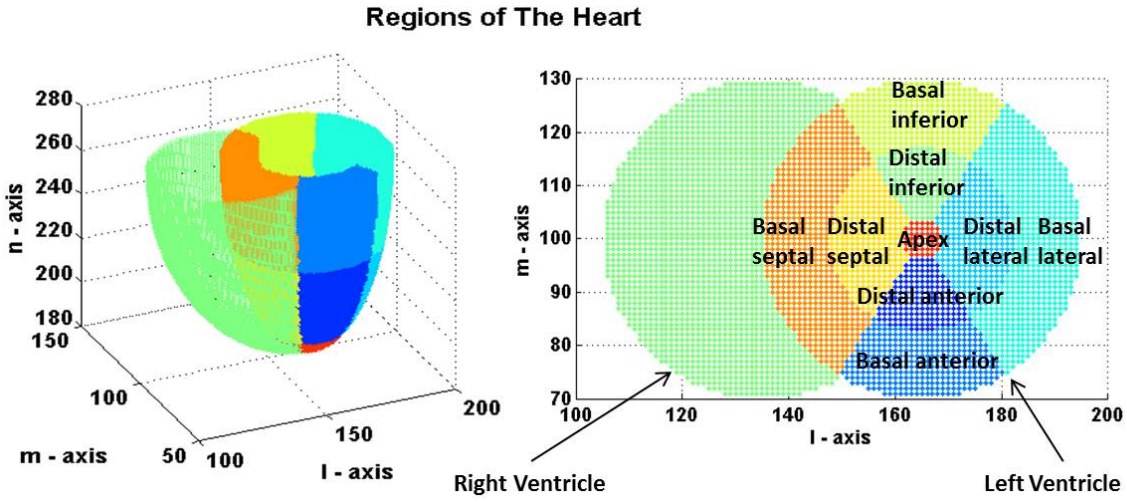

Figure 2.4 Division of the regions of left ventricle (3D view, left; top view, right).

These resulted in a three-dimensional array of 129,826 points representing the ventricles of the heart. The construction of the model and following simulations were performed in MATLAB.

2.3.2.2 Normal Electrical Activity of Heart – Activation Sequence

Production of Normal Activation. Clinical endocardial excitation map of human left ventricle showed that the site with the earliest excitation of the left ventricle was located in an area between the middle and anterior septum near the apex (personal communication with Dr. Morales). Therefore, at the left side of the septum, one point between middle and anterior area near the apex was assigned with the earliest activation time (Figure 2.5). In the right ventricle, two points at the free wall and the septum near the apex were assigned an activation time 5 msec later than that of the left ventricle, as indicated by the activation sequence of an isolated human heart (33).

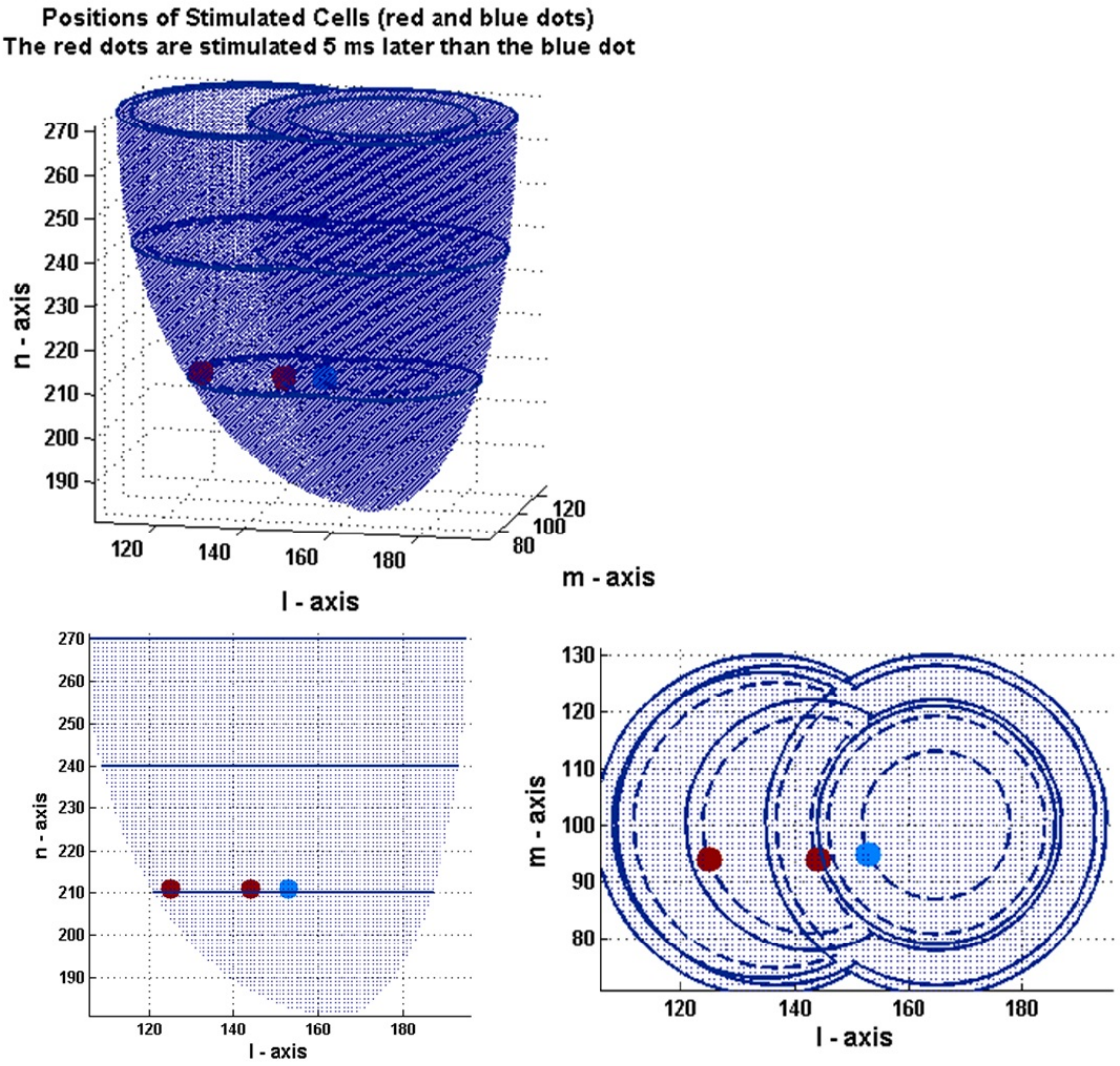

Figure 2.5 Production of normal electrical activities of left and right ventricles (3D view, top; front view, bottom left; top view, bottom right).

Electrical Excitation Propagations to Six Nearest Neighbors. When one element was activated, the excitation propagated to its six nearest neighbors at the next time step or in the next few time steps, according to the conduction velocity. With 1mm distance between elements and the largest conduction velocity of 4 m/s, the smallest time step was set to be 0.25 msec. The activation propagation to neighbors was delayed in regions with a slower conduction velocity. The transmural velocity ranged from 0.222 m/s to 0.45 m/s (33). The

slowest transmural velocity speed was at the septum, and the transmural velocity increased gradually from 0.25 m/s, at the apex, to 0.45 m/s, at the base of the free walls. This difference in velocity was adopted from the excitation isochrone of the isolated human heart, in which transmural velocity was slower in the area where excitation occurred earlier (33). Therefore, in this model, the transmural velocity described above was assigned to make the earlier excitation area have slower transmural velocity. Faster conduction velocities were assigned to endocardia to simulate the Purkinje network. As shown in Figure 2.6, the endocardia had a fast conduction velocity 4 m/s in a fan pattern, and other endocardia between the lines of the fan had conduction velocity of 2 m/s. This arrangement of conduction velocity between endocardial cells led the propagation of excitation from apex to base.

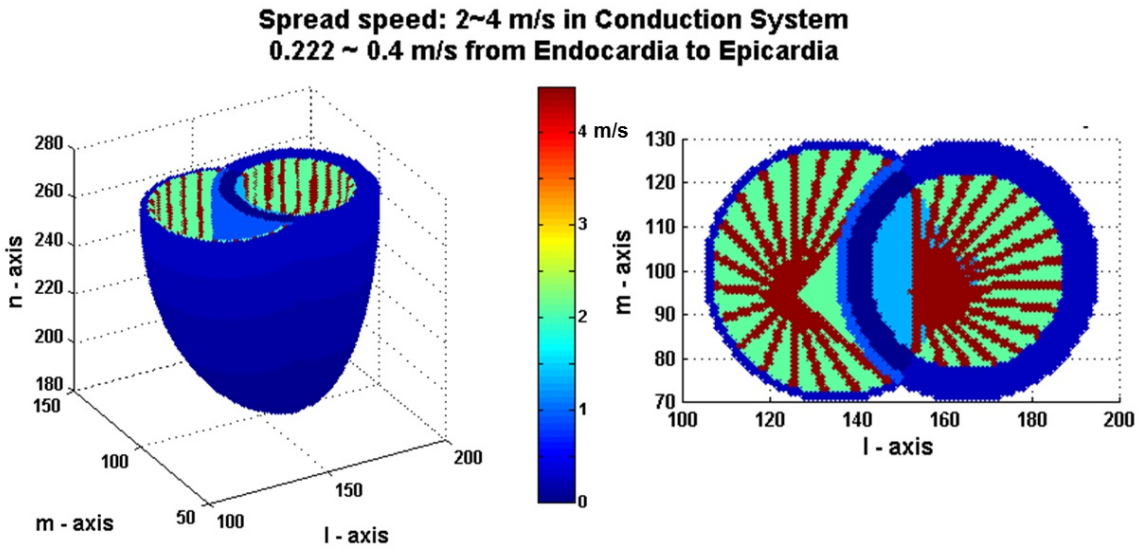

Figure 2.6 Propagation speed of electrical activation to six neighbors (3D view, left; top view, right).

The resultant activation sequence is shown at a series of horizontal cross-sections, a middle-front cross-section (Figure 2.7), endocardial layers and epicardial layers (Figure 2.8).

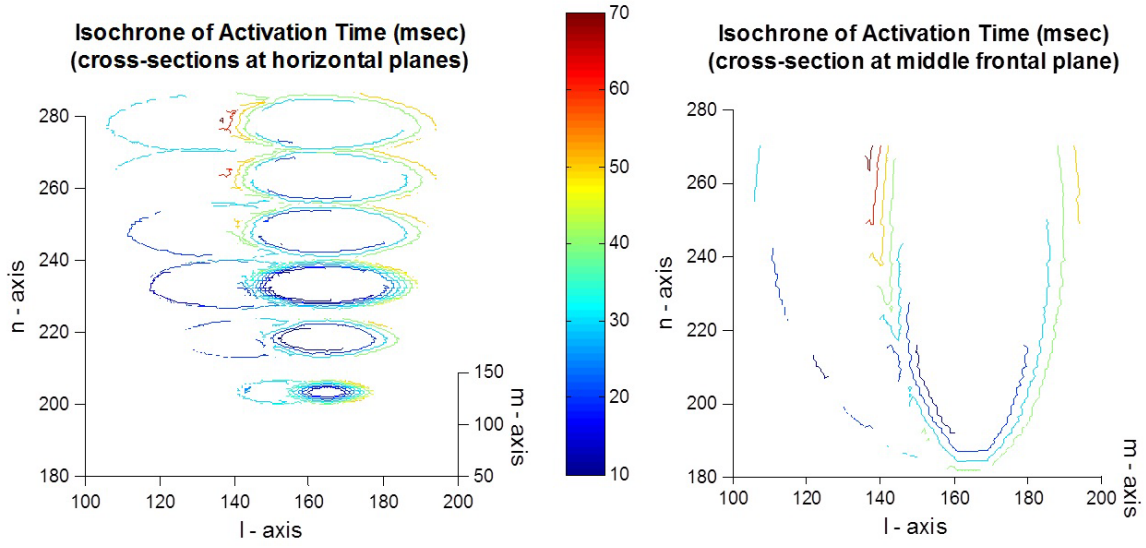

Figure 2.7 Activation sequence at horizontal cross-sections (left) and middle frontal cross-section (right).

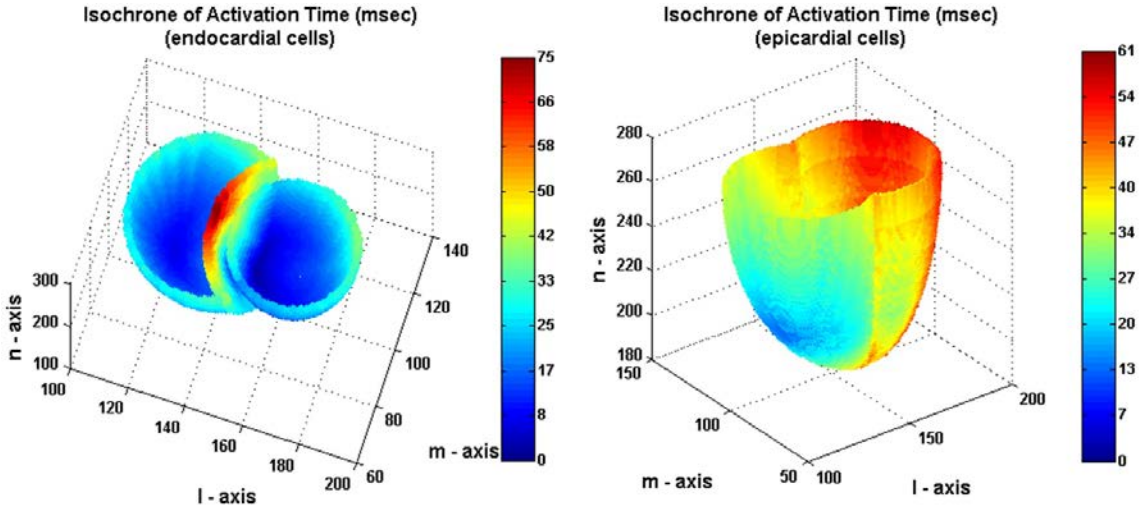

Figure 2.8 Activation map of endocardium (left) and epicardium (right).

2.3.2.3 Normal Electrical Activity of Heart – Repolarization

Distribution of Action Potential Duration (APD). The length of APD was different in the three types of myocardium: midmyocardium longest, endocardium shorter and epicardium shortest (138). The APDs increased gradually from endocardium to midmyocardium, and decreased sharply from subepicardium to

epicardium transmurally (138). In addition, APDs at the apex were slightly longer than those at the base (118). In the septum, APDs progressively lengthened from right ventricular to left ventricular endocardium (89). In this model, the normal APD distribution had a transmural gradient and an apex-to-base gradient. At the apex, APDs of the elements from epicardium layer to endocardium layer at the free wall of the left ventricle were 216, 222, 246, 252, 258, 264, 270, 264, 258 msec, at the septum were 224, 227, 230, 233, 236, 239, 242, 245, 248 msec, and at the free wall of right ventricle were 206, 230 and 224 msec. The APD decreased gradually from apex to base, so that APDs were 10 msec shorter at the base than those at the apex. The distribution of APD is shown in Figure 2.9.

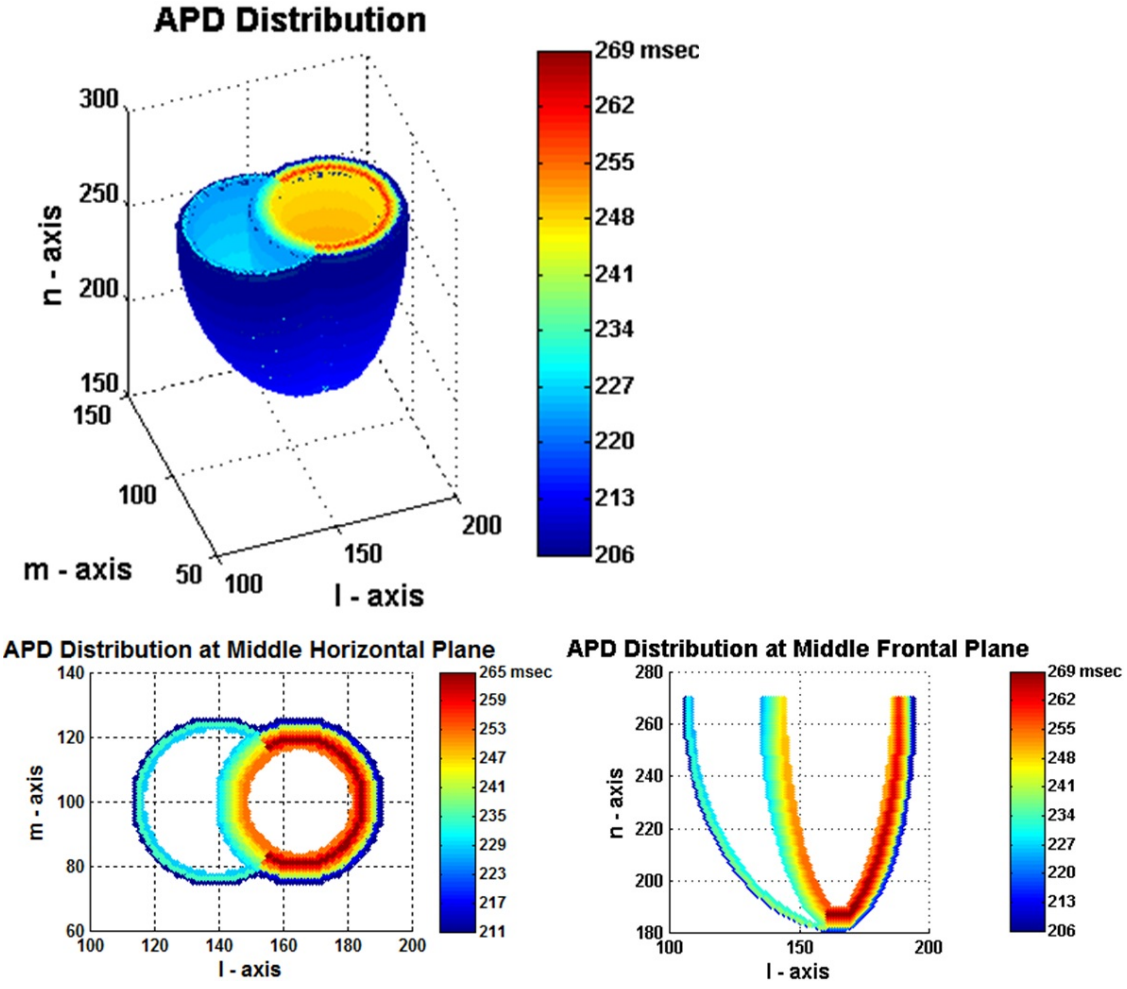

Figure 2.9 Distribution of action potential durations (3D view, top; middle horizontal cross section, bottom left; middle front cross section, bottom right).

Cellular Action Potential Model. The intracellular action potential model consisted of a step change from resting potential -90 mV to 10 mV simulating depolarization, followed by six linear lines changing from 10 mV to -90 mV simulating repolarization. Similar to a previous study (86), the differences of APD were accomplished by proportionally changing the lengths of the first two lines of repolarization (Figure 2.10). In the abnormal model, the prolongation or shortening of APD was accomplished by proportionally prolonging or shortening the lengths of the first two lines of repolarization.

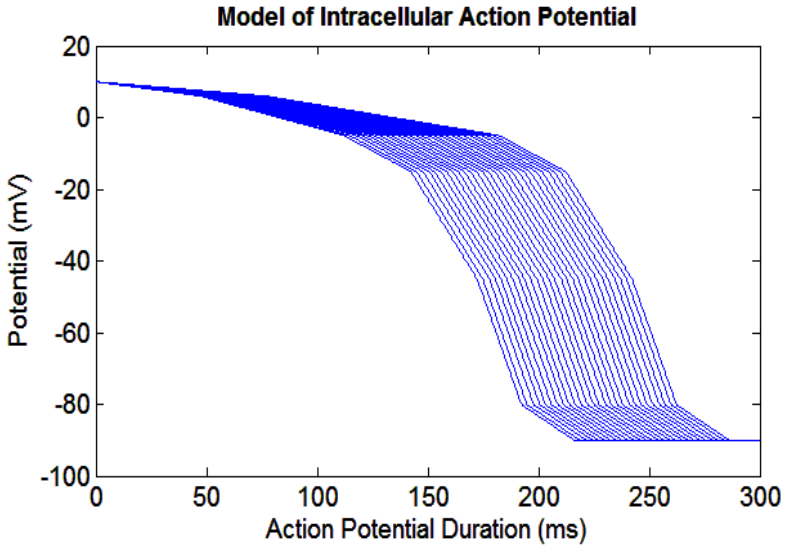

Figure 2.10 Model of intracellular action potential with different durations.

2.3.2.4 Heart-Torso Model

Position of Heart in Torso. The torso was modeled as an homogeneous volume conductor. The torso has a cylinder shape with maximum length 300 mm from left to right, maximum length 200 mm from front to back and 350 mm from top to bottom (Figure 2.11). The heart model, located inside the torso model, was surrounded by the point elements on the torso surface. The position of the heart inside the torso was determined by first setting the center of the heart model the same with that of the torso model except 50 mm higher than the torso model.

This resulted in the anterior side of both ventricles facing the front side of the torso model. Then the heart model was rotated by 45 deg along the longitudinal axis of the torso and then 45 deg along the mediolateral axis of the heart model. After the rotations, the heart model was displaced to the left side of the torso by 90 mm and the front side by 45 mm. This resulted in the heart model being closer to the left and front side of the torso model and the apex pointing towards the left down side. The locations of the electrodes of 12-lead ECG were determined on the body surface according to the standard placement.

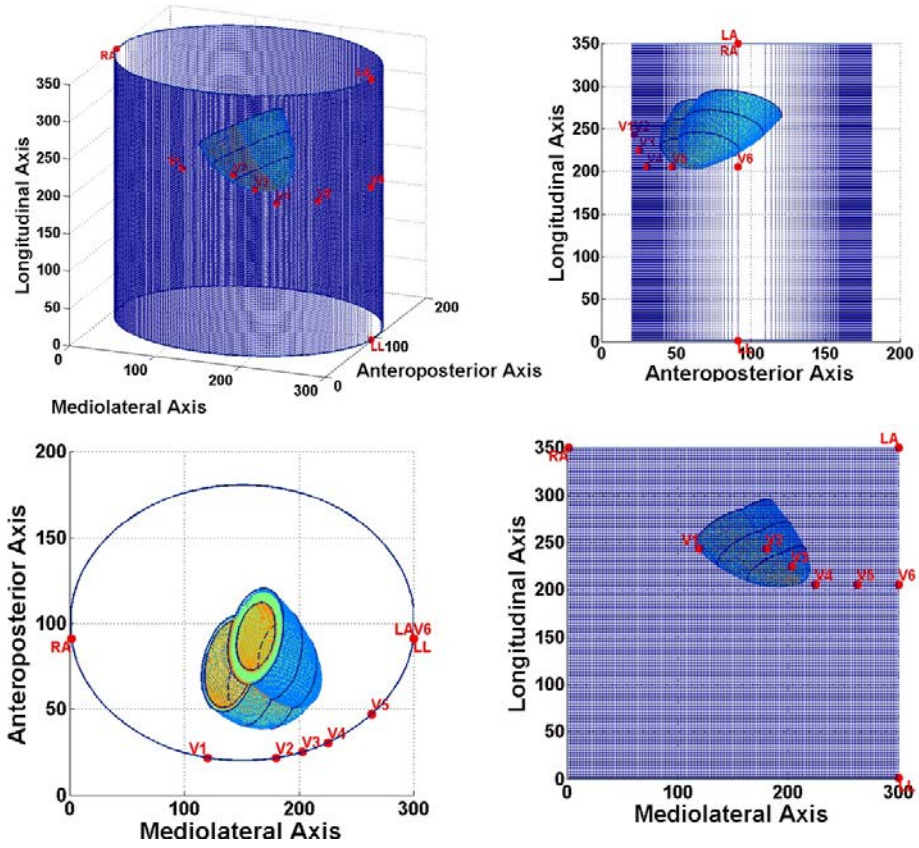

Figure 2.11 Views of heart inside torso, heart rotation and positions of electrodes (3D view, top left; lateral view from left, top right; top view, bottom left; front view, bottom right).

Body surface potential: solution of forward problem. The computation of surface potentials was similar to that of Miller et al. (86) except that this study calculated the current dipole at each point of the heart model, instead of dividing the heart model into 23 regions. Considering a three dimensionally distributed myocardia network, if the gradient of the intracellular potential exists, there will be a current flow from high intracellular potential to low intracellular potential as

$$\bar{J}_i = -\sigma_i \nabla \emptyset_i$$

where $\bar{J}_i$ is intracellular current density, σ_i is the effective conductance of intracellular network (set to equal to 1 in the model) and $\emptyset_i$ is the intracellular potential.

In this model, the individual myocardial segments were discrete points in a rectangular grid, therefore the gradient function at one point can be approximated as the potential differences of it six neighbors as

$$\Delta\emptyset_{l,m,n} = \frac{\emptyset_{l+1,m,n} - \emptyset_{l-1,m,n}}{2\Delta l}\bar{l} + \frac{\emptyset_{l,m+1,n} - \emptyset_{l,m-1,n}}{2\Delta m}\bar{m} + \frac{\emptyset_{l,m,n+1} - \emptyset_{l,m,n-1}}{2\Delta n}\bar{n}$$

where $\emptyset_{l,m,n}$ is the intracellular potential at point l, m, n in the three dimensional grid, Δl is the distance between two points and $\bar{l}$ is the unit vector along the l axis. The directions of the unit vectors are shown in Figure 2.12. The unit vectors were fixed three-element arrays acquired by scaling the length of the three vectors.

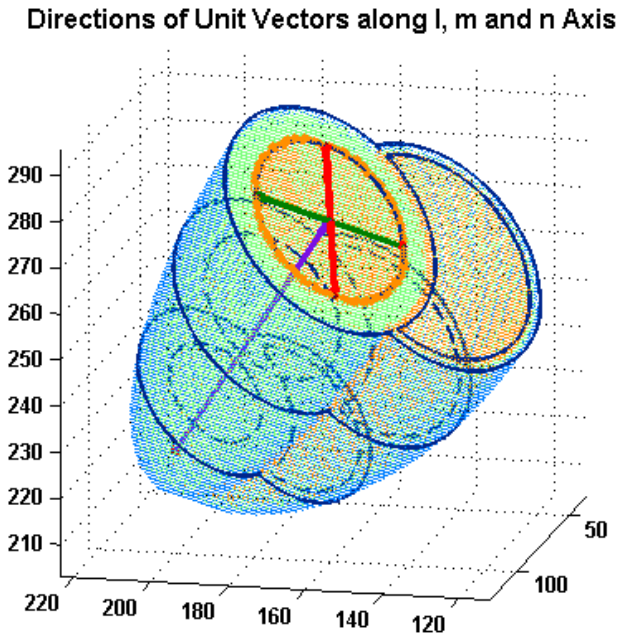

Figure 2.12 Directions of unit vectors of the heart coordinates along the dimension of the cell grid in the directions of the l, m and n axes (green, red and purple lines).

The volume integral of the current density $\bar{J}_i$ at the small space around a point can be approximated as following and is equivalent to a current dipole (105)

$$\bar{P}_{l,m,n} = -\sigma_i(\nabla\emptyset_{l,m,n})d_l d_m d_n$$

The simulation sources are thus a set of 129,826 time-varying current dipoles. The electrical field of one observation point on the body surface (x_p, y_p, z_p) can be calculated as follows

$$\Phi(x_p, y_p, z_p) = \frac{1}{4\pi\varepsilon_0}\int_{volume} \bar{P}_{l,m,n} \bullet \nabla\left(\frac{1}{r}\right)dxdydz = \frac{1}{4\pi\varepsilon_0}\int_{volume} \frac{\bar{P}_{l,m,n} \bullet \bar{u}_{x,y,z,x_p,y_p,z_p}}{r^2_{x,y,z,x_p,y_p,z_p}}dxdydz$$

where $\bar{u}_{x,y,z,x_p,y_p,z_p}$ is a three-element array, representing the unit vector pointing from an element at (x, y, z) of the heart model towards an electrode on the body surface at (x_p, y_p, z_p). r is the distance between the element at (x, y, z) of the heart model and the electrode on the body surface at (x_p, y_p, z_p). ε_0 is the permittivity of free space. In the model, the permittivity was set to be 1 according to the assumption that the torso was an homogenous conductor.

Twelve-lead ECG is calculated from the 9 body surface potentials at the locations of the electrodes RA, LA, LL, V1, V2, V3, V4, V5 and V6 as the following:

1) limb leads

$$I = LA - RA$$
$$II = LL - RA$$
$$III = LL - LA$$

2) augmented limb leads

$$aVR = RA - \frac{1}{2}(LA + LL)$$
$$aVL = LA - \frac{1}{2}(RA + LL)$$
$$aVF = LL - \frac{1}{2}(RA + LA)$$

3) precordial leads

$$V_W = \frac{1}{3}(RA + LA + LL)$$
$$V_1 = V1 - V_W, \quad V_2 = V2 - V_W$$
$$V_3 = V3 - V_W, \quad V_4 = V4 - V_W$$
$$V_5 = V5 - V_W, \quad V_6 = V6 - V_W$$

where V_W is the Wilson's central terminal used as the negative electrode for the precordial leads.

QT interval measurement of modeled ECG. The T wave end of modeled ECG was determined by using a voltage threshold method. The peak of the T wave was identified at the time when the ECG arrived at its maximum absolute value after the QRS complex. The end of the T wave was identified when the absolute voltage of the T wave decreased to ten percent of the voltage of the T peak (Figure 2.13). The QT interval was computed as the time difference between first activation and the T wave end.

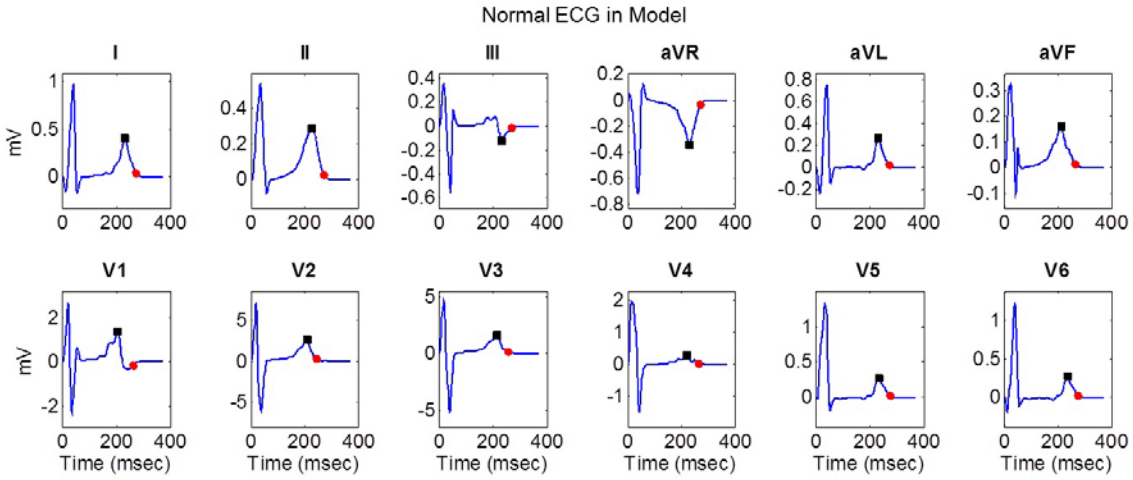

Figure 2.13 Twelve-lead ECG generated from normal model and the detection of the T peak and the T wave end.

Regional dipoles and 12-lead ECG. The activities of the heart model with all parts integrated are shown in the movie 'Heart Model and ECG.wmv'. Dipoles were estimated at every cell element as a source of the electrical field of the extracellular space, which were proportional to the differences of the intracullular potentials of its six neighbors. In order to visualize the contribution of the dipoles of all regions, the dipoles of one region were averaged and ploted as a green quiver located at the average of the coordinates of the cell elements in that region. The direction of the quiver corresponds to the direction pointing from the negative charge to the positive charge of the dipole. In order to visualize the major force of the heart model, which is reflective of the general morphology of the ECG, the average dipole of all cell elements of the heart was plotted as a red quiver located at the average of the coordinates of all cell elements. The intracellular potentials and dipoles changed with time during the processes of depolarization and repolarization of the heart, generating the QRS complex and T wave in ECG (see movie).

2.3.2.5 Diabetes Effects on Normal Heart

Prolongation and Shortening of Action Potential. In two previous animal studies, cardiac sympathetic denervation by stellate ganglionectomy or phenol resulted in prolongation of the functional refractory period (139) or activation-

recovery interval (140), while in another animal study, cardiac sympathetic denervation by bilateral sympathetic ganglionegtomy resulted in shortening of the APD (136). In this study, both prolongation and shortening of the action potential were simulated.

Transmural differences of APD changes. It has been shown that the stained area of tyrosin hydroxylase- and NPY- immunoreactive nerves (sympathetic nerves) was largest in epicardium followed by endocardium, and was smallest in midmyocardium in pig heart (26). The ratio of the stained areas was approximately 5:3:1 in epicardium, endocardium and midmyocardium, respectively (26). In this study, APD changes applied in epicardium, endocardium and midmyocardium in the heart model were set accordingly with this ratio.

Regions in the heart model being affected. Four patterns of abnormal cardiac sympathetic innervation have been reported in studies of diabetic cardiac autonomic neuropathy, shown by MIBG-SPECT or HED-PET images: 1) low tracer uptake in one region, 2) low tracer uptake in more than one region, 3) reduced uptake in the whole heart, and 4) denervation in distal regions complicated by hyperinnervation in basal regions. In the heart model, regions of the left ventricular walls and septum were divided according to the polar map, which was used previously in a MIBG-SPECT study (55). Hyperinnervation was simulated by applying the opposite APD changes of denervation. Figure 2.14 and Figure 2.15 show examples of prolonging and shortening of APD at one region, the basal anterior region.

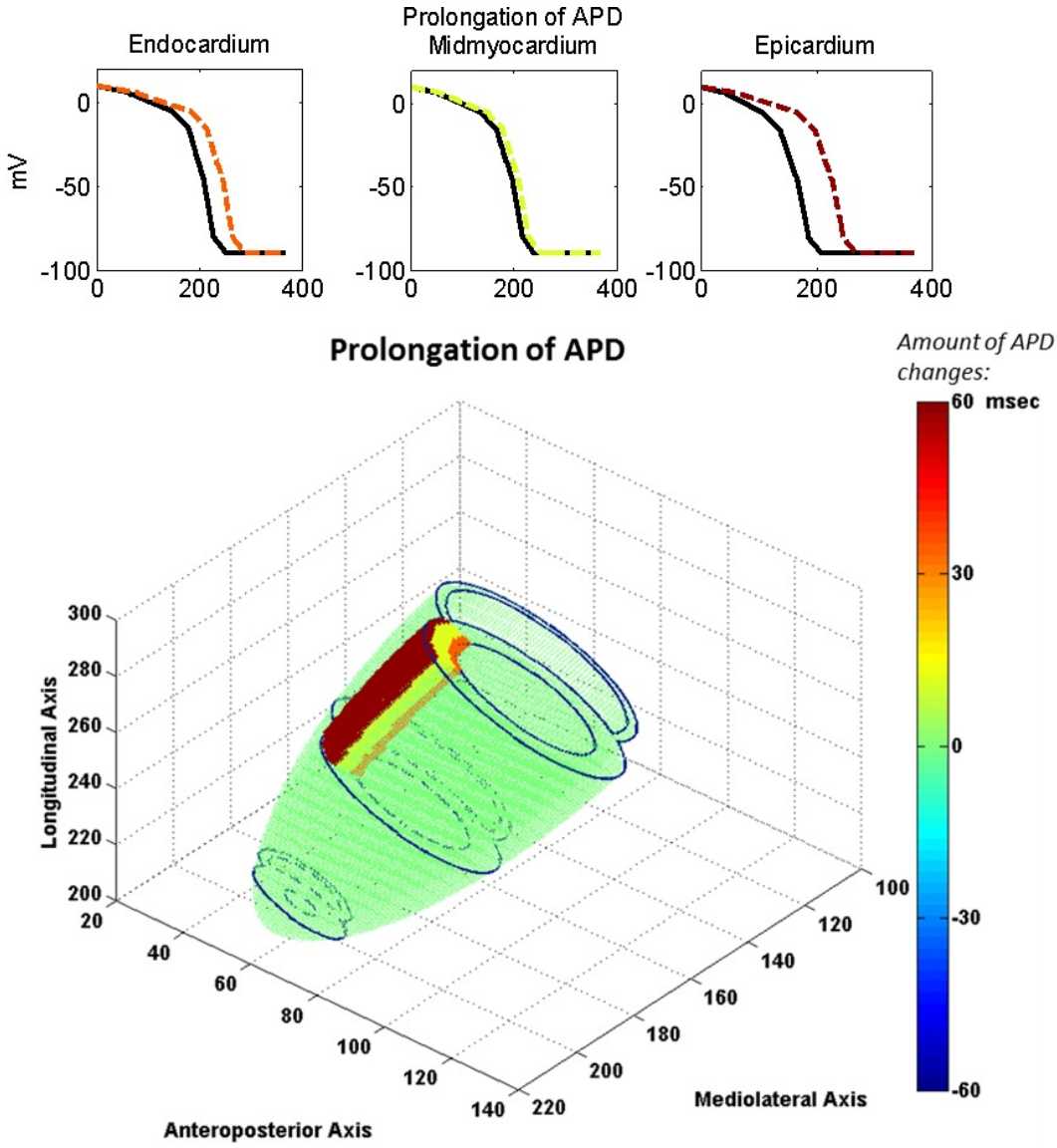

Figure 2.14 Example of simulation of possible effects of diabetic neuropathy to the heart: prolongation of APD at basal anterior region.

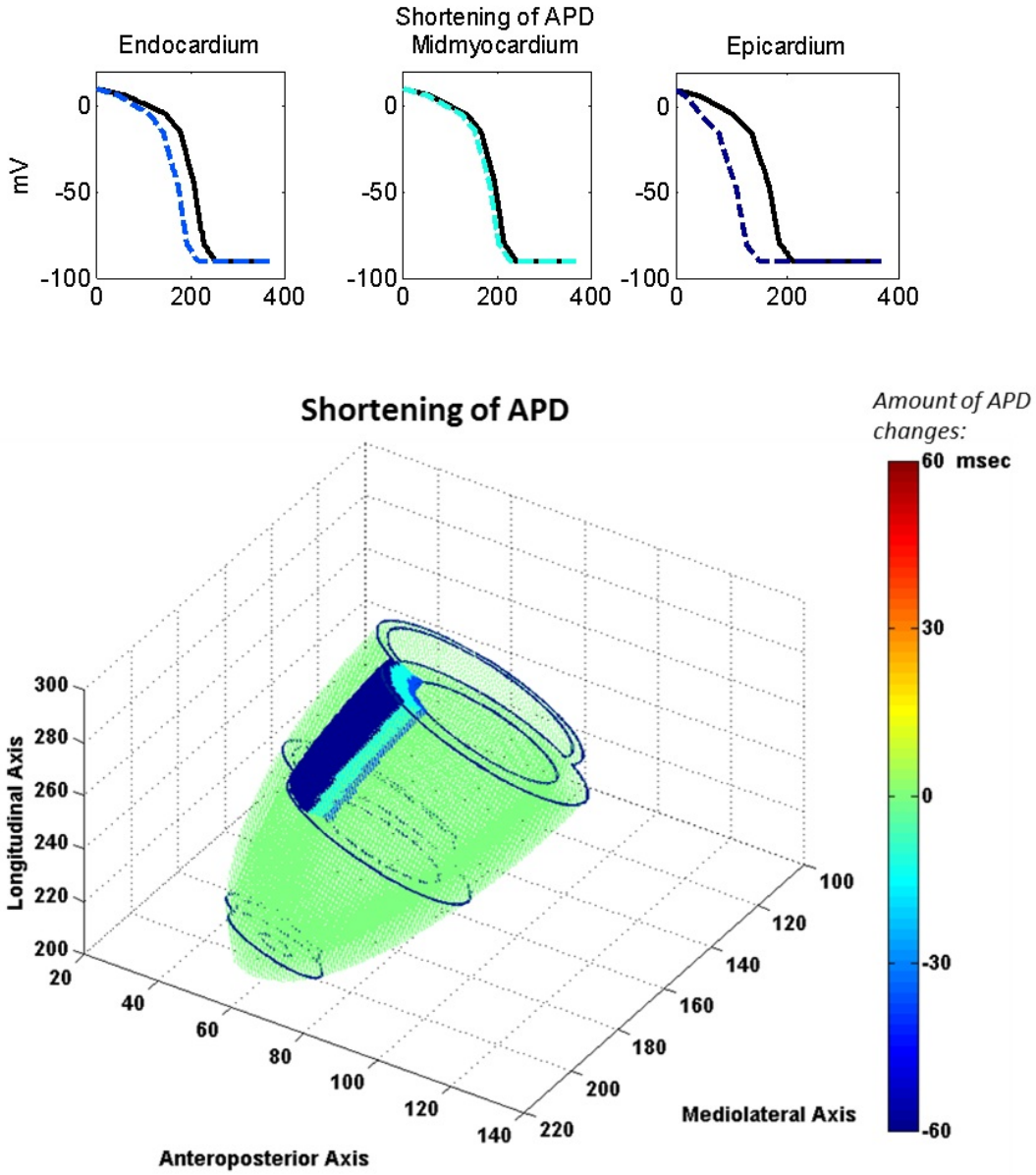

Figure 2.15 Example of simulation of possible effects of diabetic neuropathy to the heart: shortening of APD at basal anterior region.

Matching procedure. In order to link clinically observed QT interval changes, to cardiac sympathetic denervation or hyperinnervation seen in cardiac imaging studies, the following procedure was followed:

1) In experimental ECG, QT interval changes in diabetic patients with neuropathy, compared to those of able-bodied subjects were characterized.

2) In the model, simulations of abnormal heart with different patterns of cardiac sympathetic denervation or hyperinnervation were performed.

3) Within the results of simulation, the pattern that generated 12-lead ECG and QT intervals which best matched the characteristics of experimental QT intervals of diabetics with neuropathy was chosen as an inverse solution.

4) In the model, abnormal patterns were further modified to determine whether the characteristics of experimental QT intervals could be better matched.

2.4 Chapter Four: Results

2.4.1 Experimental ECG

Group mean RR intervals of supine able-bodied subjects, diabetics without neuropathy, diabetics with mild neuropathy and diabetics with severe neuropathy are shown in Figure 2.16. RR interval tended to be different among groups (p=0.0829, ANOVA).

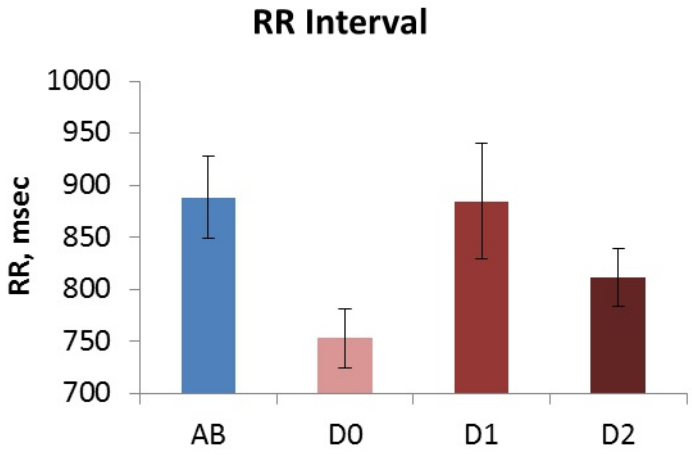

Figure 2.16 Five-minute, resting, average ± SEM RR interval of able-bodied subjects (AB), diabetics without neuropathy (D0), diabetics with mild neuropathy (D1) and diabetics with severe neuropathy (D2).

Group mean QT intervals and heart rate-corrected QT interval (QTc) of 12 leads are shown in Figure 2.17. QT intervals of able-bodied subjects did not differ from those of diabetics with severe neuropathy. QTc of able-bodied subjects tended to be shorter than diabetics with severe neuropathy (p=0.051 for lead aVL, p=0.104 for lead I, using two-tail t test between able-bodied subjects and diabetics with severe neuropathy). QTc intervals of diabetics without neuropathy tended to be the longest in the four groups.

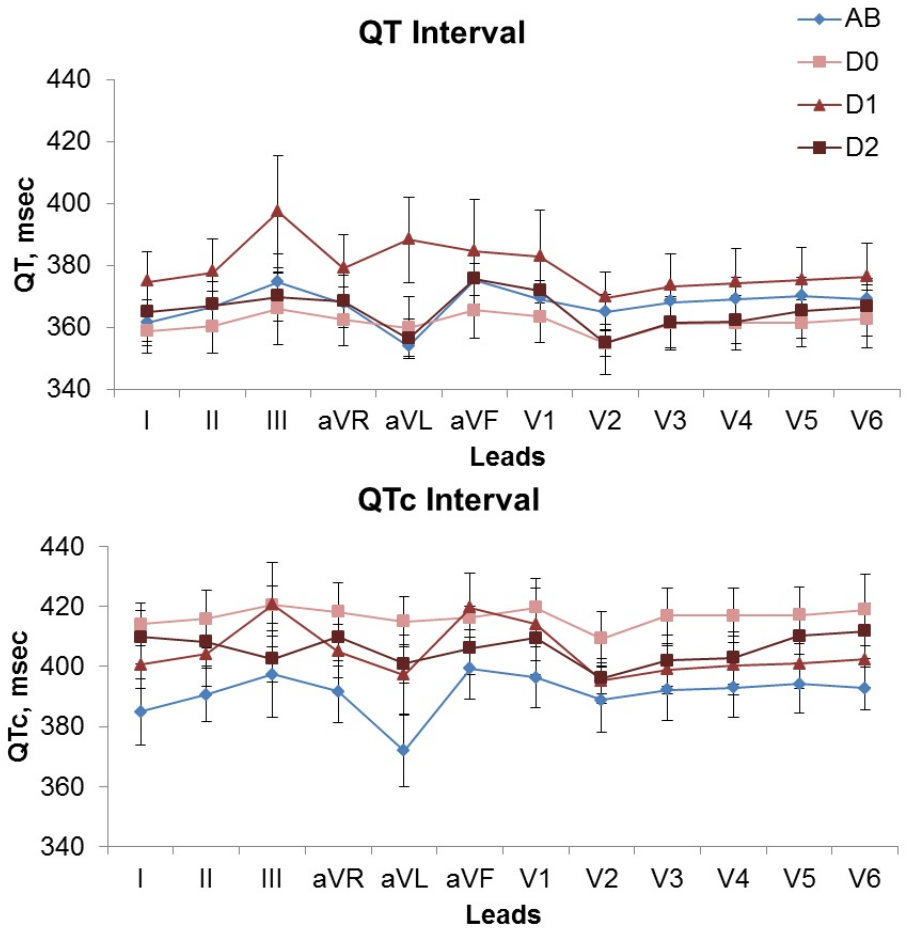

Figure 2.17 Average ± SEM QT interval (top) and heart rate-corrected QT interval (QTc, bottom) of 12-lead ECG of four groups.

Maximum and minimum QTc of all leads measured over supine control period are shown in Figure 2.18. Maximum QTc was not different between able-bodied subjects and diabetics with severe neuropathy. Minimum QTc was not different between able-bodied subjects and diabetics with severe neuropathy, but demonstrated a tendency to be different.

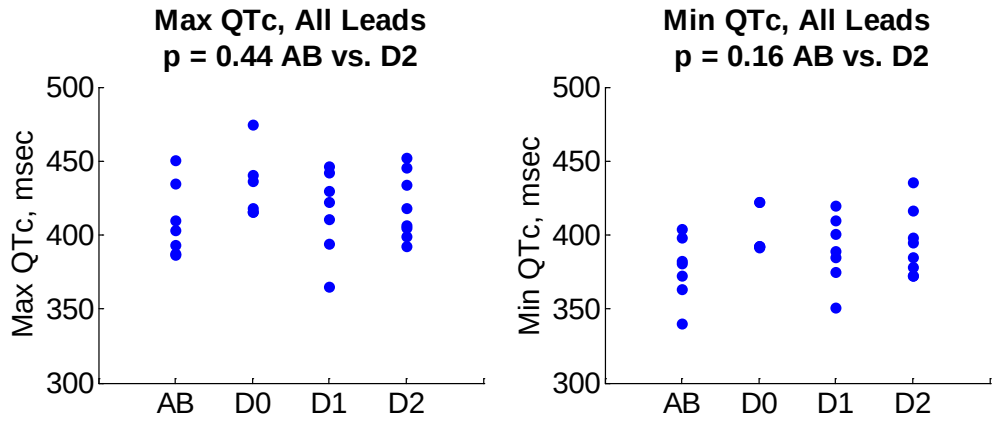

Figure 2.18 Individual maximum QTc (left) and minimum QTc (right) of all leads in the four groups.

Minimum QTc of septal leads, anterior leads, lateral leads and inferior leads for all subjects are shown in Figure 2.19. Minimum QTc of lateral leads tended to be different between able-bodied subjects and diabetics with severe neuropathy ($p = 0.095$, two-tail t test between able-bodied subjects and diabetics with severe neuropathy).

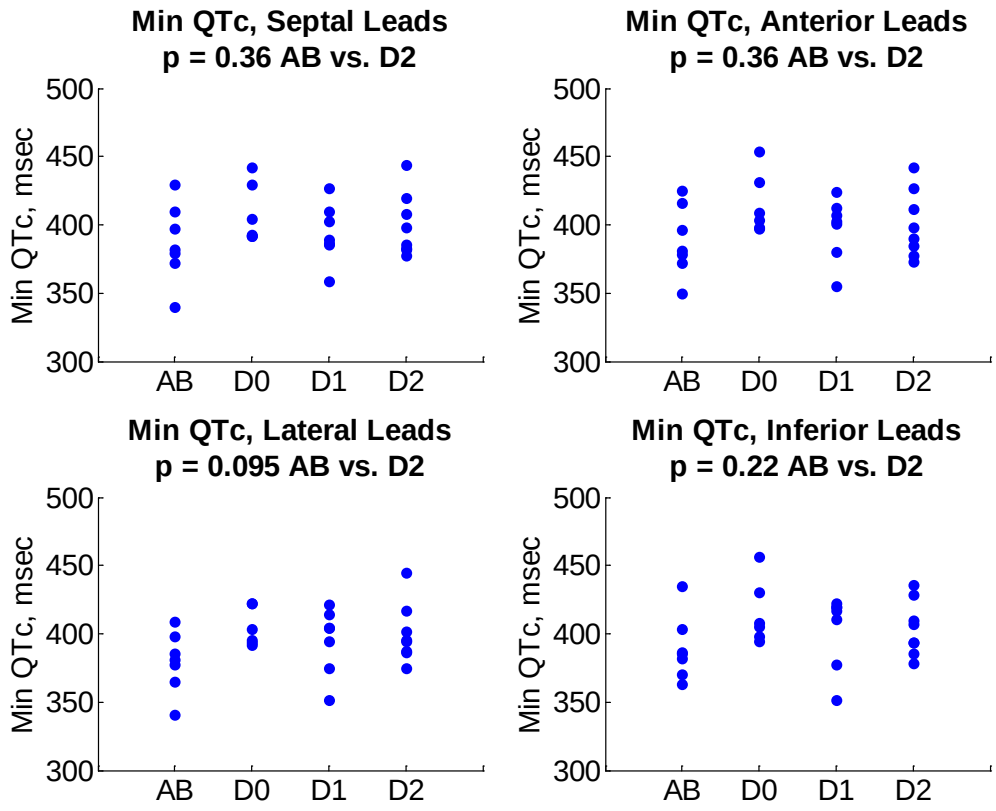

Figure 2.19 Individual minimum QTc of septal leads (top left), anterior leads (top right), lateral leads (bottom left) and inferior leads (bottom right) of the four groups.

Two characteristics were identified in QTc interval to be matched by the model. First, diabetics with severe neuropathy tended to have longer QTc interval in all leads than did able-bodied subjects. Second, minimum QTc interval from lateral leads demonstrated greater group difference between able-bodied subjects and diabetics with severe neuropathy when compared to other leads. In addition, a third characteristic of ECG, morphology, needed to be matched. Specifically, the T waves of lateral leads V5 and V6 should be positive which was observed in the ECG of all subjects.

2.4.2 Modeled ECG – Normal Model

QT intervals of 12-lead ECG from the model of the normal heart are shown in Figure 2.20. Compared to the QTc interval of 12-lead ECG from able-bodied subjects, there was a similar dip at lead V2. The lack of a dip at aVL in the model, compared to the able-bodied subjects, did not appear to be an important factor in model function, perhaps due to the anatomy of the model vs. real heart. In the subsequent simulation of abnormal heart, changes from normal QT intervals were computed.

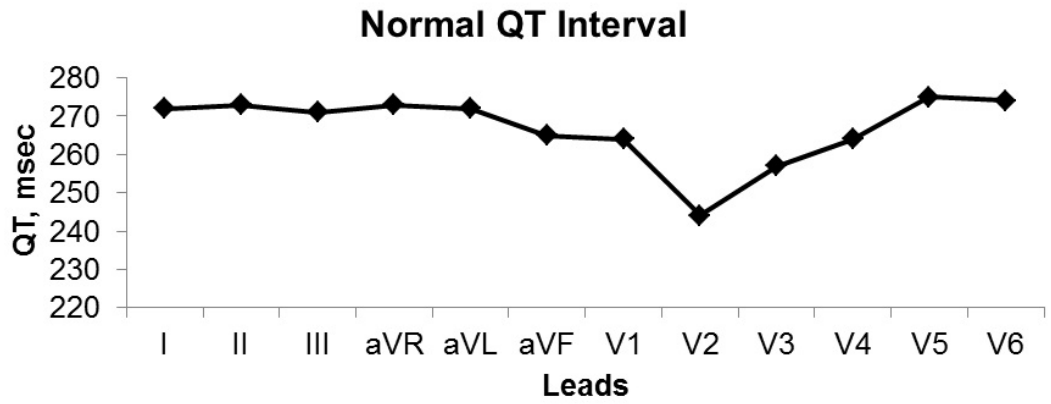

Figure 2.20 QT interval of 12 leads generated from normal model.

2.4.3 Modeled ECG - Diabetic Effect on Normal Model

Determination of the amount of APD changes in simulation. In order to determine the amount of APD changes, the effects of changing APD on 12-lead ECG and QT interval were assessed, by prolonging and shortening APD to different extent at one region (Figure 2.21, Figure 2.22). The shape of ECG showed that shortening APD at one region, for example, in the distal inferior region, primarily modified the ST segment and the ascending part of the T wave (blue lines in Figure 2.21). Conversely, prolonging APD in the distal inferior region primarily modifed the descending part of the T wave (red lines in Figure 2.21). Greater APD prolongation generated greater changes in QT interval

(Figure 2.22). In subsequent simulations, a 60 msec change in epicardial APD, 36 msec endocardial and 12 msec midmyocardial generated changes of QT interval by the desired amount of 20 msec, as observed in the QTc interval of lateral leads. Some exceptions occurred; 1) at the septum, 36 msec change was applied at both sides of the endocardium; 2) to simulate diffuse reduction of innervation, 20 msec change in APD at the epicardium, 12 msec at the endocardium and 4 msec at the midmyocardium were applied to the whole septem and left ventricular walls, in order to correspond to the definition of diffuse uptake of MIBG observed in a previous study that reported reduced global heart-to-mediastinum ratio without obvious regional defect in SPECT polar map (115). Although shortening APD in the distal inferior region did not produced QT interval prolongation in most leads, as did prolonging APD (Figure 2.22), it did prolong QT interval in several leads. Therefore, both prolonged and shortened APD were applied, respectively.

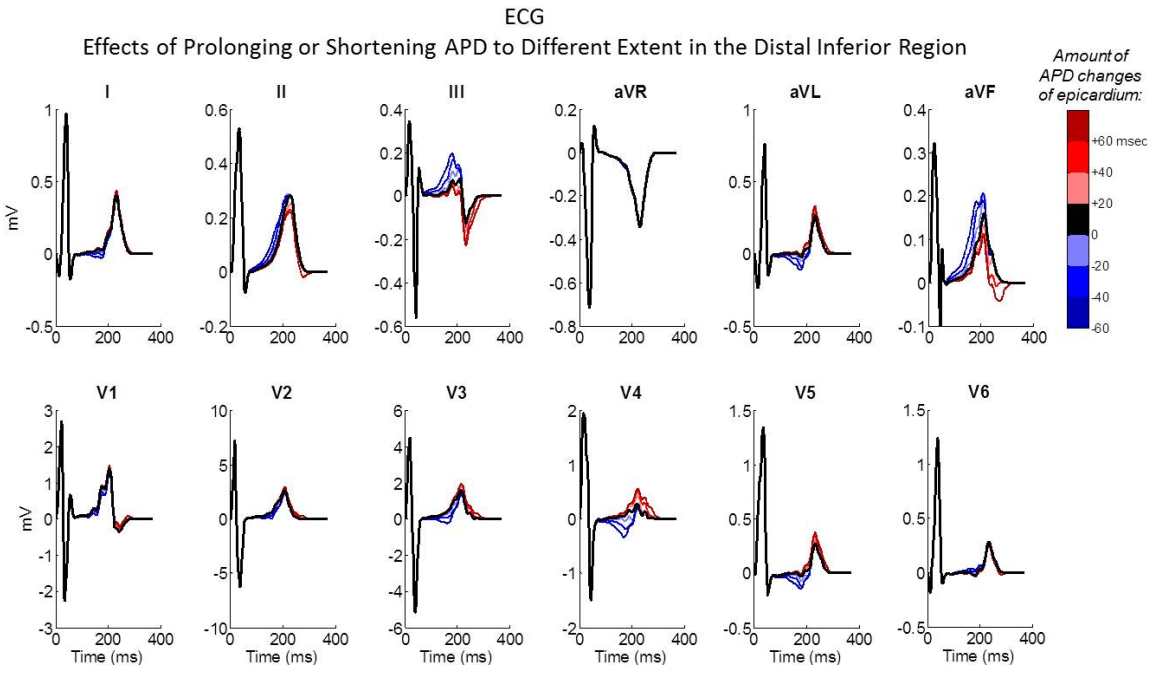

Figure 2.21 Twelve-lead ECG of normal model and abnormal models by prolonging or shortening APD to different extent in the distal inferior region.

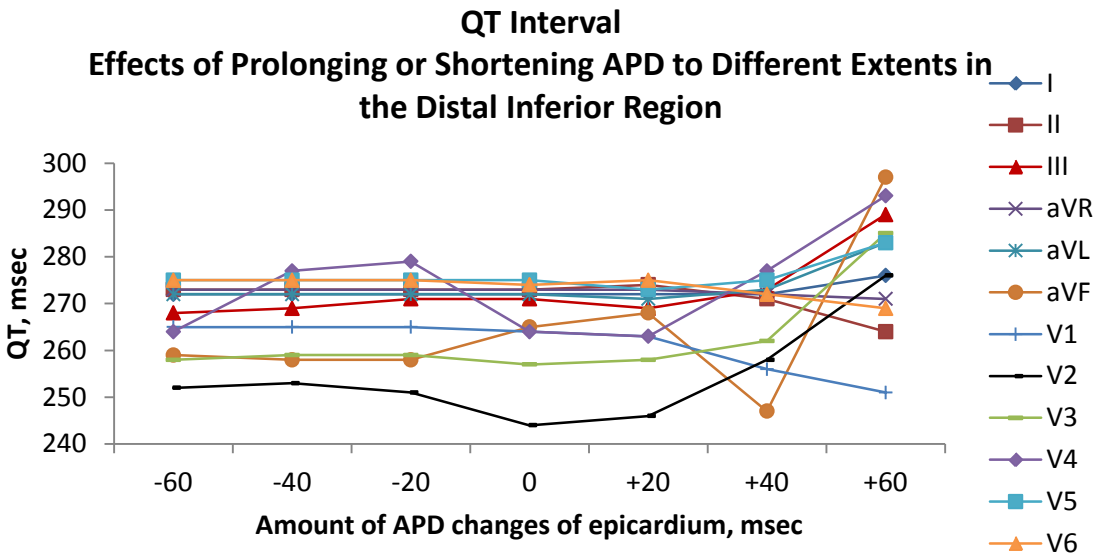

Figure 2.22 QT interval of 12 leads of normal model and abnormal models by prolonging or shortening APD in the distal inferior region, when applying different magnitudes of APD changes.

QT interval from simulation of regional abnormalities of cardiac sympathetic innervation. Action potential durations were prolonged or shortened by 60 msec at the epicardium, 36 msec at the endocardium and 12 msec at the midmyocardium in the following single regions respectively: distal inferior, basal inferior, distal lateral, basal lateral, distal anterior, basal anterior, distal septal, basal septal regions and apex. QT intervals were computed in every trial. QT interval changes due to *prolonging* APD at these regions are shown in Figure 2.23. QT interval changes due to *shortening* APD at these regions are shown in Figure 2.24. The patterns that prolonged APD in the distal lateral or basal septal regions were selected because these modifications generated increases in QT intervals of all leads.

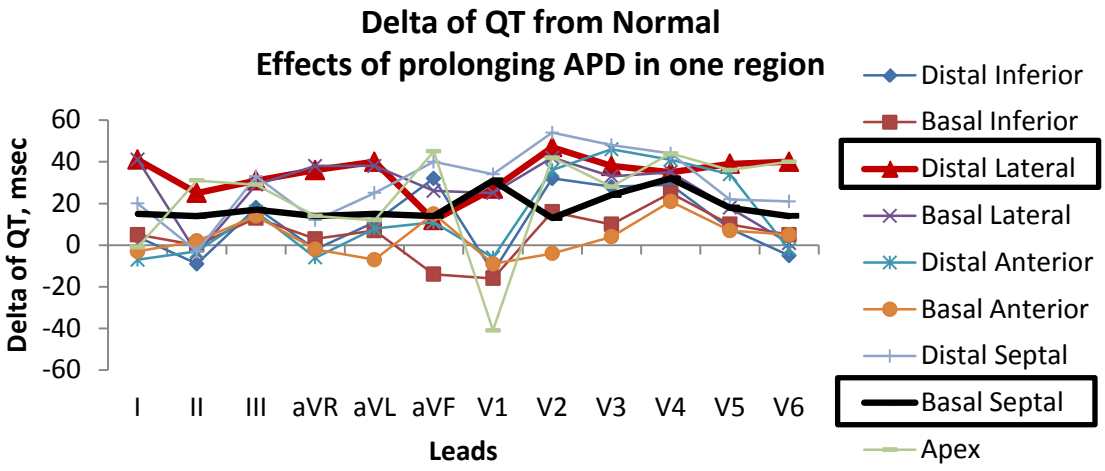

Figure 2.23 Delta of QT interval of 12 leads from normal model, resulting from *prolonging* APD in one region.

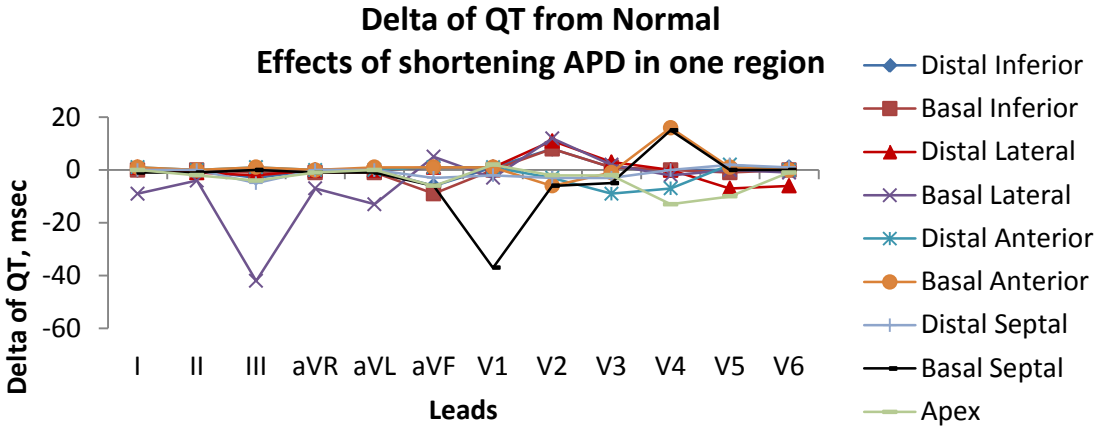

Figure 2.24 Delta of QT interval of 12 leads from normal model, resulting from *shortening* APD in one region.

Simulations of hyperinnervation in the basal region complicated by the loss of innervation in the distal region were simulated by *prolonging* APD in the distal region and *shortening* APD in basal region. Results of QT interval changes due to this simulation are shown in Figure 2.25. QT interval changes due to *shortening* APD in the distal region and *prolonging* APD in the basal region are shown in Figure 2.26. The pattern of prolonging APD in the distal, and shortening

APD in the basal septal region was selected because this modification generated increases in QT interval of all leads.

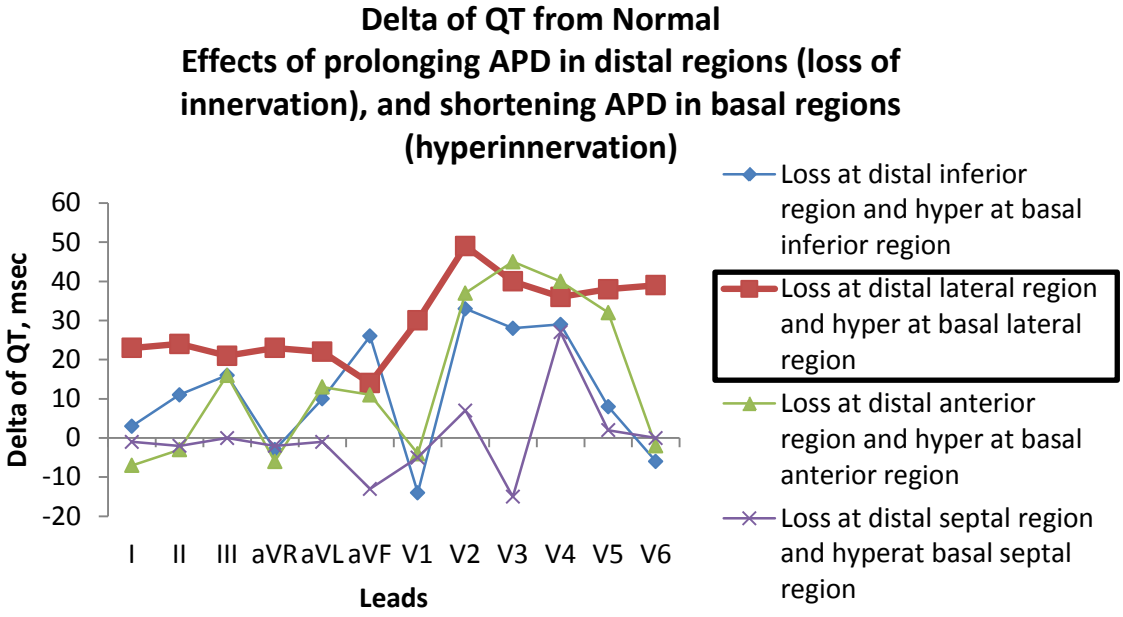

Figure 2.25 Delta of QT interval of 12 leads from normal model, resulting from *prolonging* APD in distal, and *shortening* APD in basal regions.

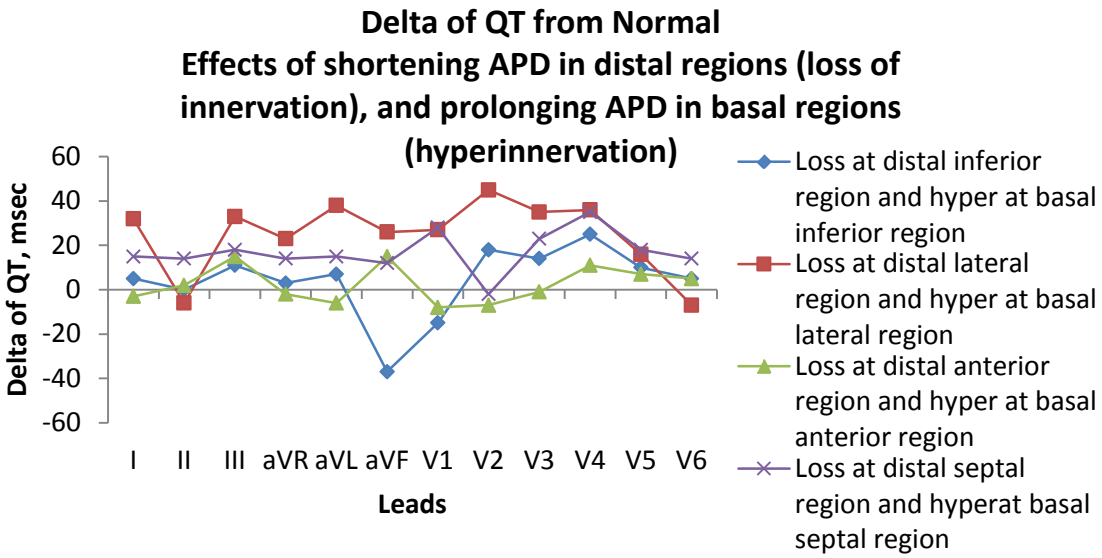

Figure 2.26 Delta of QT interval of 12 leads from normal model, resulting from *shortening* APD in distal, and *prolonging* APD in basal regions.

Finally, because the distal inferior region has frequenty been reported to be the first region affected, and an extension from this region has been observed in patients with more severe neuropathy, simulations of loss of innervation in two regions, extending from distal inferior to basal inferior, distal septal,distal lateral or apical regions were performed. In addition, diffuse denervation was also simulated by changing APD in the whole left ventricle. QT interval changes due to *prolonging* APD in these regions are shown in Figure 2.27. QT interval changes due to *shortening* APD in these regions are shown in Figure 2.28. The pattern that prolonged APD at distal inferior and distal lateral regions was selected because this pattern generated increases in QT interval of all leads.

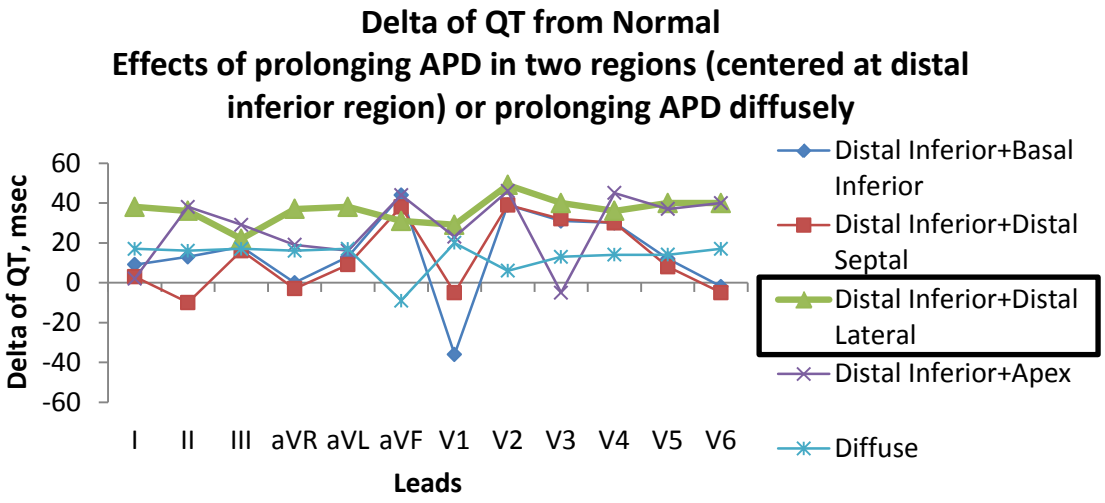

Figure 2.27 Delta of QT interval of 12 leads from normal model, resulting from *prolonging* APD in two regions or *prolonging* APD diffusely.

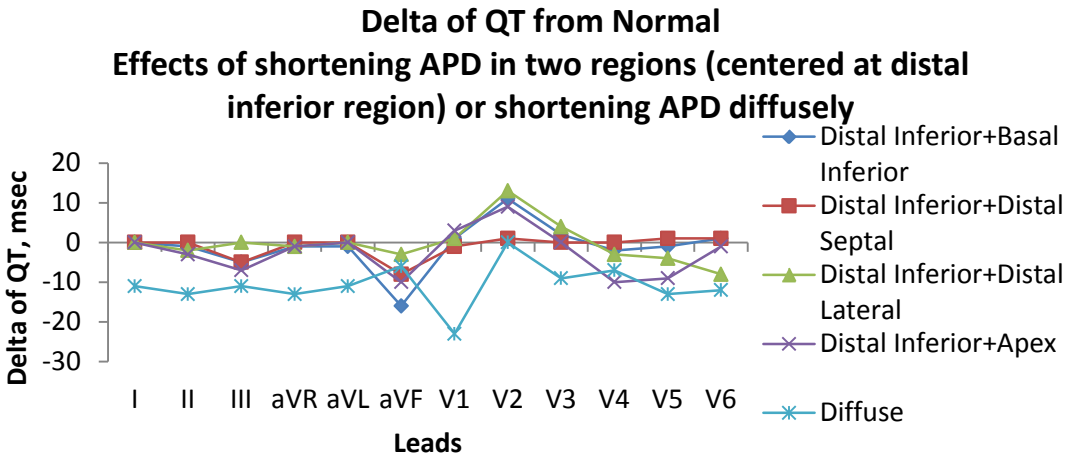

Figure 2.28 . Delta of QT interval of 12 leads from normal model, resulting from *shortening* APD in two regions or *shortening* APD diffusely.

Twelve-lead ECG of selected patterns were then plotted against normal 12-lead ECG to compare the morpholoy of ECG. Figure 2.29 shows ECGs from the simulation that prolonged APD in the distal lateral region. Prolonging APD in

this region resulted in changes in the morphology of ECGs and generated an inverted T wave in leads V5 and V6.

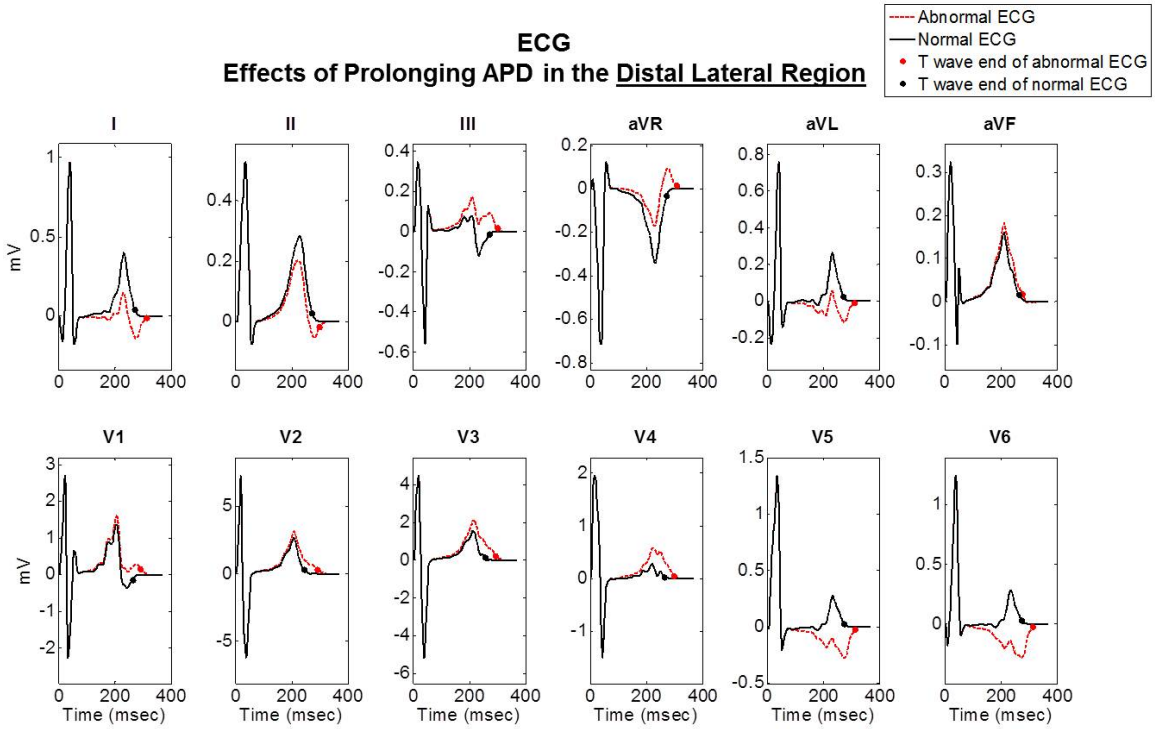

Figure 2.29 Twelve-lead ECG of the simulation that prolonged APD in the distal lateral region, plotted against normal ECG.

Figure 2.30 shows ECGs of the simulation that prolonged APD in the basal septal region. Prolonging APD in the basal septal region preserved the morphology of ECG.

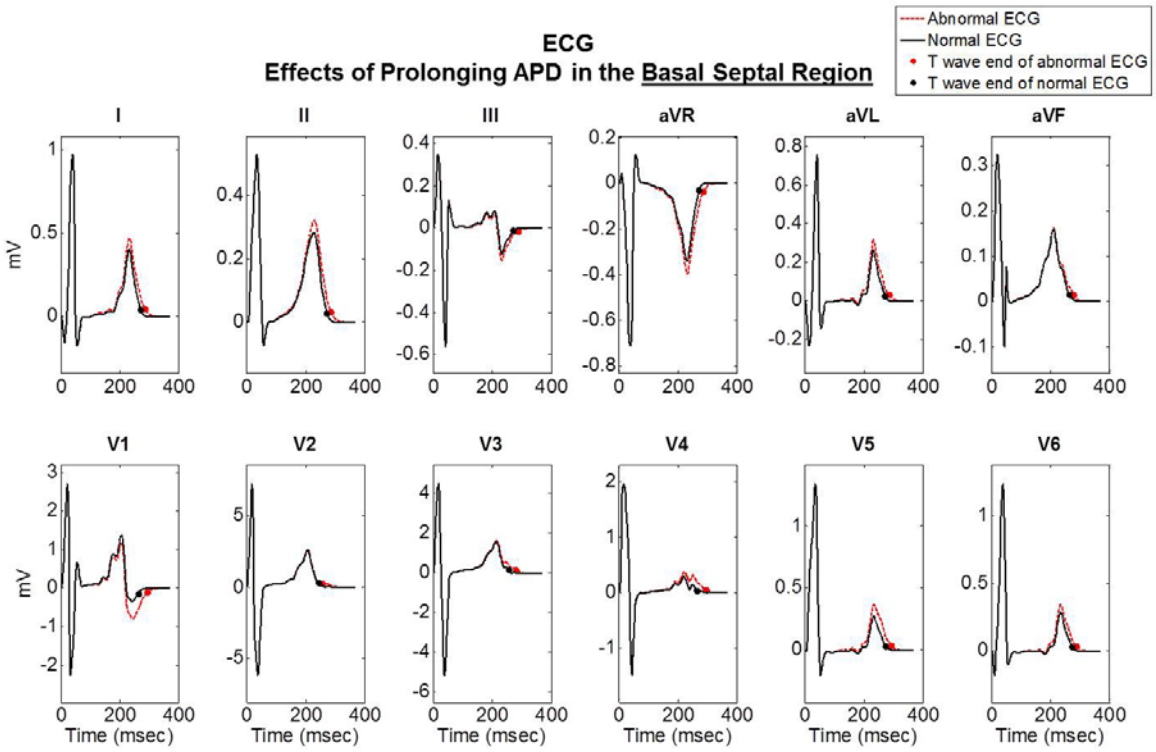

Figure 2.30 Twelve-lead ECG of the simulation that prolonged APD in the basal septal region, plotted against normal ECG.

Figure 2.31 shows ECGs from the simulation that prolonged APD in the distal lateral region and shortened APD in the basal lateral region. Prolonging APD in the distal lateral region with shortening APD in the basal lateral region resulted in changes in the morphology of ECG and generated inverted T wave in leads V5 and V6.

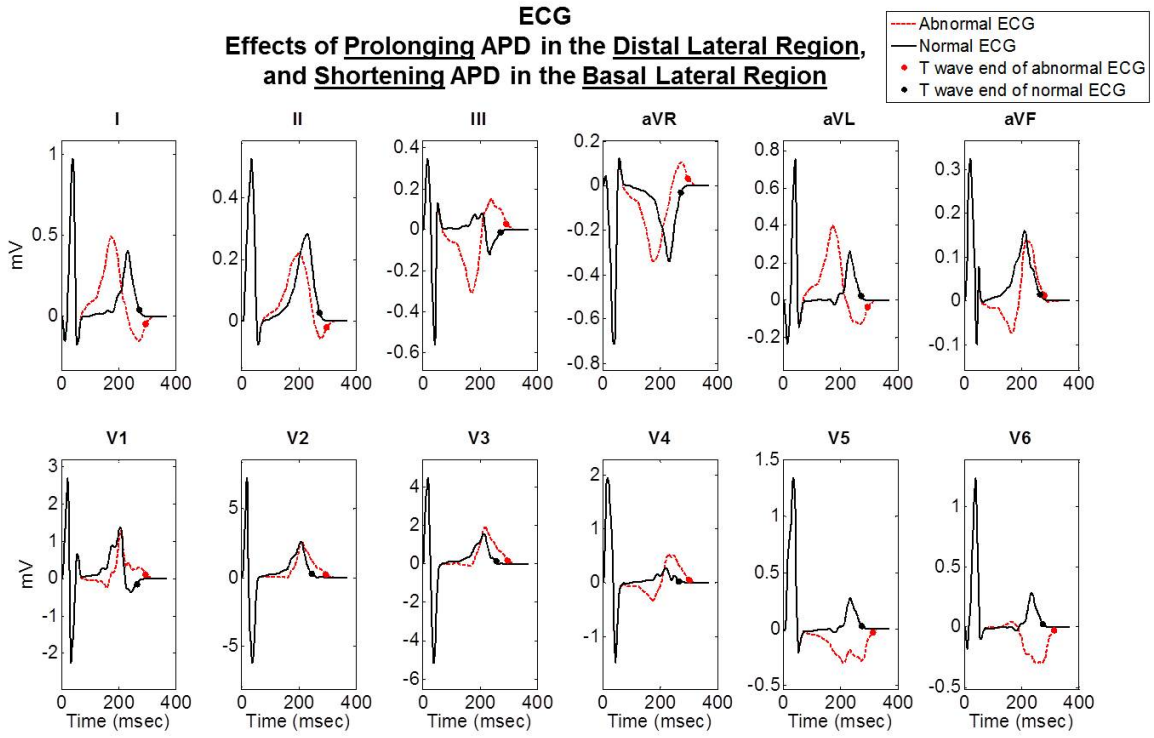

Figure 2.31 Twelve-lead ECG of the simulation that prolonged APD in the distal lateral region and shortened APD in the basal lateral region, plotted against normal ECG.

Figure 2.32 shows ECGs of the simulation that prolonged APD at distal inferior and distal lateral regions. Prolonging APD at distal inferior and distal lateral regions resulted in changes in the morphology of ECG and generated inverted T wave in leads V5 and V6.

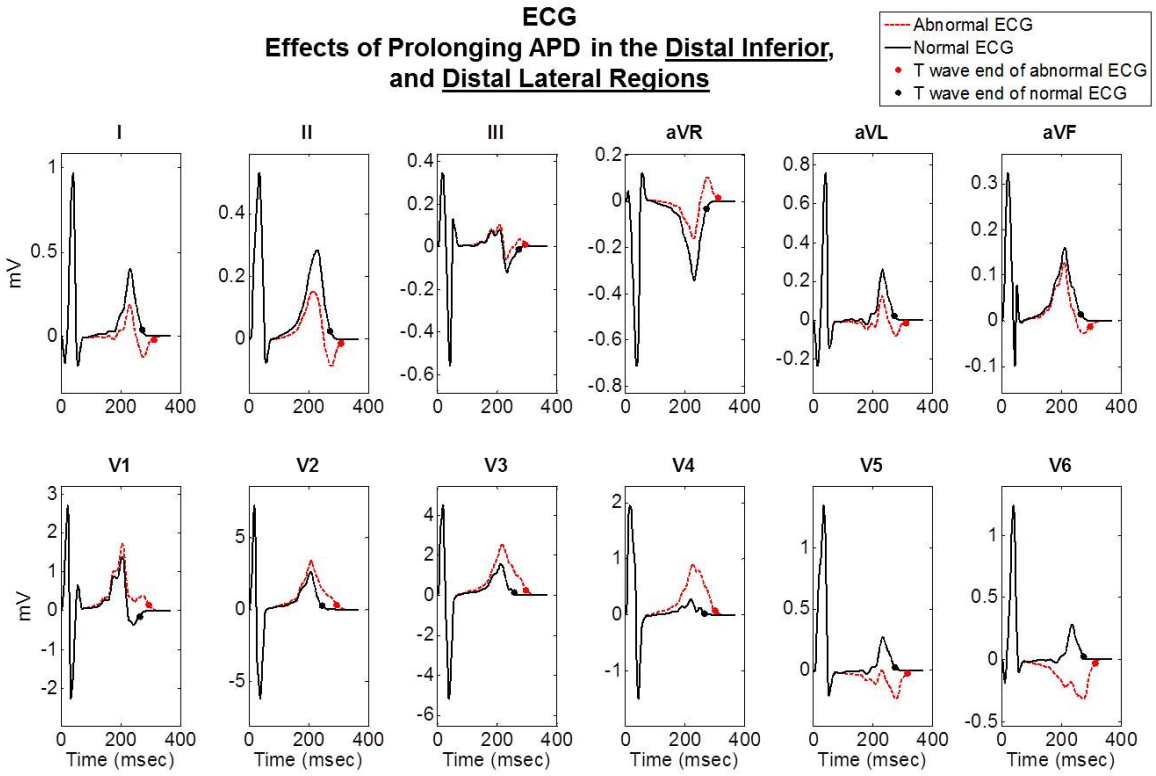

Figure 2.32 Twelve-lead ECG of the simulation that prolonged APD in the distal inferior and distal lateral regions, plotted against normal ECG.

Determination of the pattern with the best match. From the comparison of the change in QT interval and morphology of ECGs, the pattern of prolonging APD in the basal septal region yielded the best match to experimental data. Specifically, 1) QT interval increased in all leads, and 2) the morphology of ECG was preserved. In addition, the minimum QT interval of lateral leads increased by 15 msec, 2 msec longer than from all leads.

Further modifcations. Because in diabetic patients with more severe autonomic neuropathy, the loss of tracer activity in the same region is more pronounced and the affected region extends to other regions (91, 93, 113, 123), the simulations of longer prolongation of APD (60 msec at endocardium and 20 msec at midmyocardim) in the basal septal region, and prolonging APD in regions near the basal septal region were performed, respectively. QT interval changes due to prolonging APD in two regions (basal septal and distal septal

regions, basal septal and basal inferior regions, basal septal and basal anterior regions) are shown in Figure 2.33. Compared to changing APD in a single basal septal region, extension of regions did not alter QT intervals of lateral leads (leads I, aVL, V5 and V6), but other leads. Prolonging APD in the single basal septal region was chosen to be the pattern that best matched observed results.

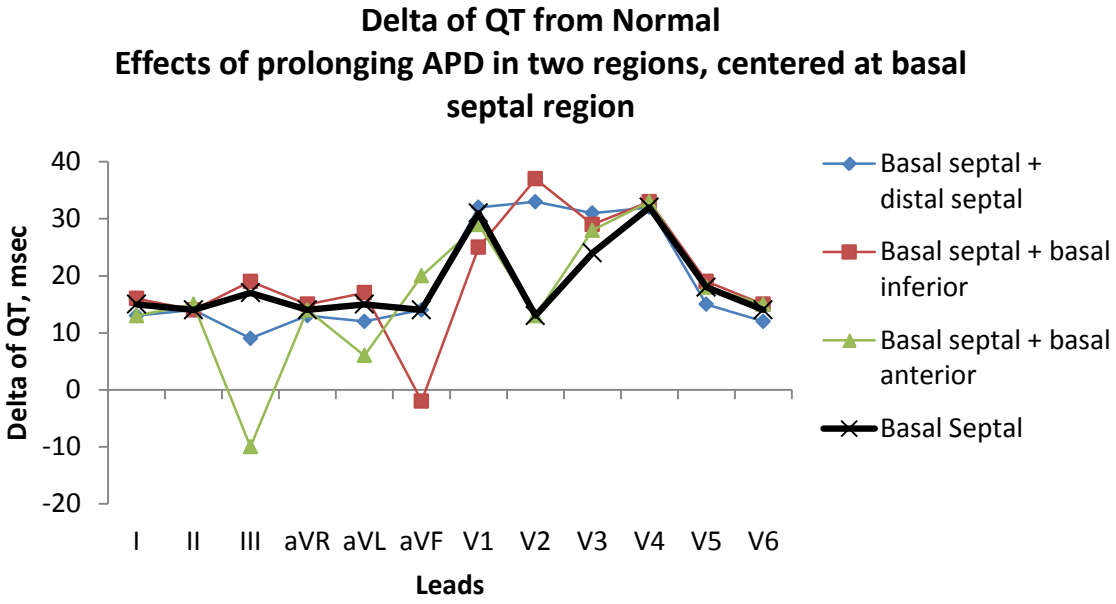

Figure 2.33 Delta of QT interval of 12 leads from the normal model, resulting from prolonging APD in two regions, extended from the basal septal region.

QT interval changes due to longer prolongation of APD in the basal septal region are shown in Figure 2.34. Additional prolongation of APD generated larger changes in QT interval in most leads.

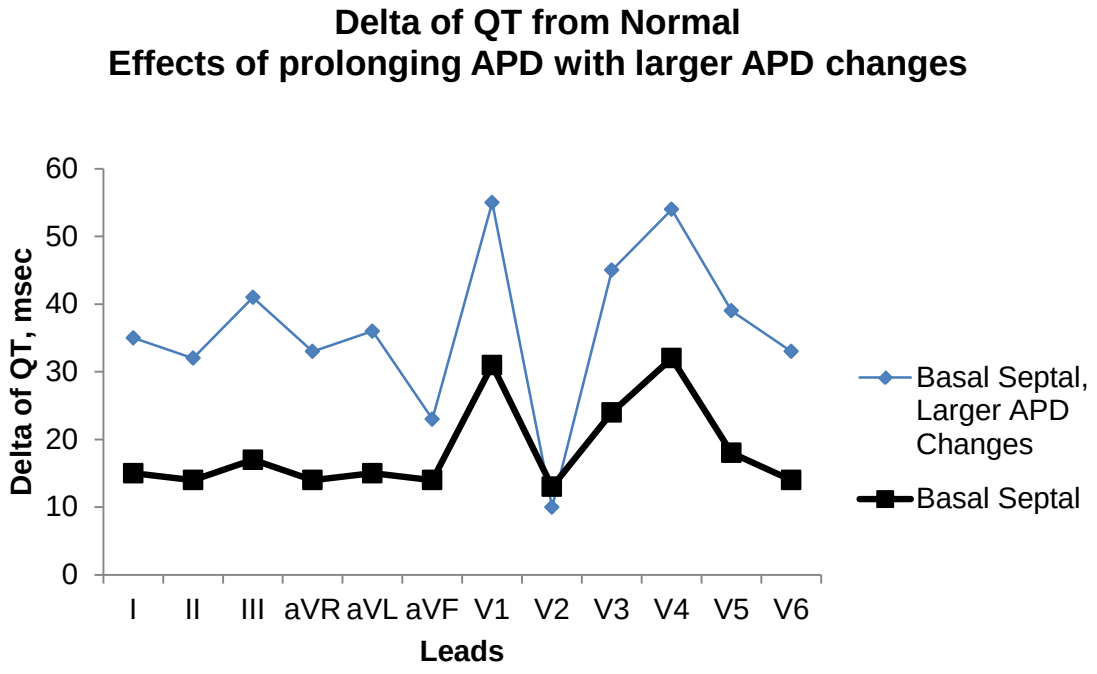

Figure 2.34 Delta of QT interval of 12 leads from thenormal model, resulting from prolonging APD with larger prolongation in the basal septal region.

Intracellular potential and dipoles in normal model and abnormal model. In order to verify the changes in the forward solution, the cardiac source of modified model with the chosen pattern was plotted against that of the normal model. The intracellular potentials of the nine transmural layers (from epicardium to endocardium) of the left ventricle of the normal model were shown at the top left side of Figure 2.35, Figure 2.36 and Figure 2.37, for different times. In order to show the septum, the right ventricle is not included. At the end of the QRS of the normal ECG, all cell elements were activated and intracellular potentials were homogeneous (Figure 2.35). At the peak of the T wave, intracellur potentials were inhomogenous, representing different stages of repolarization (Figure 2.36). At the end of the T wave, all cell elements were back to resting potentials (Figure 2.37). The intracellular potentials of the left ventricle of the abnormal model, obtained by prolonging APD in the basal septal region, are shown at the top right

side of Figure 2.35, Figure 2.36 and Figure 2.37, for different times. At the time of the end of the QRS of the normal ECG (Figure 2.35), all cell elements were activated, similar to those of the normal model. At the peak of the T wave (Figure 2.36), repolarizations were more heterogeneous, due to higher potentials in the basal septal region (red and orange areas). Unlike the normal model, the cell elements in the basal septal region were still repolarizing at the end of the T wave (Figure 2.36).

Dipoles and ECG of lateral leads of the normal heart model are also shown at the bottom of Figure 2.35, Figure 2.36 and Figure 2.37 for different times. Dipoles were estimated at every cell element as a source of the electrical field of the extracellular space, and were proportional to the differences of the intracullular potentials of its six neighbors. Similar to the dipoles shown in the movie ‘Heart Model and ECG’, the dipoles of one region were averaged and plotted as a green quiver located at the average of the coordinates of the cell elements in that region. The average dipole of all cell elements of the heart was plotted as a red quiver located at the average of the coordinates of all cell elements. The time at which these plots were made was marked on the ECG of the four lateral leads.

At the end of QRS, in the normal heart model, the dipoles were small in amplitude and almost invisible (Figure 2.35, bottom left). It was similar in the abnormal model (Figure 2.35, bottom right).

In the normal heart model, at the peak of the T wave, the major force of the heart model, reflected by the red quiver, pointed toward the lateral wall of left ventricle, generating positive T waves in lateral leads (Figure 2.36, bottom left). In the abnormal model, although the amplitude of the red quiver was larger, the direction was similar to that of the normal model, generating a more positive T wave (Figure 2.36, bottom right).

At the end of the T wave, in the normal heart model, the dipoles again were small in amplitude and almost invisible (Figure 2.37, bottom left). The

voltages of normal ECGs were close to zero. In the abnormal model, the major force was larger than that of the normal model, due to the repolarizing cell elements at the basal septal region (Figure 2.37, bottom right). The voltages of the abmormal ECGs were greater than zero.

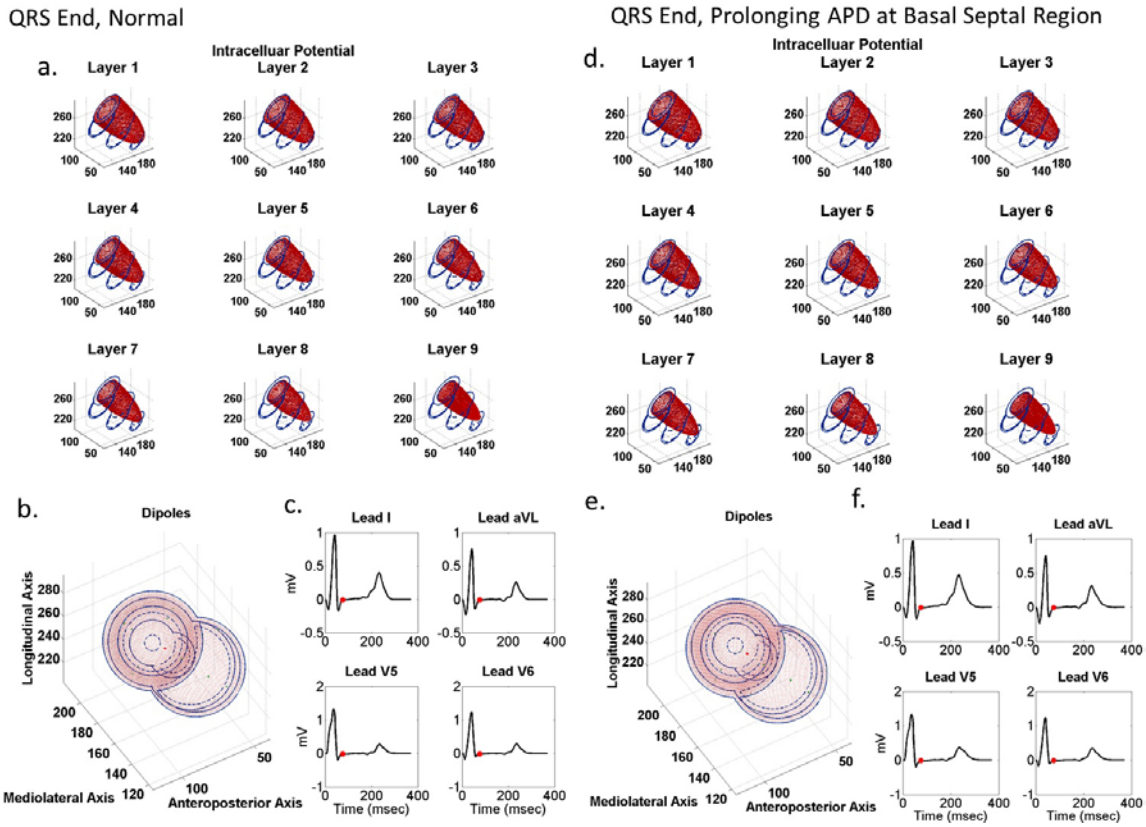

Figure 2.35 Intracellular potentials of nine transmural layers (from epicardium to endocardium), dipoles and the ECGs of lateral leads of the normal model (a, b, c, left) and the abnormal model, obtained by prolonging APD in the basal septal region (d, e, f, right) at the end of the QRS of normal ECG.

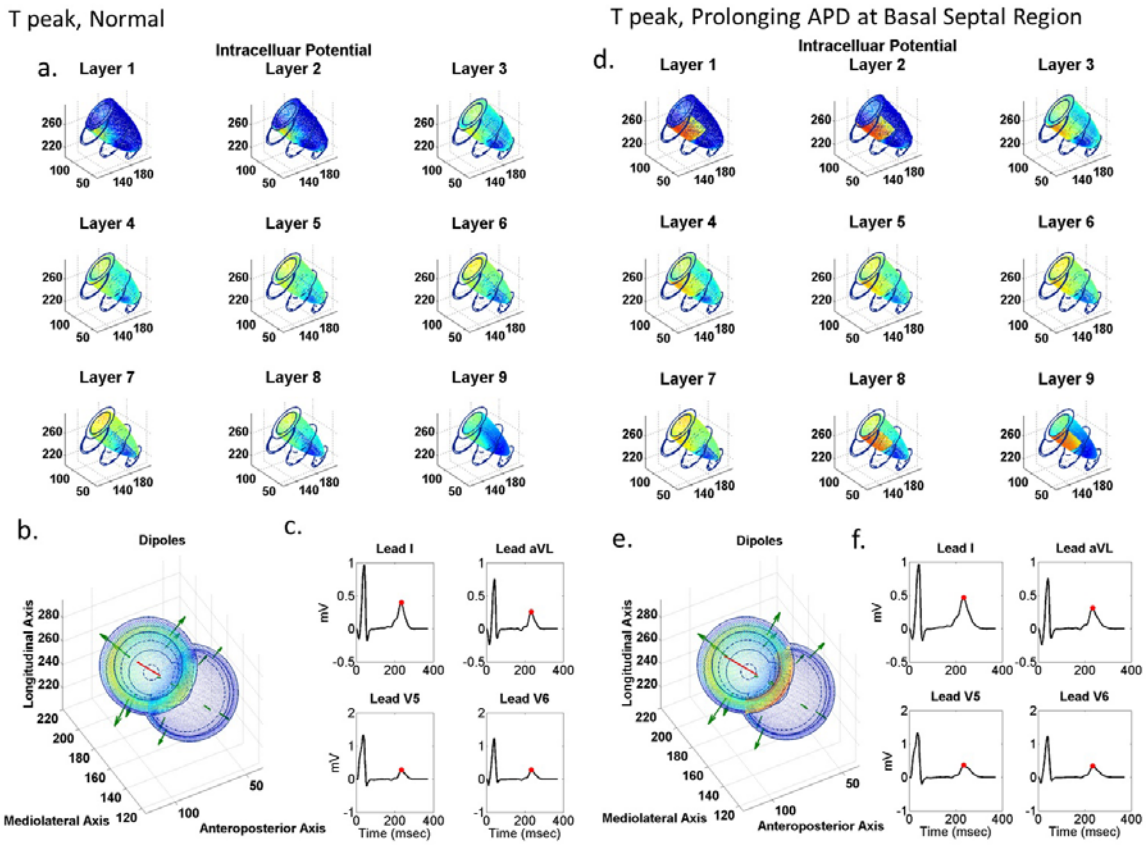

Figure 2.36 Intracellular potentials of nine transmural layers (from epicardium to endocardium), dipoles and the ECGs of lateral leads of the normal model (a, b, c left) and the abnormal model, obtained by prolonging APD in the basal septal region (d, e, f, right) at the peak of the T wave of normal ECG.

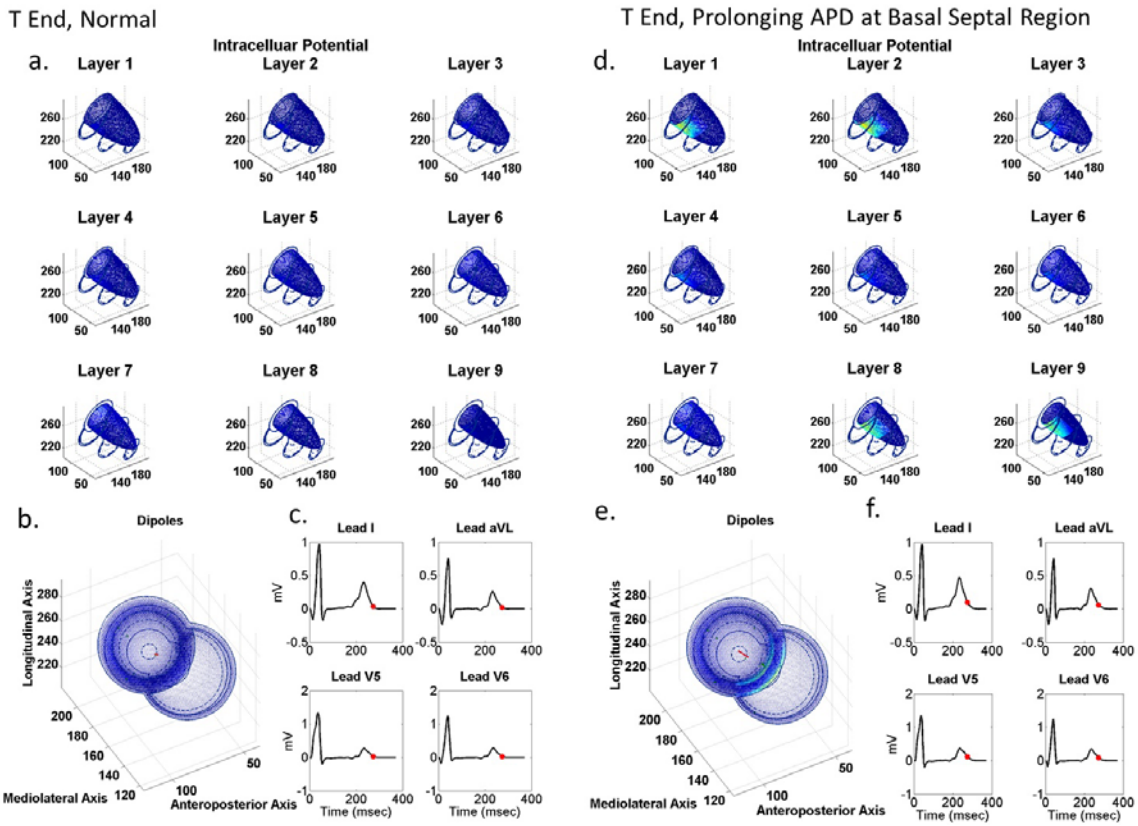

Figure 2.37 Intracellular potentials of nine transmural layers (from epicardium to endocardium), dipoles and the ECGs of lateral leads of the normal model (a, b, c left) and the abnormal model, obtained by prolonging APD in the basal septal region (d, e, f, right) at the end of the T wave of normal ECG.

2.5 Chapter Five: Discussion

2.5.1 QT Interval Changes in Diabetic Patients with Autonomic Neuropathy.

In this study, diabetic patients with severe neuropathy tended to have longer QTc intervals in lateral leads of 12-lead ECG, compared to those of able-bodied subjects.

It has been reported that diabetic patients with cardiovascular autonomic neuropathy, diagnosed by two abnormal results in cardiovascular reflex tests, had longer QTc interval than the control group (51, 83, 125). The association between QTc interval and the severity of autonomic neuropathy has also been reported (69, 83, 100). However, Gonin et al reported that 57% of the patients with cardiovascular autonomic neuropathy had a normal QTc interval (51). In those studies, the numbers of subjects were greater than that in our study, with the number of diabetic patients ranging from 73 to 266 patients. In addition, QTc interval was measured in one ECG lead in those studies. In contrast, in the present study, QTc intervals were also compared in regional leads recorded in the 12-lead ECG. This resulted in a more significant group difference in the minimum QTc interval of lateral leads when comparing diabetic patients with severe neuropathy to able-bodied subjects. Therefore, minimum QTc interval of lateral leads in 12-lead ECG may be more diagnostic that that of a single lead.

Veglio et al reported that, in 3,250 insulin-dependent diabetic patients, prolonged QTc interval, measured on V5 lead of resting ECG, was more prevalent in female subjects, resulting in longer QTc in female, than in male, subjects (126). However, in the same study, the relation between QTc prolongation and autonomic neuropathy was not observed among females although it was observed among males. In our study, diabetes without neuropathy were dominated by female subjects (5 of 6 subjects were female). Therefore, the tendency for diabetics without neuropathy to have longer QTc interval than diabetics with neuropathy may be due to this gender difference (Figure 2.38).

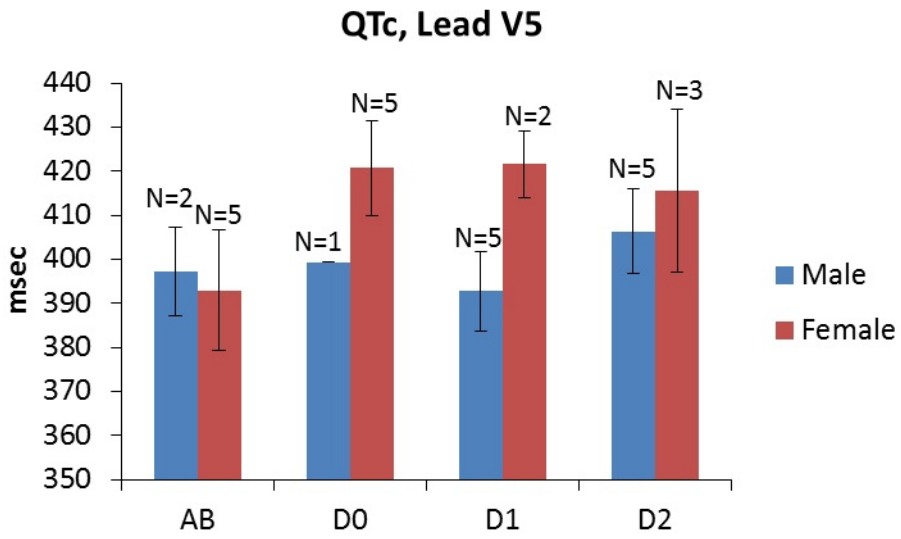

Figure 2.38 Gender differences in QTc interval of lead V5 for able-bodied subjects (AB), diabetics without neuropathy (D0), diabetics with mild neuropathy (D1) and diabetics with severe neuropathy (D2).

Conversely to prolongation of QTc interval, Ong et al reported a higher heart rate and shorter QTc interval in diabetic patients with autonomic neuropathy, diagnosed by reduced heart rate variability (98). However, different from our study, they recorded a much longer data record, one that lasted for 24 hours.

2.5.2 Regional Sympathetic Denervation to Left Ventricle in Diabetic Patients

In studies of MIBG-SPECG or HED-PET images, which reveal sympathetic innervation to the left ventricle, diabetic patients without or with mild autonomic neuropathy demonstrate low uptake of tracer in the posterior wall (112, 113), posterior-inferior wall (91), inferior wall (56, 93), distal inferior wall (123) and to a less extend, septal wall (114). In diabetic patients with autonomic neuropathy, the defects in these regions were more pronounced and extended to other areas (91, 93, 113, 123). It has also been reported that reduced uptake of tracer was observed in anterior, lateral and apical regions (75, 115). In addition,

Claus et al reported a lack of tracer activity in dorso-septal region in diabetic patients, within whom 79% had somatic polyneuropathy (22). The finding of a defect in the dorso-septal region agreed with the simulations of the present study. The similarity between the defect region in the study of Claus et al and this study may be due to a similar stage of neuropathy in both studies of diabetic patients with polyneuropathy.

2.5.3 Mechanisms of QT Interval Prolongation in Diabetic Neuropathy

This simulation study suggested that different patterns of regional prolongation of APD in the left ventricle caused changes in QT intervals of 12-lead ECG. It has been reported that regional defects in MIBG uptake was not correlated with QTc interval in diabetic patients (22, 112-114). However, in those studies, ECG was recorded in one lead. In fact, in the current simulation study, there were relatively smaller increases or even decreases in QT interval of lead II when prolonging APD. These results were seen in many patterns (for example, 1) those involving distal inferior, basal inferior, distal anterior, basal anterior, or basal lateral regions, 2) with complications of hyperinnervation in inferior, anterior or septal regions, and 3) in two regions involving distal inferior, basal inferior, distal anterior and distal septal regions). Therefore, QTc interval of lead II may not be reflective of most patterns of regional denervation. Another possibility is that QTc interval of lead II is reflective of a more severe autonomic neuropathy, since QT interval was correlated with abnormal results in cardiovascular reflex tests, which is known to represent a more severe neuropathy (49). In this simulation study, increases in APD prolongation led to increases in QT interval prolongation of lead II (Figure 2.34), although extension of affected area did not have an effect on lead II ECG (Figure 2.33).

2.5.4 Limitations

Movement of the heart during contraction and relaxation was not considered in this model, which may influence the results of the morphology of the modeled ECG. In addition, the lack of effects of muscle orientation on the

propagation of excitation, the simplicity of the structure of the ventricles, and the assumption of an homogeneous conductor in the torso may also explain differences in the detail of the morphology of the ECG and the QT interval pattern of 12 leads, between the model and able-bodied subjects. In addition, the lack of direct comparison of simulation results with individual cardiac denervation pattern from cardiac images limits the interpretation of results. However, this model demonstrates the feasibility of using forward and inverse solutions to detect cardiac sympathetic denervation.

2.6 Chapter Six: Conclusions

Diabetic patients with severe neuropathy tended to have longer QTc intervals in 12-lead ECG. The minimum QTc interval of lateral leads was more diagnostic than that from other leads. The change of QTc interval in diabetic patients with severe neuropathy compared to able-bodied subject may be due to a mechanism involving prolongation of APD at the basal septal region, due to cardiac sympathetic denervation.

2.7 Chapter Seven: Future Work

Validation studies need to be performed by collecting MIBG-SPECT images and QT intervals in 12-lead ECG in diabetic patients. Results from these data sets would be used to verify the model. In addition, the inverse solution from body surface potential acquired from more electrodes could provide the potential to locate cardiac sympathetic denervation, and thus provide a time efficient and cost effective method to detect cardiac denervation in diabetic patients. Finally, refining the model by adding complexity (for example, inhomogeneity of the torso or orientation of muscle fibers) may improve the similarity between the model and a real heart.

REFERENCES

1. *Comprehensive electrocardiology*. New York: Springer, 2010.

2. Aoki M, Okamoto Y, Musha T, and Harumi K. Three-dimensional simulation of the ventricular depolarization and repolarization processes and body surface potentials: normal heart and bundle branch block. *IEEE Trans Biomed Eng* 34: 454-462, 1987.

3. Armour JA, and Ardell JL. *Neurocardiology*. New York: Oxford University Press, 1994, p. xi, 443 p.

4. Armstrong RG, Seely AJ, Kilby D, Journeay WS, and Kenny GP. Cardiovascular and Thermal Responses to Repeated Head-Up Tilts Following Exercise-Induced Heat Stress. *Aviat Space Environ Med* 81: 646-653, 2010.

5. Aslan SC, Randall DC, Donohue KD, Knapp CF, Patwardhan AR, McDowell SM, Taylor RF, and Evans JM. Blood pressure regulation in neurally intact human vs. acutely injured paraplegic and tetraplegic patients during passive tilt. *Am J Physiol Regul Integr Comp Physiol* 292: R1146-1157, 2007.

6. Bailey JJ, Berson AS, Garson A, Jr., Horan LG, Macfarlane PW, Mortara DW, and Zywietz C. Recommendations for standardization and specifications in automated electrocardiography: bandwidth and digital signal processing. A report for health professionals by an ad hoc writing group of the Committee on Electrocardiography and Cardiac Electrophysiology of the Council on Clinical Cardiology, American Heart Association. *Circulation* 81: 730-739, 1990.

7. Barnett SR, Morin RJ, Kiely DK, Gagnon M, Azhar G, Knight EL, Nelson JC, and Lipsitz LA. Effects of age and gender on autonomic control of blood pressure dynamics. *Hypertension* 33: 1195-1200, 1999.

8. Bernardi L, Hayoz D, Wenzel R, Passino C, Calciati A, Weber R, and Noll G. Synchronous and baroceptor-sensitive oscillations in skin microcirculation: evidence for central autonomic control. *American Journal of Physiology - Heart and Circulatory Physiology* 273: H1867-H1878, 1997.

9. Bernardi L, Radaelli A, Solda PL, Coats AJ, Reeder M, Calciati A, Garrard CS, and Sleight P. Autonomic control of skin microvessels: assessment by power

spectrum of photoplethysmographic waves. *Clinical science (London, England : 1979)* 90: 345-355, 1996.

10. Bernardi L, Rossi M, Fratino P, Finardi G, Mevio E, and Orlandi C. Relationship between phasic changes in human skin blood flow and autonomic tone. *Microvascular Research* 37: 16-27, 1989.

11. Bernardi L, Rossi M, Leuzzi S, Mevio E, Fornasari G, Calciati A, Orlandi C, and Fratino P. Reduction of 0.1 Hz microcirculatory fluctuations as evidence of sympathetic dysfunction in insulin-dependent diabetes. *Cardiovascular Research* 34: 185-191, 1997.

12. Bertinieri G, di Rienzo M, Cavallazzi A, Ferrari AU, Pedotti A, and Mancia G. A new approach to analysis of the arterial baroreflex. *J Hypertens Suppl* 3: S79-81, 1985.

13. BOURGEOIS MJ, GILBERT BK, DONALD DE, and WOOD EH. Characteristics of Aortic Diastolic Pressure Decay with Application to the Continuous Monitoring of Changes in Peripheral Vascular Resistance. *Circulation Research* 35: 56-66, 1974.

14. Brown DR, Brown LV, Patwardhan A, and Randall DC. Sympathetic activity and blood pressure are tightly coupled at 0.4 Hz in conscious rats. *Am J Physiol* 267: R1378-1384, 1994.

15. Brown DR, Cassis LA, Silcox DL, Brown LV, and Randall DC. Empirical and theoretical analysis of the extremely low frequency arterial blood pressure power spectrum in unanesthetized rat. *American Journal of Physiology - Heart and Circulatory Physiology* 291: H2816-H2824, 2006.

16. Butler GC, Yamamoto Y, Xing HC, Northey DR, and Hughson RL. Heart rate variability and fractal dimension during orthostatic challenges. *J Appl Physiol* 75: 2602-2612, 1993.

17. Cardoso CR, Salles GF, and Deccache W. Prognostic value of QT interval parameters in type 2 diabetes mellitus: results of a long-term follow-up prospective study. *J Diabetes Complications* 17: 169-178, 2003.

18. Cavaletti G, Bogliun G, Marzorati L, Zincone A, Piatti M, Colombo N, Parma G, Lissoni A, Fei F, Cundari S, and Zanna C. Grading of chemotherapy-

induced peripheral neurotoxicity using the Total Neuropathy Scale. *Neurology* 61: 1297-1300, 2003.

19. Cerutti C, Barres C, and Paultre C. Baroreflex modulation of blood pressure and heart rate variabilities in rats: assessment by spectral analysis. *Am J Physiol* 266: H1993-2000, 1994.

20. Chang AT, Boots RJ, Brown MG, Paratz JD, and Hodges PW. Ventilatory changes following head-up tilt and standing in healthy subjects. *Eur J Appl Physiol* 95: 409-417, 2005.

21. Charkoudian N. Skin blood flow in adult human thermoregulation: how it works, when it does not, and why. *Mayo Clin Proc* 78: 603-612, 2003.

22. Claus D, Meudt O, Rozeik C, Engelmann-Kempe K, Huppert PE, and Wietholtz H. Prospective investigation of autonomic cardiac neuropathy in diabetes mellitus. *Clin Auton Res* 12: 373-378, 2002.

23. Colantuoni A, Bertuglia S, and Intaglietta M. Microvascular vasomotion: origin of laser Doppler flux motion. *International journal of microcirculation, clinical and experimental / sponsored by the European Society for Microcirculation* 14: 151-158, 1994.

24. Combe H, Bauduceau B, Chanudet X, Chau NP, Rabasa R, Meyer L, Mayaudon H, Larroque P, and Gautier D. [Cardiovascular autonomic neuropathy and blood pressure variability in insulin-dependent diabetes]. *Arch Mal Coeur Vaiss* 86: 1149-1152, 1993.

25. Cooke WH, Rickards CA, Ryan KL, Kuusela TA, and Convertino VA. Muscle sympathetic nerve activity during intense lower body negative pressure to presyncope in humans. *J Physiol* 587: 4987-4999, 2009.

26. Crick SJ, Anderson RH, Ho SY, and Sheppard MN. Localisation and quantitation of autonomic innervation in the porcine heart II: endocardium, myocardium and epicardium. *Journal of anatomy* 195 (Pt 3): 359-373, 1999.

27. de Sousa MR, Huikuri HV, Lombardi F, Perez AA, Gomes ME, Barros MV, Barros VC, Rocha MO, and Ribeiro AL. Abnormalities in fractal heart rate dynamics in Chagas disease. *Ann Noninvasive Electrocardiol* 11: 145-153, 2006.

28. Di Flaviani A, Picconi F, Di Stefano P, Giordani I, Malandrucco I, Maggio P, Palazzo P, Sgreccia F, Peraldo C, Farina F, Frajese G, and Frontoni S. Impact of Glycemic and Blood Pressure Variability on Surrogate Measures of Cardiovascular Outcomes in Type 2 Diabetic Patients. *Diabetes Care* 2011.
29. Di Rienzo M, Castiglioni P, Parati G, Mancia G, and Pedotti A. Effects of sino-aortic denervation on spectral characteristics of blood pressure and pulse interval variability: a wide-band approach. *Medical and Biological Engineering and Computing* 34: 133-141, 1996.
30. Di Rienzo M, Parati G, Castiglioni P, Omboni S, Ferrari AU, Ramirez AJ, Pedotti A, and Mancia G. Role of sinoaortic afferents in modulating BP and pulse-interval spectral characteristics in unanesthetized cats. *American Journal of Physiology - Heart and Circulatory Physiology* 261: H1811-H1818, 1991.
31. Di Rienzo M, Parati G, Castiglioni P, Tordi R, Mancia G, and Pedotti A. Baroreflex effectiveness index: an additional measure of baroreflex control of heart rate in daily life. *Am J Physiol Regul Integr Comp Physiol* 280: R744-751, 2001.
32. Ducher M, Cerutti C, Gustin MP, Abou-Amara S, Thivolet C, Laville M, Paultre CZ, and Fauvel JP. Noninvasive exploration of cardiac autonomic neuropathy. Four reliable methods for diabetes? *Diabetes Care* 22: 388-393, 1999.
33. Durrer D, van Dam RT, Freud GE, Janse MJ, Meijler FL, and Arzbaecher RC. Total excitation of the isolated human heart. *Circulation* 41: 899-912, 1970.
34. Eke A, Herman P, Kocsis L, and Kozak LR. Fractal characterization of complexity in temporal physiological signals. *Physiol Meas* 23: R1-38, 2002.
35. England JD, Gronseth GS, Franklin G, Miller RG, Asbury AK, Carter GT, Cohen JA, Fisher MA, Howard JF, Kinsella LJ, Latov N, Lewis RA, Low PA, and Sumner AJ. Distal symmetric polyneuropathy: a definition for clinical research: report of the American Academy of Neurology, the American Association of Electrodiagnostic Medicine, and the American Academy of Physical Medicine and Rehabilitation. *Neurology* 64: 199-207, 2005.

36. Evans JM, Leonelli FM, Ziegler MG, McIntosh CM, Patwardhan AR, Ertl AC, Kim CS, and Knapp CF. Epinephrine, vasodilation and hemoconcentration in syncopal, healthy men and women. *Auton Neurosci* 93: 79-90, 2001.
37. Evans JM, Ziegler MG, Patwardhan AR, Ott JB, Kim CS, Leonelli FM, and Knapp CF. Gender differences in autonomic cardiovascular regulation: spectral, hormonal, and hemodynamic indexes. *J Appl Physiol* 91: 2611-2618, 2001.
38. Ewing D, Boland O, Neilson J, Cho C, and Clarke B. Autonomic neuropathy, QT interval lengthening, and unexpected deaths in male diabetic patients. *Diabetologia* 34: 182-185, 1991.
39. Ewing DJ, and Clarke BF. Diagnosis and management of diabetic autonomic neuropathy. *Br Med J (Clin Res Ed)* 285: 916-918, 1982.
40. Fallouh HB, Bardswell SC, McLatchie LM, Shattock MJ, Chambers DJ, and Kentish JC. Esmolol cardioplegia: the cellular mechanism of diastolic arrest. *Cardiovascular Research* 87: 552-560, 2010.
41. Farina D, and Dossel O. Model-based approach to the localization of infarction. In: *Computers in Cardiology, 2007*IEEE, 2007, p. 173-176.
42. Foo JY, and Lim CS. Dual-channel photoplethysmography to monitor local changes in vascular stiffness. *J Clin Monit Comput* 20: 221-227, 2006.
43. Frattola A, Parati G, Castiglioni P, Paleari F, Ulian L, Rovaris G, Mauri G, Di Rienzo M, and Mancia G. Lacidipine and Blood Pressure Variability in Diabetic Hypertensive Patients. *Hypertension* 36: 622-628, 2000.
44. Frattola A, Parati G, Gamba P, Paleari F, Mauri G, Di Rienzo M, Castiglioni P, and Mancia G. Time and frequency domain estimates of spontaneous baroreflex sensitivity provide early detection of autonomic dysfunction in diabetes mellitus. *Diabetologia* 40: 1470-1475, 1997.
45. Freeman R, Saul JP, Roberts MS, Berger RD, Broadbridge C, and Cohen RJ. Spectral analysis of heart rate in diabetic autonomic neuropathy. A comparison with standard tests of autonomic function. *Arch Neurol* 48: 185-190, 1991.

46. Fu Q, Shook RP, Okazaki K, Hastings JL, Shibata S, Conner CL, Palmer MD, and Levine BD. Vasomotor sympathetic neural control is maintained during sustained upright posture in humans. *J Physiol* 577: 679-687, 2006.
47. Furlan R, Porta A, Costa F, Tank J, Baker L, Schiavi R, Robertson D, Malliani A, and Mosqueda-Garcia R. Oscillatory patterns in sympathetic neural discharge and cardiovascular variables during orthostatic stimulus. *Circulation* 101: 886-892, 2000.
48. Ghosh S, Rhee EK, Avari JN, Woodard PK, and Rudy Y. Cardiac memory in patients with Wolff-Parkinson-White syndrome: noninvasive imaging of activation and repolarization before and after catheter ablation. *Circulation* 118: 907-915, 2008.
49. Giordano A, Calcagni ML, Verrillo A, Pellegrinotti M, Frontoni S, Spallone V, and Gambardella S. Assessment of sympathetic innervation of the heart in diabetes mellitus using 123I-MIBG. *Diabetes Nutr Metab* 13: 350-355, 2000.
50. Goldberger AL, and West BJ. Fractals in physiology and medicine. *Yale J Biol Med* 60: 421-435, 1987.
51. Gonin JM, Kadrofske MM, Schmaltz S, Bastyr EJ, and Vinik AI. Corrected Q-T Interval Prolongation as Diagnostic Tool for Assessment of Cardiac Autonomic Neuropathy in Diabetes Mellitus. *Diabetes Care* 13: 68-71, 1990.
52. Gregoire J, Tuck S, Yamamoto Y, and Hughson RL. Heart rate variability at rest and exercise: influence of age, gender, and physical training. *Can J Appl Physiol* 21: 455-470, 1996.
53. Gulrajani RM. The forward and inverse problems of electrocardiography. *IEEE engineering in medicine and biology magazine : the quarterly magazine of the Engineering in Medicine & Biology Society* 17: 84-101, 122, 1998.
54. Hage FG, and Iskandrian AE. Cardiac autonomic denervation in diabetes mellitus. *Circulation Cardiovascular imaging* 4: 79-81, 2011.
55. Hattori N, Rihl J, Bengel FM, Nekolla SG, Standl E, Schwaiger M, and Schnell O. Cardiac autonomic dysinnervation and myocardial blood flow in long-term Type 1 diabetic patients. *Diabetic Medicine* 20: 375-381, 2003.

56. Hattori N, Tamaki N, Hayashi T, Masuda I, Kudoh T, Tateno M, Tadamura E, Yonekura Y, Nakao K, and Konishi J. Regional abnormality of iodine-123-MIBG in diabetic hearts. *Journal of nuclear medicine : official publication, Society of Nuclear Medicine* 37: 1985-1990, 1996.

57. Hertzman AB, Randall WC, Peiss CN, and Seckendorf R. Regional rates of evaporation from the skin at various environmental temperatures. *J Appl Physiol* 5: 153-161, 1952.

58. Hodges GJ, and Johnson JM. Adrenergic control of the human cutaneous circulation. *Applied Physiology, Nutrition, and Metabolism* 34: 829-839, 2009.

59. Holowatz LA. Sex differences in the control of acral skin blood flow in humans: differential regulation of cyclooxygenase in alpha-adrenergic signalling. *J Physiol* 589: 5017, 2011.

60. Howorka K, Pumprla J, and Schabmann A. Optimal parameters of short-term heart rate spectrogram for routine evaluation of diabetic cardiovascular autonomic neuropathy. *J Auton Nerv Syst* 69: 164-172, 1998.

61. Ishaque MR, Ahmed SA, and Abid I. Comparison of the ambulatory blood pressure variability in diabetic hypertensive and non diabetic hypertensive patients. *Ann Pak Inst Med Sci* 5: 174-177, 2009.

62. Jepsen H, and Gaehtgens P. Postural vascular response vs. sympathetic vasoconstriction in human skin during orthostasis. *American Journal of Physiology - Heart and Circulatory Physiology* 269: H53-H61, 1995.

63. Ji S, and Travin M. Radionuclide imaging of cardiac autonomic innervation. *Journal of Nuclear Cardiology* 17: 655-666, 2010.

64. Johansson M, Gao SA, Friberg P, Annerstedt M, Bergstrom G, Carlstrom J, Ivarsson T, Jensen G, Ljungman S, Mathillas O, Nielsen FD, and Strombom U. Reduced baroreflex effectiveness index in hypertensive patients with chronic renal failure. *Am J Hypertens* 18: 995-1000; discussion 1016, 2005.

65. Johnson JM, Pergola PE, Liao FK, Kellogg DL, and Crandall CG. Skin of the dorsal aspect of human hands and fingers possesses an active vasodilator system. *Journal of Applied Physiology* 78: 948-954, 1995.

66. Kamath GS, and Mittal S. The Role of Antiarrhythmic Drug Therapy for the Prevention of Sudden Cardiac Death. *Progress in Cardiovascular Diseases* 50: 439-448, 2008.
67. Kardos A, Rudas L, Simon J, Gingl Z, and Csanady M. Effect of postural changes on arterial baroreflex sensitivity assessed by the spontaneous sequence method and Valsalva manoeuvre in healthy subjects. *Clin Auton Res* 7: 143-148, 1997.
68. Keller DU, Seemann G, Weiss DL, Farina D, Zehelein J, and Dossel O. Computer based modeling of the congenital long-QT 2 syndrome in the Visible Man torso: from genes to ECG. *Conf Proc IEEE Eng Med Biol Soc* 2007: 1410-1413, 2007.
69. Kempler P, Varadi A, Szalay F, and Tamas G. Autonomic neuropathy and corrected QT interval prolongation. There is a relationship. *Diabetes Care* 17: 454-456, 1994.
70. Kikuya M, Hozawa A, Ohokubo T, Tsuji I, Michimata M, Matsubara M, Ota M, Nagai K, Araki T, Satoh H, Ito S, Hisamichi S, and Imai Y. Prognostic Significance of Blood Pressure and Heart Rate Variabilities : The Ohasama Study. *Hypertension* 36: 901-906, 2000.
71. Kilpatrick ES, Rigby AS, and Atkin SL. The Role of Blood Pressure Variability in the Development of Nephropathy in Type 1 Diabetes. *Diabetes Care* 33: 2442-2447, 2010.
72. Krause M, Rudiger H, Bald M, Nake A, and Paditz E. Autonomic blood pressure control in children and adolescents with type 1 diabetes mellitus. *Pediatr Diabetes* 10: 255-263, 2009.
73. Krishnamurthy S, Wang X, Bhakta D, Bruce E, Evans J, Justice T, and Patwardhan A. Dynamic cardiorespiratory interaction during head-up tilt-mediated presyncope. *Am J Physiol Heart Circ Physiol* 287: H2510-2517, 2004.
74. Langen KJ, Ziegler D, Weise F, Piolot R, Boy C, Hubinger A, Gries FA, and Muller-Gartner HW. Evaluation of QT interval length, QT dispersion and myocardial m-iodobenzylguanidine uptake in insulin-dependent diabetic patients with and without autonomic neuropathy. *Clin Sci (Lond)* 93: 325-333, 1997.

75. Langer A, Freeman MR, Josse RG, and Armstrong PW. Metaiodobenzylguanidine imaging in diabetes mellitus: Assessment of cardiac sympathetic denervation and its relation to autonomic dysfunction and silent myocardial ischemia. *Journal of the American College of Cardiology* 25: 610-618, 1995.
76. Langley P, Smith FE, King ST, Zheng D, Haigh AJ, and Murray A. Fully automated computer measurement of QT interval from the 12-lead electrocardiogram. In: *Computers in Cardiology, 2006*2006, p. 345-348.
77. Leahy MJ, de Mul FF, Nilsson GE, and Maniewski R. Principles and practice of the laser-Doppler perfusion technique. *Technol Health Care* 7: 143-162, 1999.
78. Leonelli FM, Wang K, Evans JM, Patwardhan AR, Ziegler MG, Natale A, Kim CS, Rajikovich K, and Knapp CF. False positive head-up tilt: hemodynamic and neurohumoral profile. *J Am Coll Cardiol* 35: 188-193, 2000.
79. Levick JR. *An introduction to cardiovascular physiology*. London, New York: Arnold; Distributed in the United States of America by Oxford University Press, 2003, p. 265 p.
80. Liao D, Barnes RW, Chambless LE, Simpson RJ, Jr., Sorlie P, and Heiss G. Age, race, and sex differences in autonomic cardiac function measured by spectral analysis of heart rate variability--the ARIC study. Atherosclerosis Risk in Communities. *Am J Cardiol* 76: 906-912, 1995.
81. Linnemann B, and Janka HU. Prolonged QTc interval and elevated heart rate identify the type 2 diabetic patient at high risk for cardiovascular death. The Bremen Diabetes Study. *Exp Clin Endocrinol Diabetes* 111: 215-222, 2003.
82. Malik M, and Batchvarov VN. Measurement, interpretation and clinical potential of QT dispersion. *J Am Coll Cardiol* 36: 1749-1766, 2000.
83. Matel D, Chiochina AD, and Stratone A. [Utility of QTc interval for the diagnosis of cardiac autonomic neuropathy in type 2 diabetes mellitus]. *Rev Med Chir Soc Med Nat Iasi* 114: 282-286, 2010.
84. Meendering JR, Torgrimson BN, Houghton BL, Halliwill JR, and Minson CT. Menstrual cycle and sex affect hemodynamic responses to combined

orthostatic and heat stress. *Am J Physiol Heart Circ Physiol* 289: H631-642, 2005.

85. Meyer MF, Rose CJ, Hülsmann JO, Schatz H, and Pfohl M. Impaired 0.1-Hz vasomotion assessed by laser Doppler anemometry as an early index of peripheral sympathetic neuropathy in diabetes. *Microvascular Research* 65: 88-95, 2003.

86. Miller WT, and Geselowitz DB. Simulation studies of the electrocardiogram. I. The normal heart. *Circ Res* 43: 301-315, 1978.

87. Mokhtar RH, Ayob A, and Mohd Noor N. Blood Pressure Variability in Patients with Diabetes Mellitus. *Asian Cardiovasc Thorac Ann* 18: 344-348, 2010.

88. Morillo CA, Eckberg DL, Ellenbogen KA, Beightol LA, Hoag JB, Tahvanainen KUO, Kuusela TA, and Diedrich AM. Vagal and Sympathetic Mechanisms in Patients With Orthostatic Vasovagal Syncope. *Circulation* 96: 2509-2513, 1997.

89. Morita ST, Zipes DP, Morita H, and Wu J. Analysis of action potentials in the canine ventricular septum: no phenotypic expression of M cells. *Cardiovasc Res* 74: 96-103, 2007.

90. Naas AA, Davidson NC, Thompson C, Cummings F, Ogston SA, Jung RT, Newton RW, and Struthers AD. QT and QTc dispersion are accurate predictors of cardiac death in newly diagnosed non-insulin dependent diabetes: cohort study. *BMJ* 316: 745-746, 1998.

91. Nagamachi S, Hoshi H, Ohnishi T, Jinnouchi S, Futami S, Watanabe K, Nakatsuru K, Toshimori T, and Matsukura S. [123I-MIBG myocardial scintigraphy in diabetic patients: association with autonomic neuropathy]. *Kaku Igaku* 31: 1059-1069, 1994.

92. Nagamachi S, Jinnouchi S, Kurose T, Ohnishi T, Flores LG, 2nd, Nakahara H, Futami S, Tamura S, and Matsukura S. 123I-MIBG myocardial scintigraphy in diabetic patients: relationship with 201Tl uptake and cardiac autonomic function. *Ann Nucl Med* 12: 323-331, 1998.

93. Nagamachi S, Jinnouchi S, Nakahara H, Flores LG, 2nd, Ohnishi T, Hoshi H, Futami S, Watanabe K, Nakatsuru K, Toshimori T, and Matsukura S. 123I-

MIBG myocardial scintigraphy in diabetic patients: relationship to autonomic neuropathy. *Nucl Med Commun* 17: 621-632, 1996.

94. Norman AE. *12 Lead ECG Interpretation: A Self-teaching Manual*. McGraw-Hill, 1992.

95. O'Leary DD, Kimmerly DS, Cechetto AD, and Shoemaker JK. Differential effect of head-up tilt on cardiovagal and sympathetic baroreflex sensitivity in humans. *Exp Physiol* 88: 769-774, 2003.

96. O'Leary DD, Lin DC, and Hughson RL. Determination of baroreflex gain using auto-regressive moving-average analysis during spontaneous breathing. *Clin Physiol* 19: 369-377, 1999.

97. Omboni S, Parati G, Di Rienzo M, Wieling W, and Mancia G. Blood pressure and heart rate variability in autonomic disorders: a critical review. *Clin Auton Res* 6: 171-182, 1996.

98. Ong JJ, Sarma JS, Venkataraman K, Levin SR, and Singh BN. Circadian rhythmicity of heart rate and QTc interval in diabetic autonomic neuropathy: implications for the mechanism of sudden death. *Am Heart J* 125: 744-752, 1993.

99. Pagani M, Malfatto G, Pierini S, Casati R, Masu AM, Poli M, Guzzetti S, Lombardi F, Cerutti S, and Malliani A. Spectral analysis of heart rate variability in the assessment of autonomic diabetic neuropathy. *J Auton Nerv Syst* 23: 143-153, 1988.

100. Pappachan JM, Sebastian J, Bino BC, Jayaprakash K, Vijayakumar K, Sujathan P, and Adinegara LA. Cardiac autonomic neuropathy in diabetes mellitus: prevalence, risk factors and utility of corrected QT interval in the ECG for its diagnosis. *Postgrad Med J* 84: 205-210, 2008.

101. Parati G, Saul JP, Di Rienzo M, and Mancia G. Spectral analysis of blood pressure and heart rate variability in evaluating cardiovascular regulation. A critical appraisal. *Hypertension* 25: 1276-1286, 1995.

102. Patwardhan AR, Vallurupalli S, Evans JM, Bruce EN, and Knapp CF. Override of spontaneous respiratory pattern generator reduces cardiovascular parasympathetic influence. *J Appl Physiol* 79: 1048-1054, 1995.

103. Peralta AO, John RM, Gaasch WH, Taggart PI, Martin DT, and Venditti FJ. The class III antiarrhythmic effect of sotalol exerts a reverse use-dependent positive inotropic effect in the intact canine heart. *Journal of the American College of Cardiology* 36: 1404-1410, 2000.
104. Philip J. Weston MAJ, Ronnie B. Panerai, Paul G. McNally, John F. Potter and Herbert Thurston. Evidence of defective cardiovascular regulation in insulin-dependent diabetic patients without clinical autonomic dysfunction. *Diabetes Research and Clinical Practice* 42: 141-148, 1998.
105. Plonsey R, and Fleming DG. *Bioelectric phenomena*. New York,: McGraw-Hill, 1969, p. xiv, 380 p.
106. Rana BS, Lim PO, Naas AA, Ogston SA, Newton RW, Jung RT, Morris AD, and Struthers AD. QT interval abnormalities are often present at diagnosis in diabetes and are better predictors of cardiac death than ankle brachial pressure index and autonomic function tests. *Heart* 91: 44-50, 2005.
107. Ribeiro AL, Lombardi F, Sousa MR, Lins Barros MV, Porta A, Costa Val Barros V, Gomes ME, Santana Machado F, and Otavio Costa Rocha M. Power-law behavior of heart rate variability in Chagas' disease. *Am J Cardiol* 89: 414-418, 2002.
108. Rossing P, Breum L, Major-Pedersen A, Sato A, Winding H, Pietersen A, Kastrup J, and Parving HH. Prolonged QTc interval predicts mortality in patients with Type 1 diabetes mellitus. *Diabet Med* 18: 199-205, 2001.
109. Rowell LB. *Human cardiovascular control*. New York: Oxford University Press, 1993, p. xv, 500 p.
110. Ruiz J, Monbaron D, Parati G, Perret S, Haesler E, Danzeisen C, and Hayoz D. Diabetic Neuropathy Is a More Important Determinant of Baroreflex Sensitivity Than Carotid Elasticity in Type 2 Diabetes. *Hypertension* 46: 162-167, 2005.
111. Sagawa S, Shiraki K, Miki K, and Tajima F. Cardiovascular responses to upright tilt at a simulated altitude of 3,700 m in men. *Aviat Space Environ Med* 64: 219-223, 1993.

112. Schnell O, Hammer K, Muhr-Becker D, Ziegler A, Weiss M, Tatsch K, and Standl E. Cardiac sympathetic dysinnervation in Type 2 diabetes mellitus with and without ECG-based cardiac autonomic neuropathy. *J Diabetes Complications* 16: 220-227, 2002.
113. Schnell O, Kirsch CM, Stemplinger J, Haslbeck M, and Standl E. Scintigraphic evidence for cardiac sympathetic dysinnervation in long-term IDDM patients with and without ECG-based autonomic neuropathy. *Diabetologia* 38: 1345-1352, 1995.
114. Schnell O, Muhr D, Weiss M, Dresel S, Haslbeck M, and Standl E. Reduced myocardial 123I-metaiodobenzylguanidine uptake in newly diagnosed IDDM patients. *Diabetes* 45: 801-805, 1996.
115. Scholte AJ, Schuijf JD, Delgado V, Kok JA, Bus MT, Maan AC, Stokkel MP, Kharagitsingh AV, Dibbets-Schneider P, van der Wall EE, and Bax JJ. Cardiac autonomic neuropathy in patients with diabetes and no symptoms of coronary artery disease: comparison of 123I-metaiodobenzylguanidine myocardial scintigraphy and heart rate variability. *Eur J Nucl Med Mol Imaging* 37: 1698-1705, 2010.
116. Scott LA, and Kench PL. Cardiac autonomic neuropathy in the diabetic patient: does 123I-MIBG imaging have a role to play in early diagnosis? *Journal of nuclear medicine technology* 32: 66-71, 2004.
117. Shibasaki M, Davis SL, Cui J, Low DA, Keller DM, Durand S, and Crandall CG. Neurally mediated vasoconstriction is capable of decreasing skin blood flow during orthostasis in the heat-stressed human. *J Physiol* 575: 953-959, 2006.
118. Sicouri S, Fish J, and Antzelevitch C. Distribution of M cells in the canine ventricle. *J Cardiovasc Electrophysiol* 5: 824-837, 1994.
119. Stansberry KB, Shapiro SA, Hill MA, McNitt PM, Meyer MD, and Vinik AI. Impaired Peripheral Vasomotion in Diabetes. *Diabetes Care* 19: 715-721, 1996.
120. Stauss HM, Anderson EA, Haynes WG, and Kregel KC. Frequency response characteristics of sympathetically mediated vasomotor waves in humans. *American Journal of Physiology - Heart and Circulatory Physiology* 274: H1277-H1283, 1998.

121. Stemper B, Bernardi L, Axelrod FB, Welsch G, Passino C, and Hilz MJ. Sympathetic and parasympathetic baroreflex dysfunction in familial dysautonomia. *Neurology* 63: 1427-1431, 2004.
122. Stevens MJ. New imaging techniques for cardiovascular autonomic neuropathy: a window on the heart. *Diabetes Technol Ther* 3: 9-22, 2001.
123. Stevens MJ, Raffel DM, Allman KC, Dayanikli F, Ficaro E, Sandford T, Wieland DM, Pfeifer MA, and Schwaiger M. Cardiac sympathetic dysinnervation in diabetes: implications for enhanced cardiovascular risk. *Circulation* 98: 961-968, 1998.
124. Sundkvist G. Autonomic nervous function in asymptomatic diabetic patients with signs of peripheral neuropathy. *Diabetes Care* 4: 529-534, 1981.
125. Tentolouris N, Katsilambros N, Papazachos G, Papadogiannis D, Linos A, Stamboulis E, and Papageorgiou K. Corrected QT interval in relation to the severity of diabetic autonomic neuropathy. *Eur J Clin Invest* 27: 1049-1054, 1997.
126. Veglio M, Borra M, Stevens LK, Fuller JH, and Perin PC. The relation between QTc interval prolongation and diabetic complications. The EURODIAB IDDM Complication Study Group. *Diabetologia* 42: 68-75, 1999.
127. Veglio M, Sivieri R, Chinaglia A, Scaglione L, and Cavallo-Perin P. QT interval prolongation and mortality in type 1 diabetic patients: a 5-year cohort prospective study. Neuropathy Study Group of the Italian Society of the Study of Diabetes, Piemonte Affiliate. *Diabetes Care* 23: 1381-1383, 2000.
128. Vinik AI, and Erbas T. Cardiovascular autonomic neuropathy: diagnosis and management. *Curr Diab Rep* 6: 424-430, 2006.
129. Vinik AI, and Erbas T. Recognizing and treating diabetic autonomic neuropathy. *Cleve Clin J Med* 68: 928-930, 932, 934-944, 2001.
130. Vinik AI, Maser RE, Mitchell BD, and Freeman R. Diabetic autonomic neuropathy. *Diabetes Care* 26: 1553-1579, 2003.
131. Vinik AI, and Mehrabyan A. Diagnosis and management of diabetic autonomic neuropathy. *Compr Ther* 29: 130-145, 2003.

132. Wagner CD, Mrowka R, Nafz B, and Persson PB. Complexity and "chaos" in blood pressure after baroreceptor denervation of conscious dogs. *Am J Physiol* 269: H1760-1766, 1995.
133. Wagner CD, and Persson PB. Two ranges in blood pressure power spectrum with different 1/f characteristics. *American Journal of Physiology - Heart and Circulatory Physiology* 267: H449-H454, 1994.
134. Wallin BG, Sundlof G, and Delius W. The effect of carotid sinus nerve stimulation on muscle and skin nerve sympathetic activity in man. *Pflugers Arch* 358: 101-110, 1975.
135. White WB. Diurnal blood pressure and blood pressure variability in diabetic normotensive and hypertensive subjects. *Journal of Hypertension* 10: S43, 1992.
136. Xie X, Visweswaran R, Guzman PA, Smith RM, Osborn JW, and Tolkacheva EG. The effect of cardiac sympathetic denervation through bilateral stellate ganglionectomy on electrical properties of the heart. *American Journal of Physiology - Heart and Circulatory Physiology* 301: H192-H199, 2011.
137. Yan GX, and Antzelevitch C. Cellular basis for the normal T wave and the electrocardiographic manifestations of the long-QT syndrome. *Circulation* 98: 1928-1936, 1998.
138. Yan GX, Shimizu W, and Antzelevitch C. Characteristics and distribution of M cells in arterially perfused canine left ventricular wedge preparations. *Circulation* 98: 1921-1927, 1998.
139. Yanowitz F, Preston JB, and Abildskov JA. Functional distribution of right and left stellate innervation to the ventricles. Production of neurogenic electrocardiographic changes by unilateral alteration of sympathetic tone. *Circ Res* 18: 416-428, 1966.
140. Yoshioka K, Gao D-W, Chin M, Stillson C, Penades E, Lesh M, O'Connell W, and Dae M. Heterogeneous Sympathetic Innervation Influences Local Myocardial Repolarization in Normally Perfused Rabbit Hearts. *Circulation* 101: 1060-1066, 2000.

141. Zhang Q, Zhang X, Chang B, Qiu B, Zhang Y, Li J, and Zeng Z. Blood pressure variability correlates with target-organ damage in elderly patients with hypertension]. *Sichuan da xue xue bao Yi xue ban= Journal of Sichuan University Medical science edition* 42: 252, 2011.
142. Ziegler D. Diabetic cardiovascular autonomic neuropathy. *Diabetic Neuropathy Edit by Aventis Pharma, Inc* 140-169, 2001.
143. Ziegler D, Gries FA, Spuler M, and Lessmann F. The epidemiology of diabetic neuropathy. Diabetic Cardiovascular Autonomic Neuropathy Multicenter Study Group. *J Diabetes Complications* 6: 49-57, 1992.
144. Ziegler D, Laude D, Akila F, and Elghozi JL. Time- and frequency-domain estimation of early diabetic cardiovascular autonomic neuropathy. *Clin Auton Res* 11: 369-376, 2001.
145. Zipes DP, and Jalife J. *Cardiac electrophysiology : from cell to bedside*. Philadelphia: Saunders, 2004, p. xvi, 1144 p.

VITA

Student Name: Siqi Wang

Educational Institutions

September 2004 - July 2008 Sun Yat-sen University, China, Bachelor of Science in Biomedical Engineering

Professional Positions

August 2008 - December 2012 Research Assistant, Center for Biomedical Engineering, Wenner-Gren Research Laboratory, University of Kentucky

Peer Reviewed Publications

1. **Siqi Wang**, David C. Randall, Charles F. Knapp, Abhijit R. Patwardhan, Kevin R. Nelson, Dennis G. Karounos, Joyce M. Evans. Blood pressure regulation in diabetic patients with and without peripheral neuropathy. *Am J Physiol Regul Integr Comp Physiol* 302: R541-550, 2012.

Abstract

1. **Siqi Wang**, André Diedrich, Vladimir Kostas, Rachel Moore, Mat Stasuk, Charles Knapp, Joyce Evans. Postural Changes in Human Stroke Volume: Bio-Impedance vs. Ultrasound Estimates. *Gill Heart Institute, 15th Annual Cardiovascular Research Day*, October, 2012

2. **Siqi Wang**, André Diedrich, Vladimir Kostas, Rachel Moore, Mat Stasuk, Charles Knapp, Joyce Evans. Estimation of Postural Changes in Human Stroke Volume from Bio-Impedance. *BMES Annual Meeting*, Atlanta, GA, October, 24-27, 2012

3. Qingguang Zhang, Joyce M Evans, Vladimir Kostas, **Siqi Wang**, Charles F Knapp, Cardiovascular Responses of Men and Women to Orthostasis in Simulated Lunar and Martian Gravities. *BMES Annual Meeting*, Atlanta, GA, October, 24-27, 2012

4. **Siqi Wang,** David Randall, Charles Knapp, Kevin Nelson, Abhijit Patwardhan, Joyce Evans. Noninvasive assessment of cardiovascular autonomic neuropathy. *Gill Heart Institute, 14th Annual Cardiovascular Research Day*, October, 2011

5. JM Evans, **S Wang**, V Kostas, Q Zhang, SC Elayi, MB Stenger, CF Knapp. Orthostatic Fluid Shifts in Earth and Simulated Moon and Mars Environments. *AGSB/ISGP annual meeting*, San Jose, CA, November 3-7, 2011.

6. VI Kostas, MB Stenger, CF Knapp, RS. Shapiro, EE. Salmon, **S Wang**, A Diedrich, and JM Evans**.** Cardiovascular responses to standing in earth and simulated moon and mars gravity environments. *American College of Sports Medicine*, Denver, CO, June, 2011.

7. VI Kostas, MB Stenger, CF Knapp, RS. Shapiro, EE. Salmon, **S Wang**, A Diedrich, and JM Evans**.** Cardiovascular models of simulated moon and mars gravities: Head up tilt vs lower body unweighting. *Humans in Space Conference*, Houston Texas, April, 2011

8. **S Wang**, DC Randall, CF Knapp, KR Nelson, AR Patwardhan and JM Evans**.** Noninvasive assessment of cardiovascular autonomic neuropathy. FASEB *Jnl* 25, 2011.

9. **Siqi Wang,** David Randall, Charles Knapp, Kevin Nelson, Abhijit Patwardhan, Joyce Evans. Autonomic regulation in patients with diabetic neuropathy. *Gill Heart Institute, 13th Annual Cardiovascular Research Day*, October, 2010

10. **S Wang**, DC Randall, CF Knapp, KR Nelson, AR Patwardhan, PJ Kilfoil, and JM Evans. Autonomic regulation in patients with diabetic neuropathy. FASEB *Jnl* 24, 2010.

11. JM Evans, PJ Kilfoil, **S Wang**, L Mohney and CF Knapp. Cardiovascular responses to standing and walking in earth and simulated moon and mars gravities. FASEB *Jnl* 24, 2010.

12. **Siqi Wang**, David Randall, Charles Knapp, Abhijit Patwardhan, Peter Kilfoil, Joyce Evans. Dysfunction of autonomic regulation of short term blood pressure in diabetes. *Gill Heart Institute, 12th Annual Cardiovascular Research Day*, October, 2009

Scholastic and Professional Honors

2012 University of Kentucky, Graduate School, Max Steckler Fellowship

2012 University of Kentucky, Office of International Affairs, International

Student Tuition Scholarship

2012 University of Kentucky, College of Engineering, Halcomb Fellowhsip